



**UNIVERSIDADE FEDERAL DO PARÁ  
INSTITUTO DE GEOCIÊNCIAS  
PROGRAMA DE PÓS-GRADUAÇÃO EM GEOLOGIA E GEOQUÍMICA**

---

**DISSERTAÇÃO DE MESTRADO Nº 602**

**FONTES FOSFÁTICAS: DIFERENCIAÇÃO POR ESPECTROSCOPIA  
IV E RECICLAGEM POR PRECIPITAÇÃO DE ESTRUVITA A  
PARTIR DE SOLUÇÃO AQUOSA**

**Dissertação apresentada por:**

**PAULO VICTOR CAMPOS SOUSA**

**Orientadora: Prof.<sup>a</sup> Dr.<sup>a</sup> Simone Patrícia Aranha da Paz (UFPA)**

---

**BELÉM - PARÁ  
2021**

**Dados Internacionais de Catalogação na Publicação (CIP) de acordo com  
ISBD Sistema de Bibliotecas da Universidade Federal do Pará  
Gerada automaticamente pelo módulo Ficat, mediante os dados fornecidos pelo(a)  
autor(a)**

---

S725f Sousa, Paulo Victor Campos.  
Fontes fosfáticas : diferenciação por espectroscopia IV e  
reciclagem por precipitação de estruvita a partir de solução aquosa  
/ Paulo Victor Campos Sousa. — 2021.  
xv, 84 f. : il. color.

Orientador(a): Prof<sup>a</sup>. Dra. Simone Patrícia Aranha da  
Paz Dissertação (Mestrado) - Universidade Federal do  
Pará,  
Instituto de Geociências, Programa de Pós-Graduação em  
Geologia e Geoquímica, Belém, 2021.

1. Mineralogia. 2. Geoquímica. 3. Fosfatos Amazônicos.  
4. Estruvita. 5. Planejamento Experimental Sequencial. I.  
Título.

CDD 549.131

---



**Universidade Federal Do Pará**  
**Instituto De Geociências**  
**Programa De Pós-Graduação Em Geologia E Geoquímica**

**FONTES FOSFÁTICAS: DIFERENCIAÇÃO POR  
ESPECTROSCOPIA IV E RECICLAGEM POR PRECIPITAÇÃO  
DE ESTRUVITA A PARTIR DE SOLUÇÃO AQUOSA**

**DISSERTAÇÃO APRESENTADA POR:**

**PAULO VICTOR CAMPOS SOUSA**

**Como requisito parcial à obtenção do Grau de Mestre em Ciências na Área de  
GEOQUÍMICA E PETROLOGIA Linha de pesquisa em MINERALOGIA E  
GEOQUÍMICA**

Data da aprovação: 04 / 06 / 2021

Banca Examinadora:

Prof.<sup>a</sup> Dr.<sup>a</sup> Simone Patrícia Aranha da Paz  
(Orientadora – UFPA)

Prof.<sup>a</sup> Dr.<sup>a</sup> Verônica Scarpini Candido  
(Membro – UFPA)

Prof. Dr. Samuel Rodrigues Castro  
(Membro – UFJF)

## AGRADECIMENTOS

Sem a bondade divina, meus caminhos não teriam sentido. Sem apoio de grandes mentes, minha trajetória não teria fundamento. Sem amor familiar, minhas conquistas não teriam motivos. Sem a luz dos amigos, minhas perspectivas não teriam força. Por tudo isso, reservo este espaço para demonstrar minha gratidão a todos que impulsionaram direta ou indiretamente na construção desse trabalho.

A Deus, provedor de todas as coisas, que com Seu bondoso amparo me guiou até aqui, dando-me coragem nos caminhos tortuosos, acalanto no meio das aflições, respostas aos meus intrínsecos questionamentos, inspiração e sabedoria.

As minhas amadas mães Maria das Graças Campos e Valdeni Marinho por minha primeira formação, a formação de dignidade, ensinando-me sobre a vida com humildade, justiça, caráter e confiança, sempre almejando o melhor para o meu crescimento como ser humano e me apoiando em minhas escolhas.

Ao meu Irmão Pedro Henrique e Cunhada Antonia Ariele que me deram grande apoio durante essa fase da minha vida.

A minha grande família, em especial a minha tia Valdirene Marinho, por toda preocupação e compreensão.

A minha orientadora Prof.<sup>a</sup> Dr.<sup>a</sup> Simone Paz, que me concedeu a honra de ser seu orientando e me proporcionou imensurável aprendizado, contribuindo em minha construção intelectual, mostrando-me a seriedade e a beleza da ciência como instrumento de transformação e sendo uma grande inspiração de profissionalismo.

Ao Prof. Dr. Rômulo Angélica por sua parceria e grande contribuição intelectual nas diversas discussões de caráter geológico e mineralógico, além de todos os seus ensinamentos como pesquisador.

A Prof.<sup>a</sup> Dr.<sup>a</sup> Andreia Pereira por sua valiosa ajuda no entendimento dos pormenores da química analítica presentes nesse trabalho, além do seu grande incentivo durante minha trajetória no mestrado e por seus imprescindíveis conselhos.

Aos meus grandes amigos e confidentes Igor Barreto e Renata Nascimento. Amigos que encontrei ao longo dessa etapa, e que estiveram ao meu lado em diversos momentos. Amigos que tornaram o mestrado mais leve com boas e produtivas conversas e que me deram

fundamental apoio nos momentos mais difíceis. Igor, exemplo de consciência e foco. Renata cheia de doçura e perspicácia. Ambos com corações enormes, e muita sabedoria. Minha gratidão por me concederem a confiança de suas amizades.

Aos amigos do Laboratório de Caracterização Mineral (LCM), por todo auxílio fornecido e pelas inúmeras trocas de conhecimento ao longo desses anos em que pude compartilhar de muitos momentos de aprendizado e descontração em meio ao desenvolvimento dos nossos trabalhos. Agradeço em especial a Andréia Oliveira, Rebeca Castanho, Lesley Santos, Alan Albuquerque e David Porras, pelo companheirismo, apoio e amizade.

Ao Prof. Dr. José Augusto Correa por ceder espaço e instrumentos de trabalho no Laboratório de Análises Químicas do Instituto de Geociências.

A Prof.<sup>a</sup> Dr.<sup>a</sup> Rose Meira pelos ensinamentos sobre a síntese de estruvita.

Ao Prof. Dr. Lênio Faria por todos os ensinamentos acerca dos métodos de estatística de experimentos.

A Prof.<sup>a</sup> Dr.<sup>a</sup> Maria de Lourdes Santos da Universidade Federal Rural da Amazônia pelo grande apoio no fornecimento de água deionizada para a realização dos experimentos.

Ao MSc. Darllan Pinheiro pelo grande auxílio no fornecimento de água deionizada nos momentos em que precisei e pelas conversas sobre estatística.

A Dr.<sup>a</sup> Elma Oliveira pelas conversas e conselhos.

Aos técnicos do Instituto de Geociências da Universidade Federal do Pará, em especial ao Aldemir Sotero do LCM pela amizade e auxílio nas atividades, Everaldo Cunha do Laboratório de Sedimentologia pelo fornecimento de uma amostra de fosfato, Joanicy Lopes e Cleida Freitas pelo apoio nas questões acadêmicas.

A bibliotecária Lúcia Imbiriba em nome da Biblioteca Raimundo Montalvão pelas orientações em relação às normas de formatação da dissertação.

A minha grande amiga que se tornou uma irmã Bruna Baltazar por me aguentar durante nossa convivência e principalmente por me dar forças em momentos muito difíceis durante esse percurso. Sou grato por todas as experiências vividas nesse tempo, pelas palavras de conforto, pelas descontraídas e interessantes conversas e pela confiança.

A minha amiga Rosimar Adão, que me deu grande apoio e sábias palavras durante essa parte da minha trajetória.

Aos meus amigos Wynara Sandy, Amanda Éleres, Bianca Assis, Victória Eleres, Thais de Aguiar, Brenda Silva, Jhonata Vicenzott, Felipe Vidal, Maiara dos Anjos, Giovanna Coelho, Alan Palheta, Camilly Peres e Ana Beatriz Porto por confiarem na minha caminhada, pelos momentos de descontração, por entenderem minha ausência e minhas escolhas, e acima de tudo pelo grande apoio, o qual nunca irei esquecer. Sou imensamente grato por tê-los comigo.

Ao Conselho Nacional de Desenvolvimento Científico e Tecnológico (CNPq) pela concessão de bolsa de mestrado e pelo financiamento do projeto “Fertilizante de liberação lenta formulado a partir de termofosfato com aditivo de cinzas vegetais e aglomerados com bentonita magnesiana” (Proc. 429756/2018-6).

A empresa Phosfaz Fertilizantes pelas amostras de fosfato da região de Bonito-Pa.

Ao Programa de Pós-Graduação em Geologia e Geoquímica (PPGG) da Universidade Federal do Pará pela infraestrutura e recursos.

“Sometimes it is the people no one imagine anything  
of who do the things no one can imagine”

*Alan Turing*

## RESUMO

O fósforo é um elemento de múltiplas funções perante a manutenção da vida. Suas principais atribuições estão relacionadas ao seu papel de nutriente, em que atua nos organismos como componente estrutural de moléculas e na produção de energia. Por essas atribuições, o elemento é fundamentalmente requerido dentro da cadeia alimentar, sendo essencial no desenvolvimento dos vegetais, e por isso, altamente demandado no setor primário da economia. Por sua elevada reatividade com oxigênio, o fósforo encontra-se na crosta terrestre sob a forma iônica de ortofosfato ( $\text{PO}_4^{3-}$ ), distribuído como minerais fosfáticos que constituem as rochas, principais fontes para a produção de fertilizantes de fósforo. Por ser um recurso natural finito com crescente e acelerado consumo, suas reservas tendem a uma premente escassez. Devido a isso, busca-se cada vez mais por inovação e otimização de processos de produção secundária (reciclagem de fósforo), além de estratégias inteligentes de uso das fontes primárias. Nesse contexto, buscou-se nesse trabalho ampliar os estudos sobre fosfatos amazônicos no que concerne caracterização-diferenciação, e ainda, propor uma otimização na reciclagem de fósforo por precipitação de estruvita a partir de solução aquosa. Para alcançar o primeiro objetivo, fosfatos de três diferentes origens geológicas (ígnea, intempérica e biogenética), na região amazônica, foram diferenciados por espectroscopia de infravermelho com transformadas de Fourier (FTIR). As medidas foram realizadas nas regiões do infravermelho próximo e médio pelos métodos de: transmissão, reflectância difusa (DRIFT) e total atenuada (ATR). Além disso, análises complementares de difratometria de raios-X e fluorescência de raios-X também foram realizadas. Os resultados revelaram que os métodos por transmissão e DRIFT são os mais adequados e recomenda-se utilizá-los, quando possível, de maneira conjunta. As bandas características de  $\text{PO}_4$  foram observadas em todos os espectros nas faixas entre  $1200 - 984 \text{ cm}^{-1}$  e  $634 - 450 \text{ cm}^{-1}$ . A diferenciação dos materiais foi dada pela presença de bandas:  $(\text{CO}_3)^{2-}$  nos fosfatos ígneos,  $\text{Al}_2\text{OH}$  nos fosfatos intempéricos e  $\text{NH}_4$  no de origem biogenética. Ao final, um banco de dados espectral para fosfatos foi estabelecido e as assinaturas espectrais catalogadas. Para alcançar o segundo objetivo, uma otimização do processo de recuperação de P de soluções aquosas por meio de síntese de estruvita foi realizada, e para tal, uma metodologia de planejamento experimental sequencial (DOE) foi aplicada. Um planejamento Plackett-Burman seguido de um Doehlert atuaram na definição dos fatores significativamente influentes no processo de precipitação de estruvita e para otimização empregou-se a metodologia de superfície de



resposta em conjunto com a função desejabilidade. As respostas foram: recuperação de fósforo (medida química usual), padrão difratométrico e entalpia de decomposição da estruvita (medidas físicas não usuais nesse tipo de estudo, portanto uma inovação). Além disso, análises complementares de espectroscopia de fluorescência de raios-X, espectroscopia de infravermelho, granulometria a laser e microscopia eletrônica de varredura foram realizadas nos produtos. Os resultados permitiram definir as melhores condições de síntese: pH (10,2), razão N/P ( $\geq 4$ ) e concentração inicial de fósforo (183,5 mg/L), com recuperação de fósforo superior à 70% e formação de estruvita e K-estruvita. Por fim, pode-se dizer que propostas avançadas relacionadas a caracterização química e estrutural, e otimização de processo concernentes a fosfatos foram estabelecidas com base em dois métodos: um analítico (espectroscopia IV) e outro físico-químico (precipitação). Ambas as metodologias de investigação explanadas neste estudo contribuem na busca de soluções alternativas de geração e uso dos recursos fosfáticos.

**Palavras-chave:** fosfatos; diferenciação genética; FTIR; recuperação de fósforo; DOE.

## ABSTRACT

Phosphorus is an element with multiple functions in view of the maintenance of life. Its main attributions are related to its role as a nutrient, in which it acts in organisms as a structural component of molecules and in the production of energy. Due to these assignments, the element is fundamentally required within the food chain, being essential in the development of plants, and therefore, highly demanded in the primary sector of the economy. Due to its high reactivity with oxygen, phosphorus is found in the earth's crust in the ionic form of orthophosphate ( $\text{PO}_4^{3-}$ ), distributed as phosphate minerals that form the rocks, main sources for the production of phosphorus fertilizers. As it is a finite natural resource with increasing and accelerated consumption, their reserves tend to a pressing shortage. Because of this, there is an increasing search for innovation and optimization of secondary production processes (phosphorus recycling), as well as smart strategies for using primary sources. In this context, this work sought to expand studies on Amazonian phosphates with regard to characterization-differentiation, and yet, to propose an optimization in the recycling of phosphorus by struvite precipitation from aqueous solution. To achieve the first objective, phosphates from three different geological origins (igneous, weathering and biogenetics), in the Amazon region, were differentiated by infrared spectroscopy with Fourier transform (FTIR). The measurements were carried out in the near and medium infrared regions by the methods of: transmission, diffuse reflectance (DRIFT) and total attenuated (ATR). In addition, complementary analyzes of X-ray diffraction and X-ray fluorescence were also performed. The results revealed that the transmission and DRIFT methods are the most appropriate and it is recommended to use them, when possible, together. The characteristic  $\text{PO}_4$  bands were observed in all spectra in the ranges between  $1200 - 984 \text{ cm}^{-1}$  and  $634 - 450 \text{ cm}^{-1}$ . The differentiation of the materials was given by the presence of bands:  $(\text{CO}_3)^{2-}$  in igneous phosphates,  $\text{Al}_2\text{OH}$  in weathering phosphates and  $\text{NH}_4$  in the biogenetic origin. At the end, a spectral database for phosphates was established and spectral signatures were cataloged. To achieve the second objective, an optimization of the P recovery process from aqueous solutions through struvite synthesis was carried out, and for that, a sequential design of experiments methodology (DOE) was applied. A Plackett-Burman design followed by a Doehlert acted in the definition of the factors significantly influencing the struvite precipitation process and for optimization the response surface methodology was used in conjunction with the desirability function. The answers were: phosphorus recovery (usual chemical

measure), diffractometric pattern and struvite decomposition enthalpy (physical measures not usual in this type of study, therefore an innovation). In addition, complementary analyzes of X-ray fluorescence spectroscopy, infrared spectroscopy, laser granulometry and scanning electron microscopy were performed on the products. The results allowed to define the best synthesis conditions: pH (10.2), N/P ratio ( $\geq 4$ ) and initial phosphorus concentration (183.5 mg/L), with phosphorus recovery above 70% and formation of struvite and K-struvite. Finally, it can be said that advanced proposals related to chemical and structural characterization and process optimization concerning phosphates were established based on two methods: one analytical (IR spectroscopy) and the other physical-chemical (precipitation). Both research methodologies explained in this study contribute to the search for alternative solutions for the generation and use of phosphate resources.

**Keywords:** phosphates; genetic differentiation; FTIR; phosphorus recovery; DOE.

**LISTA DE ILUSTRAÇÕES**

Figura 1-A distribuição dos recursos de fosfato.....	4
Figura 2-Ciclo do fósforo .....	7
Figura 3-Estrutura da estruvita .....	11
Figura 4-Esquema básico de interação iônica de formação de estruvita e outros compostos cristalinos.....	16
Figura 5-Esquema simplificado da síntese de estruvita.....	23

**LISTA DE TABELAS**

Tabela 1-Características químicas dos cristais de estruvita.....	10
Tabela 2-Origem e Código das amostras.....	20
Tabela 3-Reagentes utilizados na composição da água residual e na análise de P .....	22
Tabela 4-Planejamento PB-12 com fatores codificados.....	27
Tabela 5-Fatores e níveis do planejamento PB-12 .....	28
Tabela 6-Matriz de Doehlert para o experimento com fatores codificados e valores experimentais.....	29

## SUMÁRIO

<b>AGRADECIMENTOS</b> .....	iv
<b>EPIÍGRAFE</b> .....	vii
<b>RESUMO</b> .....	viii
<b>ABSTRACT</b> .....	x
<b>LISTA DE ILUSTRAÇÕES</b> .....	xii
<b>LISTA DE TABELAS</b> .....	xiii
<b>1 INTRODUÇÃO</b> .....	1
1.1 APRESENTAÇÃO .....	1
1.2 JUSTIFICATIVA .....	1
<b>2 OBJETIVOS</b> .....	3
2.1 GERAL .....	3
2.2 ESPECÍFICOS .....	3
<b>3 REVISÃO BIBLIOGRÁFICA</b> .....	4
3.1 FOSFATOS .....	4
<b>3.1.1 Dinâmica e ciclo do fósforo</b> .....	6
<b>3.1.2 Recuperação de P de fontes secundárias</b> .....	7
<b>3.1.3 Estruvita</b> .....	9
<b>4 MATERIAIS E MÉTODOS</b> .....	20
4.1 PARTE I CARACTERIZAÇÃO-DIFERENCIAÇÃO DE FOSFATOS AMAZÔNICOS .....	20
<b>4.1.1 Materiais</b> .....	20
<b>4.1.2 Métodos</b> .....	21
4.2 PARTE II OTIMIZAÇÃO DA SÍNTESE DE ESTRUVITA .....	22
<b>4.2.1 Materiais</b> .....	22
<b>4.2.2 Métodos</b> .....	22
<b>4.2.3 Planejamento experimental e modelagem estatística</b> .....	26
<b>5 RESULTADOS E DISCUSSÃO</b> .....	30
5.1 ARTIGO 01 .....	30

5.2 ARTIGO 02 .....	42
<b>6 CONSIDERAÇÕES FINAIS</b> .....	<b>76</b>
<b>REFERÊNCIAS</b> .....	<b>77</b>
<b>APÊNDICE A – COMPROVANTE DE SUBMISSÃO DO ARTIGO 02</b> .....	<b>85</b>

# 1 INTRODUÇÃO

## 1.1 APRESENTAÇÃO

Apresenta-se esta monografia na forma estrutural típica de 6 tópicos principais: 1) Introdução, 2) Objetivos, 3) Revisão bibliográfica, 4) Materiais e Métodos, 5) Resultados e Discussão e 6) Considerações Finais. Apenas ressalta-se que o tópico 5 “Resultados e Discussão” compreende a apresentação de dois artigos resultantes dessa pesquisa: 5.1) Artigo 01: *FTIR spectral signatures of amazon inorganic phosphates: Igneous, weathering, and biogenetic origin*, que encontra-se publicado no periódico *Spectrochimica Acta Part A: Molecular and Biomolecular Spectroscopy*, e 5.2) Artigo 02: *A sequential Plackett-Burman and Doehlert design to optimize struvite precipitation as phosphorus recovery from wastewater aiming fertilizer production*, submetido ao periódico *Chemical Engineering Journal*. E uma vez que as conclusões estão apresentadas nos sub-tópicos 5.1 e 5.2, tem-se no tópico 6 as “Considerações Finais”.

## 1.2 JUSTIFICATIVA

O fósforo é um nutriente essencial para múltiplas funções nos organismos vivos. Sua principal atuação está relacionada ao desenvolvimento dos vegetais, nos quais o elemento é o responsável pela produção de energia química, contribuindo diretamente nas etapas de crescimento, florescimento e produção de frutos. Devido a isso, sua presença em solos agrícolas e florestais se torna fundamental (Mullen 2019, Zimdahl 2015).

Na crosta terrestre o elemento é encontrado sob a forma iônica de ortofosfato ( $\text{PO}_4^{3-}$ ), caracteristicamente disposto como minerais fosfáticos, que são as principais fontes de fósforo para a produção de fertilizantes. Devido a isso, essas fontes tendem a ficar cada vez mais escassas, tendo em vista que se trata de um recurso não renovável e de excessiva demanda pelo setor agrícola, principalmente nos países agroprodutores. Estimativas mostram que a demanda pelo nutriente ultrapassará sua oferta até 2035, e suas reservas chegarão ao esgotamento entre aproximadamente 50-100 anos (Cordell *et al.* 2009, Smil 2000).

Nesse contexto global, estratégias sustentáveis de uso dos recursos fosfáticos vêm sendo buscadas. A maioria das alternativas de manejo desses recursos estão atribuídas na recuperação secundária de suas fontes (reciclagem de fósforo), seja naquele proveniente do processo de beneficiamento/tratamento, seja naquele proveniente das etapas finais do ciclo do fósforo, principalmente em águas residuais (Daneshgar *et al.* 2019; Desmidt *et al.* 2015). Além disso,



melhorias relacionadas ao uso dos recursos primários são também demandadamente buscadas, e muitas delas carecem de tecnologias acerca da investigação inicial das suas fontes.

Metodologias que contribuem para o detalhamento químico e estrutural e/ou para a otimização de processos para obtenção de fosfatos são de grande interesse científico e tecnológico. Diversas propriedades de suas fontes podem ser estudadas através de técnicas analíticas, contribuindo na caracterização e diferenciação visando sua funcionalidade como fertilizante e garantindo o crescimento do arcabouço de dados sobre fosfatos. Além disso, tais ferramentas podem implicar em melhorias nos diversos processos de reciclagem do nutriente, incluindo os que são realizados a partir de soluções aquosas através de métodos físico-químicos como a precipitação.

Nesse sentido, visando aprimorar as investigações acerca dos fosfatos e desenvolver estratégias de uso de suas fontes, buscou-se nesse trabalho ampliar os estudos referentes à caracterização e diferenciação de fosfatos amazônicos de origens distintas, e ainda, otimizar um processo de reciclagem de fósforo tendo por base a precipitação de um composto cristalino conhecido como estruvita a partir de solução aquosa. Além disso, tais propostas possuem o intuito de permear o campo da inovação, quando se propõe: **diferenciação** de fosfatos amazônicos por espectroscopia de infravermelho, técnica com poucos bancos de dados para materiais inorgânicos e uma otimização da reciclagem de fósforo a partir de um planejamento experimental sequencial com **respostas** térmicas e estruturais, essas pouco usuais neste tipo de investigação.

## 2 OBJETIVOS

### 2.1 GERAL

Ampliar os estudos sobre fosfatos amazônicos no que concerne caracterização-diferenciação e propor uma otimização na reciclagem de fósforo por precipitação de estruvita a partir de solução aquosa visando seu uso como fertilizante.

### 2.2 ESPECÍFICOS

- Investigar a química e estruturas cristalinas de diferentes materiais fosfáticos;
- Qualificar fosfatos naturais da região amazônica a partir da diferenciação genética por espectroscopia de infravermelho com transformadas de Fourier;
- Identificar os principais grupos funcionais pertencentes às formações fosfáticas da região amazônica e catalogá-los em um banco de dados pioneiro;
- Propor uma otimização para o processo de recuperação de fósforo por precipitação de estruvita a partir de águas residuais usando estatística aplicada: metodologia de superfície de resposta, função desejabilidade e modelos empíricos baseados em regressão por mínimos quadrados
- Estabelecer as melhores condições de síntese de estruvita através da aplicação de uma metodologia de planejamento experimental sequencial com respostas: química (recuperação de fósforo), térmica (entalpia de decomposição da estruvita) e estrutural (padrão difratométrico) dos produtos de síntese.

### 3 REVISÃO BIBLIOGRÁFICA

#### 3.1 FOSFATOS

O elemento químico fósforo se apresenta distribuído na crosta terrestre sob a forma iônica de ortofosfato ( $\text{PO}_4^{3-}$ ) – também em variações como ânions ácidos de ortofosfato ( $\text{HPO}_4^{2-}$  e  $\text{H}_2\text{PO}_4^-$ ) – comumente na forma de minerais fosfatos, entre tantos, destaca-se: apatita “ $\text{Ca}_5(\text{PO}_4)_3(\text{F},\text{OH},\text{Cl})$ ”, lazulita “ $(\text{Mg},\text{Fe})\text{Al}_2(\text{PO}_4)_2(\text{OH})_2$ ” e monazita “ $(\text{Ce},\text{La},\text{Nd},\text{Th})\text{PO}_4$ ” (Attfield 1974, Straaten 2007, Zimdahl 2015). É simplesmente o elemento responsável pela produção de energia química no desenvolvimento dos vegetais (crescimento, florescimento e produção de frutos) e por isso é indispensavelmente requerido no cultivo de solos agrícolas e florestais (Zimdahl 2015). Sua forma de expressão iônica de ortofosfato é igualmente referenciada como fosfato inorgânico, o qual é expresso comumente nos resultados de análises químicas na forma de pentóxido de fósforo ( $\text{P}_2\text{O}_5$ ) (Straaten 2007). Enquanto, o fosfato orgânico é aquele sob a forma de monoéster ou diéster (ligações C-O-P) existentes nas moléculas de trifosfato de adenosina (ATP), DNA ou mesmo RNA, e também sob a forma de polifosfatos orgânicos e fosfonatos (Angert *et al.* 2011, Bünemann 2015, Huang *et al.* 2017).

Os minerais de fosfato estão agrupados em rochas fosfáticas. Estas rochas são formadas em diferentes ambientes geológicos, podendo ser de origem ígnea, sedimentar, metamórfica, biogenética ou provenientes do intemperismo (Straaten 2007, Van Straaten 2002). O gráfico na Figura 1 mostra a distribuição das fontes de fosfato de acordo com sua origem.

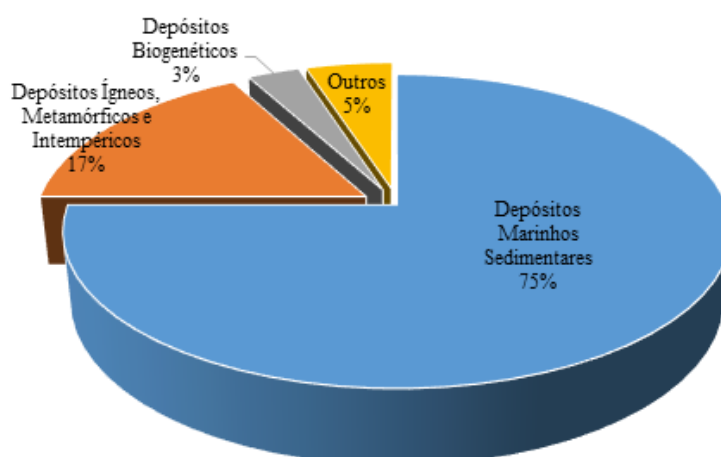


Figura 1– A distribuição dos recursos de fosfato no mundo. Adaptado de Ptáček (2016).

Os depósitos sedimentares de fosfato correspondem a cerca de 75% de todos os recursos minerais e a soma dos depósitos ígneos, metamórficos e intempéricos correspondem com ~ 17

%, enquanto os depósitos de origem biogenética (guanais), que são provenientes da interação de rochas com excrementos de pássaros e morcegos, correspondem com cerca de 3% das fontes de fosfato (Ptáček 2016, Van Straaten 2002). Tanto em rochas fosfáticas ígneas quanto sedimentares, minerais do grupo da apatita constituem-se como fosfatos predominantes. A apatita “ $\text{Ca}_5(\text{F,Cl,OH})(\text{PO}_4)_3$ ”, é essencialmente um fosfato de cálcio que apresenta transformações isomórficas de acordo com seu ambiente de origem, e pode comumente ser denominada por fluorapatita, cloroapatita ou hidroxiapatita, dependendo da concentração iônica dos íons  $\text{F}^-$ ,  $\text{Cl}^-$  e  $\text{OH}^-$ . O  $\text{Ca}^{2+}$  também pode vir a ser substituído por outros cátions bivalentes, assim como, o radical  $(\text{PO}_4)^{3-}$  pode ser substituído, parcialmente, por outros ânions, formando assim outros minerais do grupo da apatita (Dar & Khan 2017, Halder & Tišljarić 2014).

Em depósitos de origem sedimentar, os cristais de apatita normalmente ocorrem associados à calcita, dolomita, argilominerais e oxi-hidróxidos de ferro, como goethita e hematita. Nesses depósitos predominam as variedades de carbonato-apatita “ $\text{Ca}_5(\text{PO}_4,\text{CO}_3)_3(\text{OH},\text{F})$ ” e francolita ou carbonato-fluorapatita “ $\text{Ca}_5(\text{PO}_4,\text{CO}_3)_3(\text{F},\text{OH})$ ”, que geralmente são encontradas em massas criptocristalinas denominadas de colofano (Dar & Khan 2017). Outra massa criptocristalina de fosfato de cálcio proveniente de processos sedimentares é a fosforita, que consiste em uma variação amorfa da apatita, e possui depósitos com elevadas concentrações de fósforo (Dar & Khan 2017, Halder & Tišljarić 2014).

Os depósitos de fosfato são classificados como: fosfato de ferro-alumínio (Fe-Al-P), fosfato de cálcio-ferro-alumínio (Ca-Fe-Al-P) e fosfatos de cálcio (Ca-P). Essas três classes constituem uma sequência natural de intemperização dos depósitos de rocha fosfática, na qual o fosfato de cálcio representa a rocha matriz e as formas estáveis de fosfatos de ferro-alumínio como a crandalita “ $\text{CaAl}_3(\text{PO}_4)_2(\text{OH})_5 \cdot \text{H}_2\text{O}$ ” e a vivianita “ $\text{Fe}_3(\text{PO}_4)_3 \cdot 8\text{H}_2\text{O}$ ” representam o estágio mais avançado de intemperismo (Ptáček 2016).

Além dos fosfatos mais comuns, que são extraídos de rochas e representam as fontes mais plausíveis de uso, uma pequena parcela corresponde as outras diversas origens do ânion, que se constituem, em sua maioria, como fontes alternativas aos seus recursos primários. Essas fontes ainda pouco usuais são caracterizadas, principalmente, por serem residuais, tanto nas fases iniciais do ciclo do fósforo como no uso de rejeitos do beneficiamento de rochas fosfáticas, quanto nas fases finais do ciclo onde pode haver o uso do fosfato presente na biomassa, nos excrementos de animais, nos resíduos industriais e em águas residuais.

Atualmente, as fontes alternativas são alvo de importantes estudos que visam ampliar suas usabilidades ou até mesmo determinar processos que impliquem na recuperação/reciclagem do recurso, visto as crescentes demandas pelo elemento em detrimento das limitadas fontes que são disponíveis para uso.

### **3.1.1 Dinâmica e ciclo do fósforo**

A maior parte do fósforo no ambiente está contido no sistema solo sob a forma de minerais em rochas, principalmente como apatitas primárias. Por serem altamente insolúveis estes minerais não estão diretamente disponíveis para os organismos. A conversão de formas indisponíveis em ortofosfato dissolvido, que pode ser assimilado diretamente, é realizada através de diferentes reações de caráter geoquímico e bioquímico, por meio de várias etapas do ciclo global do fósforo. Estas reações podem ocorrer espontaneamente em processos químicos no solo ou por intermédio de micro-organismos presentes no meio (Mullen 2019, Ruttenberg 2001).

O ciclo do fósforo é dividido em dois subciclos interrelacionados: o geoquímico e o biológico, tendo-se o P inorgânico como ponto central do ciclo global. O subciclo geoquímico é caracterizado principalmente pelas diversas reações de intemperismo das rochas fosfáticas primárias, formando minerais fosfatos secundários de Ca, Al e Fe. Desse modo, os diferentes fosfatos presentes em depósitos minerais são passíveis de incorporação no subciclo biológico, o qual é responsável por solubilizar e ativar o fósforo para diversos processos no ambiente. No subciclo biológico, o ortofosfato solúvel, disposto através da ação de micro-organismos, é então absorvido pelas plantas ou imobilizado na biomassa microbiana. Dessa forma, os fosfatos inorgânicos são transformados em fosfatos orgânicos. O fósforo então é devolvido ao solo por meio dos excrementos e pela morte dos componentes da cadeia alimentar, podendo ser incorporado diretamente ao húmus estável, tornando-se relativamente indisponível para uso vegetal e microbiano, ou dependendo do seu teor na massa residual o P pode passar pelo processo de remineralização, sendo transformado em ortofosfato durante a decomposição microbiana do resíduo; e a parte restante de fósforo no resíduo será incorporado na biomassa microbiana durante a decomposição (Mullen 2019).

Durante o intemperismo das rochas, no ambiente superficial, uma parte do fósforo é lixiviado para fora do sistema com as águas que saem pela superfície do solo ou percolam para o lençol freático (Ruttenberg 2001). Uma vez que chega aos corpos hídricos se incorpora a cadeia trófica aquática ou se acumula nos sedimentos de fundo, aonde não pode ser aproveitado

até que possa ser reincorporado a cadeia trófica, reiniciando um novo ciclo (Condrón *et al.* 2015, Mullen 2019). A partir do fluxo do ortofosfato que circula com a movimentação das águas, novas conformações são realizadas através de combinações iônicas (Haldrar & Tišljár 2014, Ruttens 2001). O ciclo do fósforo é detalhado na Figura 2.

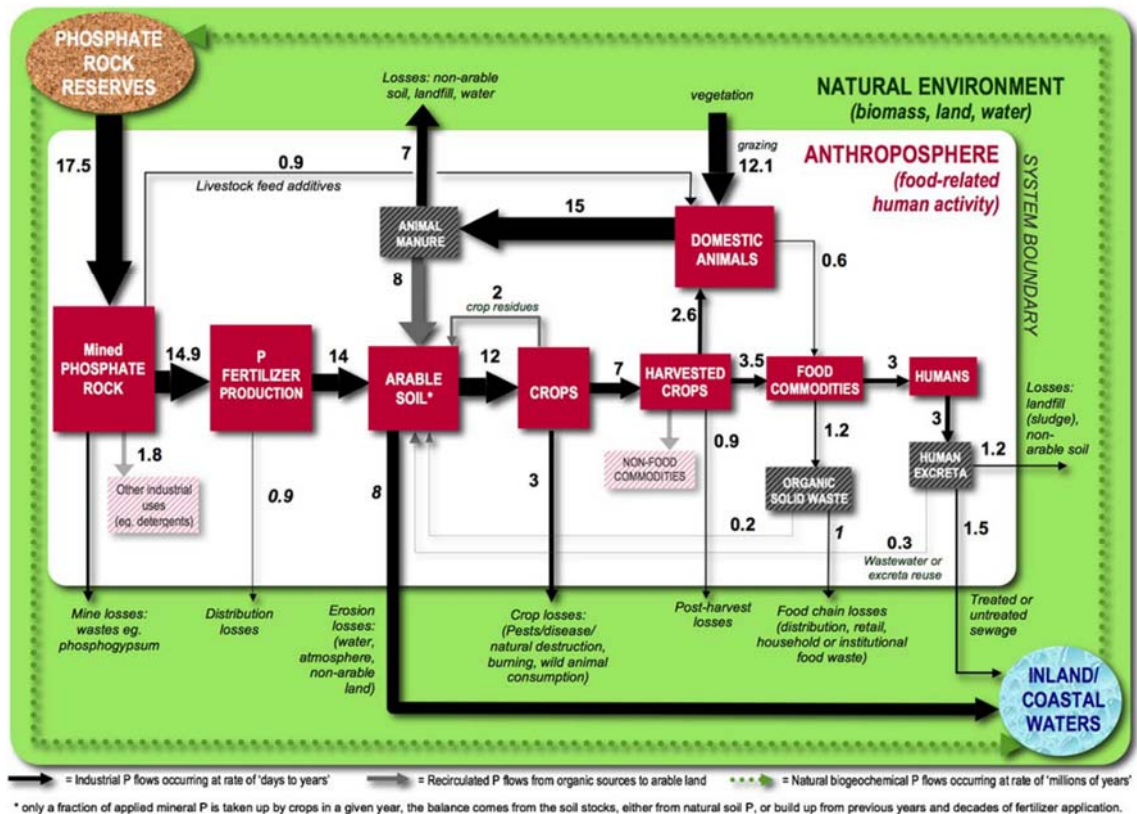


Figura 2 – Ciclo do fósforo. Fonte: Cordell *et al.* (2009).

Parte do fósforo é ainda transportada e mantida em sistemas de fluxos naturais e/ou em depósitos de resíduos, sendo provenientes de excrementos humanos e animais em escala doméstica ou industrial. Esses efluentes ricos em fosfato orgânico e inorgânico, além de outros elementos, são conhecidos como águas residuais, sendo, portanto, tidos como fontes secundárias de fósforo. O excessivo acúmulo e despejo dessas águas é capaz de gerar diversos problemas ambientais, sendo o mais comum a eutrofização de corpos hídricos (Smil 2000).

### 3.1.2 Recuperação de P de fontes secundárias

O somatório das fontes secundárias de fósforo, que engloba esgotos domésticos, dejetos de animais, chorume e rejeitos dos digeridos na produção de bioenergia, dentre outros, é de aproximadamente 7 milhões de toneladas por ano, o que corresponde com 40% do total global de recursos de fósforo primário (Cordell *et al.* 2009, Zhang *et al.* 2020). Cordell *et al.* (2009) ainda explanam diversas maneiras de como o fósforo pode ser recuperado e reutilizado como

fertilizante diretamente ou após processamento intermediário. Sendo assim, uma das alternativas citadas consiste na recuperação do elemento a partir de excrementos humanos e animais, que consistem em uma fonte renovável e estão constantemente disponíveis localmente.

O desequilíbrio molar e as concentrações variáveis do fósforo em esgotos limitam sua reciclagem e reutilização, provocando grandes perdas dentro do fluxo de resíduos líquidos, o que torna sua recuperação um grande desafio (Booker *et al.* 1999, Mehta & Batstone 2013). Como o íon ortofosfato não é volátil, diferentemente do amônio, e ainda apresenta tamanho molecular semelhante ao de outros íons presentes em águas residuais, a única abordagem viável para sua recuperação em uma forma concentrada é a precipitação como um sal insolúvel (Booker *et al.* 1999). Segundo Li *et al.* (2019) e Verstraete *et al.* (2009), a recuperação de fósforo de esgotos e demais tipos de rejeitos líquidos será altamente necessária e bastante praticada, devido a grande demanda por fertilizantes e a provável escassez do nutriente.

Dessa maneira, ao longo dos anos, diversas pesquisas avançaram dentro do contexto de recuperação e reciclagem de nutrientes como o P a partir de efluentes líquidos, e em alguns países como Japão, Canadá, Suécia, Bélgica e Holanda, o uso de materiais com elementos fertilizantes recuperados já está bem difundido (Castro 2014). Dentre os precursores em grandes projetos de recuperação de nutrientes, o Japão se destaca por ser o líder em recuperação de fosfato e por possuir várias plantas, em escala real, de recuperação de P (Adnan *et al.* 2003).

Dada a atual conjuntura agrícola mundial, tendo em vista a situação da ampla demanda por fertilizantes, juntamente com a problemática frequente da elevada disposição de elementos nutrientes em águas residuais, técnicas de recuperação do elemento vêm sendo amplamente investigadas e difundidas. Dentre as técnicas desenvolvidas, uma que ganha grande destaque é a precipitação química do elemento através da formação de diferentes fosfatos, e dentre os fosfatos que geralmente são precipitados, pode-se destacar a estruvita, que é um fosfato de amônio e magnésio hexahidratado que possui grande potencial de uso como fertilizante.

Segundo Parsons & Doyle (2002), a recuperação de nutrientes sob a forma de estruvita pode ocorrer a partir de diferentes tipos de efluentes, como lixiviados de aterros, águas residuais domésticas, industriais e agropecuárias e até mesmo com resíduos de matadouros. Dependendo do fluxo em que são gerados e tratados estes efluentes, o potencial de recuperação pode ultrapassar 1000 mg de estruvita por litro de resíduo (Parsons & Doyle 2002).

Visando uma alternativa de manejo de resíduos agropecuários, Schuiling & Andrade (1999) investigaram o potencial do uso de esterco de bezerros como fonte para a obtenção de

estruvita. Nesse estudo, uma planta de grande escala para a recuperação de nutrientes foi utilizada no local onde ocorria a deposição dos dejetos. Os resultados apresentados demonstraram que 200 m<sup>3</sup> de resíduos foram tratados, proporcionando a obtenção de centenas de kg de estruvita. Os dados referentes a recuperação de nutrientes foram expressos a partir da análise química do material obtido, o qual apresentou teores significativos de fósforo, magnésio e potássio, explanando a efetividade do tratamento.

Estudos também utilizaram a urina humana como precursora de elementos nutrientes para a precipitação de estruvita. Etter *et al.* (2011) investigaram a possibilidade da transferência de fósforo da urina humana de uma comunidade do Nepal, para a formação de um concentrado fosfático. Neste caso, o concentrado fosfático encontrado foi a estruvita. Foram utilizados dois reatores, o primeiro obteve uma eficiência correspondente à 90% de remoção de P, atribuindo-se uma baixa dosagem de Mg; já o segundo reator, que era baseado em processos de sedimentação, alcançou apenas 50% de remoção de fósforo.

Ronteltap *et al.* (2010) conduziram uma investigação acerca da precipitação de estruvita usando urina humana como fonte dos seus componentes químicos. O processo foi analisado a partir dos fatores que influenciavam no tamanho das partículas. Os resultados obtidos mostraram que a urina hidrolisada real foi capaz de gerar cristais de estruvita maiores que 90 µm em pH 9 e na temperatura de 20 °C, com uma eficiência de remoção de fósforo de aproximadamente 95%.

### 3.1.3 Estruvita

#### 3.1.3.1 Definição e características

A estruvita ( $\text{MgNH}_4\text{PO}_4 \cdot 6\text{H}_2\text{O}$ ), é um mineral pertencente ao grupo dos ortofosfatos, cuja composição química possui concentrações equimolares dos componentes iônicos –  $\text{PO}_4^{3-}$ ,  $\text{NH}_4^+$ ,  $\text{Mg}(6\text{H}_2\text{O})^{2+}$  – unidos sob a forma de cristais em ambientes aquosos característicos com elevados teores de amônia e fosfato (Le Corre *et al.* 2009, Tansel *et al.* 2018). Suas principais propriedades estão descritas na Tabela 1.

O fosfato de amônio e magnésio hexahidratado, como também é chamada a estruvita, foi inicialmente encontrado e descrito em um meio de terra turfosas acrescida de excrementos de gado no solo embaixo de uma igreja na cidade de Hamburgo, na Alemanha. Outras ocorrências típicas foram descritas em cavernas e em depósitos superficiais, onde há formações de guano de pássaros e morcegos. As raras ocorrências de estruvita na natureza podem estar



geralmente associadas a newberita  $[\text{Mg}(\text{PO}_3\text{OH}) \cdot 3(\text{H}_2\text{O})]$ , hannaita  $[(\text{NH}_4)_2\text{Mg}_3\text{H}_4(\text{PO}_4)_4 \cdot 8(\text{H}_2\text{O})]$ , brushita  $[\text{CaHPO}_4 \cdot 2\text{H}_2\text{O}]$ , e estercorita  $[\text{NaNH}_4\text{HPO}_4 \cdot 4\text{H}_2\text{O}]$  (Vollmar 1967).

Tabela 1- Características químicas dos cristais de estruvita.

Propriedade	Valor
Peso molecular	247,42 g/mol
Massa exata	247,05 g/mol
Contagem de doações de ligação de hidrogênio	10
Contagem de aceite de ligações de hidrogênio	11
Contagem de átomos pesados	13 (sem H)
Complexidade	49,8
Área de superfície polar topológica	84,8 Å <sup>2</sup>
Contagem de unidades ligadas covalentemente	9

Fonte: Adaptada do Centro Nacional de Informação Biotecnológica (2015)

Além das formações de guano, de forma geral, a ocorrência espontânea de estruvita no ambiente se dá principalmente em meios biológicos, com graus representativos de alcalinidade e turbulência. Com tais características, as usinas de tratamento de águas residuais industriais e domésticas são ambientes comuns de formação de estruvita, o que vem a ser um problema escalar, visto que nestes meios a estruvita ocorre como incrustações dentro de tubulações e em superfícies de equipamentos (Booker *et al.* 1999, Borgerding 1972, Doyle *et al.* 2003, Le Corre *et al.* 2009, Ohlinger *et al.* 1998).

Um outro ambiente típico onde há a formação de estruvita é dentro de sistemas urinários de animais, comumente nos rins, os quais possuem as características e os componentes fundamentais (compostos químicos e pH) para a precipitação deste biomineral sob a forma de algumas variedades de cálculos renais (Chatterjee *et al.* 2018, Elliot *et al.* 1958).

### 3.1.3.2 Cristalquímica

A estruvita cristaliza no sistema ortorrômbico, possuindo as células unitárias de sua estrutura com as respectivas dimensões:  $a = 6,941 \pm 0,002 \text{ \AA}$ ,  $b = 6,137 \pm 0,002 \text{ \AA}$  e  $c = 11,199 \pm 0,004 \text{ \AA}$ . Pertence então ao grupo espacial  $Pmn2_1$  e possui duas moléculas dentro de cada célula unitária. Sua estrutura se estabelece basicamente em grupos iônicos de fosfato ( $\text{PO}_4^{3-}$ ) e amônio ( $\text{NH}_4^+$ ) tetraédricos com magnésio hexahidratado  $[\text{Mg}(6\text{H}_2\text{O})^{2+}]$  octaédrico, unidos através de ligações de hidrogênio, como pode ser visto na Figura 3 (Ferraris *et al.* 1986, Whitaker & Jeffery 1970).

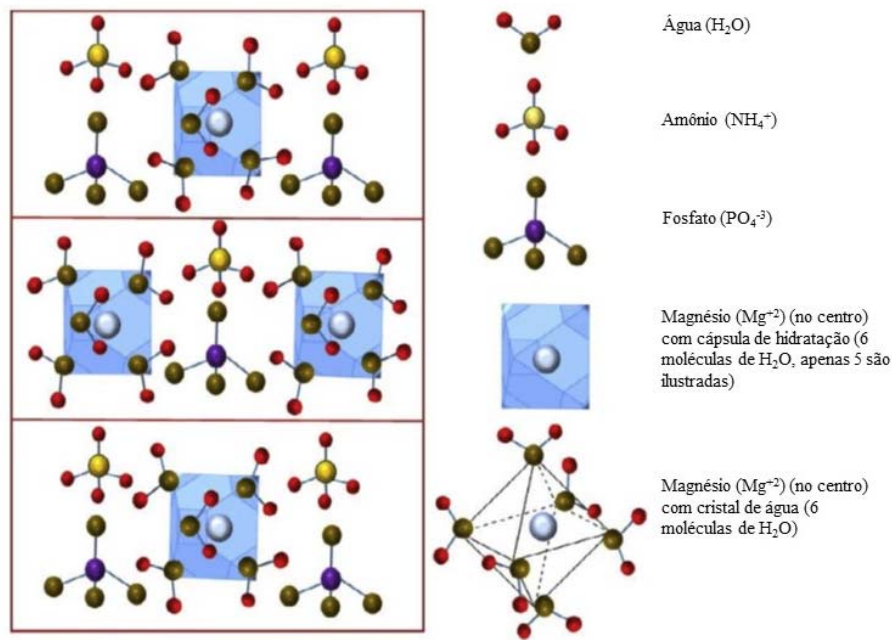


Figura 3 - Estrutura da estruvita. Traduzido de Tansel *et al.* (2018).

Os tetraedros regulares de  $\text{PO}_4^{3-}$  possuem interações P–O com valor médio de comprimento de 1,543 Å. Já os octaedros não-regulares de  $\text{Mg}\cdot 6\text{H}_2\text{O}$  contém ligações Mg–H<sub>2</sub>O e H<sub>2</sub>O–H de tamanhos médios iguais a 2,0810 Å e 0,792 Å respectivamente (Whitaker & Jeffery 1970). As moléculas de água componentes da estruvita formam seis ligações de hidrogênio, que por sua vez são consideradas ligações extremamente curtas, estando entre as menores já vistas em compostos cristalinos hidratados. Estas ligações curtas das moléculas de água são menores do que as de ligações de separação intermolecular, tendo distâncias variando de 263,0 a 269,5 pm (Ferraris *et al.* 1986, Tansel *et al.* 2018, Whitaker & Jeffery 1970).

Cada íon de  $\text{NH}_4^+$  na estrutura da estruvita é cercado por cinco átomos de oxigênio, tendo, portanto, uma das ligações N–O (comprimento de 2,818 Å), como uma forte ligação de hidrogênio, sobrepondo-se as demais ligações presentes. A amônia pode ainda apresentar ligações polifurcadas caso o grupo funcional tenha um número de coordenação maior que quatro (Abbona & Boistelle 1979, Stefov *et al.* 2005). As ligações mais fortes dentro da estrutura da estruvita são explicadas pelos seus relativos comprimentos, que são inversamente proporcionais as forças estabelecidas às mesmas. Por sua vez, ligações consideradas mais fortes demandam maior energia para serem dissociadas (Tansel *et al.* 2018).

### 3.1.3.3 Formação de estruvita

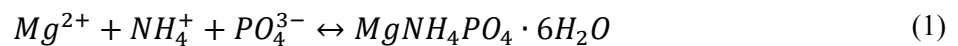
A formação de estruvita ocorre por meio de um processo físico-químico conhecido por precipitação. Fundamentalmente, para que haja a precipitação de estruvita, as concentrações

combinadas de  $PO_4^{3-}$ ,  $NH_4^+$  e  $Mg^{2+}$  devem exceder o seu limite de solubilidade. Logo, toda a química de precipitação de estruvita está intimamente ligada à solubilidade, sendo, portanto, o fator chave do entendimento de sua formação (Aage *et al.* 1997, Ohlinger *et al.* 1998, Parsons & Doyle 2002, Taylor *et al.* 1963).

A solubilidade, por sua vez, está relacionada com a disponibilidade dos íons formadores de estruvita, a qual é controlada por um sistema mútuo entre pH e a concentração das espécies totais dissolvidas. Devido a influência do pH para que haja a especiação dos componentes, há, conseqüentemente, o desencadeamento de variações da solubilidade da estruvita em relação ao pH (Ohlinger *et al.* 1998, Taylor *et al.* 1963).

Os diagramas de especiação, de maneira individual, tanto para o fósforo sob a forma de ácido fosfórico ( $H_3PO_4$ ) quanto para a amônia, possuem perfis de concentração iônica em solução aquosa bem definidos de acordo com a influência do pH. Porém, as características de especiação iônica podem ser facilmente alteradas/controladas por mudanças na temperatura do sistema e no grau de supersaturação, bem como pela presença de outros íons (Abbona *et al.* 1982, 1986, Bouropoulos & Koutsoukos 2000, Tansel *et al.* 2018).

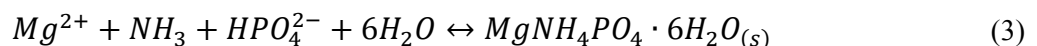
A formação de estruvita é comumente representada pela Equação 1. Esta equação é uma fórmula geral e simplificada de todo processo físico-químico envolvido na obtenção de estruvita (Abbona *et al.* 1982, Le Corre *et al.* 2007, Parsons & Doyle 2002, Rahaman *et al.* 2008).



Devido as variações no pH ocasionadas pela formação de estruvita, a participação de  $HPO_4^{2-}$  na reação é usualmente mais indicada do que o íon  $PO_4^{3-}$  em si, sendo, portanto, o mecanismo de reação descrito na Equação 2, o mais completo, no que diz respeito ao processo de diminuição do pH com a formação de estruvita (Schuiling & Andrade 1999).



Todavia, a reação exposta na Equação 3 é a rota de interação iônica que melhor representa a formação de estruvita. Isso se dá tanto por esta reação agregar a alteração de equilíbrio responsável pelo aumento da concentração de  $NH_4^+$ , ocasionada pela remoção de  $NH_3$ , consequência da redução do pH; quanto pelo tamanho dos íons, estrutura cristalina e configurações atômicas (Tansel *et al.* 2018).



O processo de formação de estruvita, tendo por fundamentação o conceito químico de cristalização e precipitação, consiste em um processo físico-químico de agrupamento iônico em arranjos ordenados de acordo com um padrão de repetição. Este processo complexo é explicado por teorias termodinâmicas que envolvem equilíbrio químico e solubilidade; e fatores cinéticos que determinam as taxas de precipitação de acordo com a formação de núcleos e crescimentos dos cristais.

#### *Fatores influentes na formação de estruvita*

A precipitação de estruvita é fundamentalmente marcada pela solubilidade das espécies envolvidas na reação. Em suma, a determinação das características de nucleação e crescimento dos cristais, pautadas em termos de solubilidade, torna-se bastante complexa, visto as diversas combinações e variações de fatores que permeiam a físico-química de cristalização. Aspectos influentes como a cinética e a termodinâmica de reação, os estados cristalinos iniciais dos compostos, fenômenos de transferência de massa entre as fases sólidas e líquidas, além de fortes parâmetros como o pH, o índice de supersaturação e a presença de espécies iônicas diferentes, são capazes de comprometer as etapas do processo de cristalização de estruvita (Le Corre 2006, Morita *et al.* 2019).

##### *a) pH*

O pH é um dos fatores termodinâmicos de maior importância no que diz respeito a precipitação de estruvita, contribuindo diretamente na especiação química dos elementos componentes da solução (fração química dos reagentes), juntamente com o produto de solubilidade de atividade, afetando assim a supersaturação da solução em função da formação de estruvita. Além disso, com o aumento do valor do pH até um valor ótimo, tem-se também a diminuição da solubilidade da estruvita formada (Aidar 2012).

A literatura reporta que devido as diversas condições do meio reacional, o pH ótimo não está fixado em um único valor e sim ao longo de uma faixa de trabalho para que ocorra a cristalização. Esta faixa ótima de pH pode variar entre valores de 7 até 12, sendo que a remoção de fósforo da solução é proporcional ao aumento dos valores de pH dentro dessa faixa. Porém, muitos estudos relatam a precipitação de estruvita em ambientes com pH entre 8 e 9 (Ali & Schneider 2008, Babić-Ivančić *et al.* 2006, Carballa *et al.* 2009, Çelen *et al.* 2007, He *et al.* 2013, Negrea *et al.* 2010).

Segundo Tansel *et al.* (2018), a ampla faixa de pH pressupõe a existência de diversas condições e diferentes mecanismos que podem resultar na formação de estruvita. Estas variações dependem das interações iônicas e/ou formação de outros cristais diferentes, porém com características semelhantes às da estruvita.

Ariyanto *et al.* (2014), demonstraram em seu estudo o efeito do pH sobre a nucleação espontânea da estruvita, que de acordo com os experimentos realizados, notou-se que conforme o aumento do pH inicial das soluções o tempo de indução para a cristalização foi reduzido.

*b) Razão de supersaturação*

Em conjunto com o pH, a razão de supersaturação (SSR) se estabelece como uma variável fundamental para o controle da precipitação de estruvita (Aidar 2012, Le Corre 2006). Sabe-se, de modo geral, que quanto menor a SSR mais eficiente será a reação e a geração de precipitado, porém essa correlação não é fixa para a precipitação de estruvita, devido as diversas condições nas quais podem ocorrer a sua formação (Aidar 2012, Forrest *et al.* 2008).

A região de metaestabilidade do meio reacional possui relativa importância na SSR. De modo que independentemente da existência de estímulos termodinâmicos iniciais para a cristalização primária de estruvita, pode ocorrer a formação secundária, desde que dentro da região de metaestabilidade. Portanto, quando há as condições necessárias juntamente com uma razão de supersaturação moderada, os cristais obtidos são de maiores tamanhos (>1mm) (Forrest *et al.* 2008, Regy 2001).

Kofina & Koutsoukos (2005), demonstraram que a precipitação espontânea de estruvita era dependente da supersaturação da solução, ocorrendo através de mecanismos de difusão superficial, tendo uma dependência de alta ordem de cristalização na faixa de supersaturação entre 2,07 e 4,29. Porém, esta faixa de SSR para que haja precipitação pode variar entre 1 e 5, não havendo um ponto ótimo determinado (Adnan *et al.* 2003, Bouropoulos & Koutsoukos 2000, Le Corre 2006).

*c) Temperatura*

A temperatura se apresenta como um fator de menor impacto sobre formação de estruvita (Durrant *et al.* 1999). Este parâmetro age como fator coadjuvante na especiação iônica, podendo alterar as condições para a cristalização do material. Temperaturas mais elevadas podem influenciar na diminuição do pH, o que torna mais difícil a precipitação de estruvita. Dados de estudos laboratoriais com composições iônicas limitadas, apesar de não serem

totalmente representativos das condições nas estações de tratamento de águas residuais, explicitam que a temperatura ambiente (~ 20-35°C) proporciona a eficiente precipitação de estruvita (Battistoni *et al.* 2000, Fattah *et al.* 2008, Loewenthal *et al.* 1994, Münch & Barr 2001, Muster *et al.* 2013, Ohlinger *et al.* 1998, Uysal *et al.* 2010)

A temperatura também é capaz de influenciar no crescimento dos cristais, pois contribui para mudanças nas taxas relativas de difusão e integração da superfície dos cristais (Le Corre 2006). Elevadas temperaturas geralmente promovem o crescimento dos cristais através de mecanismos de difusão, enquanto que em temperaturas mais amenas o crescimento é dado por fenômenos de integração de superfície (Jones 2002). A temperatura ainda influencia na forma e tipo do tamanho dos cristais, e dependendo das concentrações iônicas presentes pode afetar na natureza do cristal formado, podendo ser geradas outras fases que não são de interesse (Babić-Ivančić *et al.* 2002).

Diversos autores também investigaram a influência da temperatura na decomposição da estruvita. Seus resultados mostraram que a decomposição é dependente da temperatura, das taxas de aquecimento e do pH (Babić-Ivančić *et al.* 2002, 2006, Bhuiyan *et al.* 2008, Farhana 2015, Frost *et al.* 2004, Huang *et al.* 2015, Saerens 2020). As variações de temperatura podem ocasionar transformações na estrutura do produto, devido a provável perda de amônia e de água estrutural. Fases como bobierrita, dittmarita, phorrosslerita, newberita e hayesita podem ser geradas após a decomposição da estruvita provocada pelas perdas graduais de amônia e moléculas de água (Bhuiyan *et al.* 2008, Farhana 2015, Saerens 2020). Portanto, a decomposição da estruvita sob condições de aquecimento isotérmico seco em temperaturas entre 40 °C e 60 °C não ocasiona perdas de massa bruscas nem a liberação de amônia (Novotny 2011).

#### d) Concentração de fósforo

Necessariamente, para que ocorra a precipitação de estruvita, a concentração de P-PO<sub>4</sub> deve ser superior à 50 mg/L. Concentrações menores tendem a conduzir a formação de outros ou até mesmo nenhum precipitado (Adnan *et al.* 2003). De acordo com Bitton (2010) para que ocorra uma recuperação de P eficiente a concentração mínima de P-PO<sub>4</sub> no meio reacional deve ser acima de 40 mg/L.

e) Presença de outros íons

Geralmente, em investigações realizadas em laboratório sobre as condições para a formação de estruvita, os sistemas aquosos estabelecidos são preparados para conter um grupo limitado de íons e as condições mínimas para a composição da estruvita. Todavia, em sistemas mais comuns de formação de estruvita, seja natural ou industrial, os íons presentes não se reduzem a apenas os necessários para a formação da mesma (Laridi *et al.* 2005, Tansel *et al.* 2018).

Diferentes tipos de íons podem ser encontrados nos mais diversos ambientes os quais a estruvita é formada, sendo eles:  $\text{Fe}^{3+}$ ,  $\text{Fe}^{2+}$ ,  $\text{Ca}^{2+}$ ,  $\text{Na}^+$ ,  $\text{K}^+$ ,  $\text{Cl}^-$ ,  $\text{SO}_4^{2-}$ ,  $\text{CO}_3^{2-}$ ,  $\text{HCO}_3^-$ , silicatos, oxalatos e também íons orgânicos. A presença desses íons, bem como suas dadas concentrações, afeta diretamente toda a dinâmica de interações e agrupamentos dos íons dentro de determinados sistemas (Booker *et al.* 1999).

Como consequência das diversas interações ocorridas pela presença de inúmeros íons nas soluções, há a possível alteração dos perfis de especiação iônica de  $\text{H}_3\text{PO}_4$  e amônia ( $\text{NH}_3$ ), de acordo com o pH do meio. Esta alteração se dá por meio de interações iônicas e não covalentes, juntamente com o alinhamento e agrupamento dos íons em diferentes grupos, ocasionando a formação de outros compostos, como pode ser observado na Figura 4, onde é demonstrada esquematicamente algumas interações entre os próprios íons de formação da estruvita, que dependendo de algumas condições, como variações no pH, podem gerar outras formações cristalinas (Tansel *et al.* 2018).

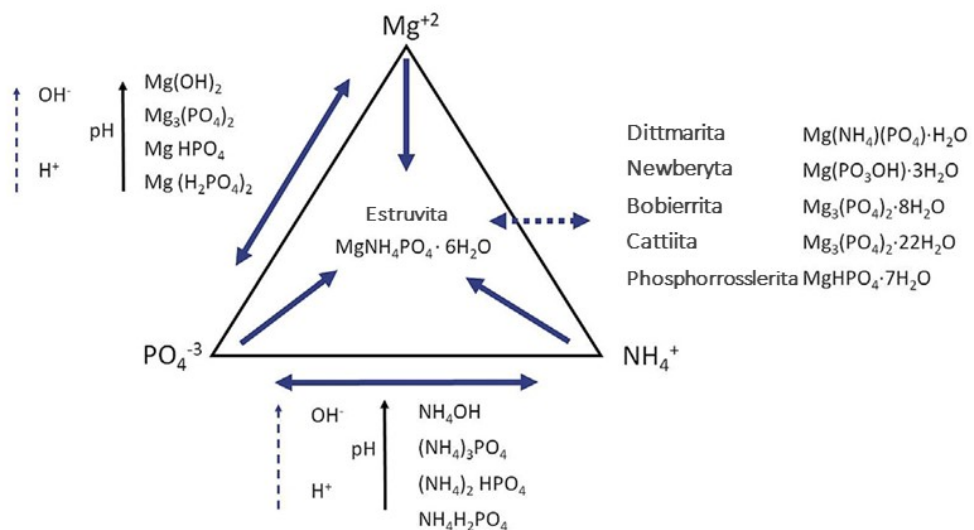


Figura 4 - Esquema básico de interação iônica de formação de estruvita e outros compostos cristalinos. Traduzido de Tansel *et al.* (2018).

A formação de estruvita, bem como a de outros sólidos possui uma interdependência com as variações das concentrações iônicas nos sistemas aquosos e do pH da solução. Os cristais de estruvita podem conter em sua estrutura apenas os seus íons principais, porém em diferentes proporções. Todavia, estes íons podem sofrer substituições pelos outros íons presentes na solução, dependendo das suas disponibilidades, ocasionando assim a formação de outros cristais aparentemente similares a estruvita, porém com composição química diferente. Estes cristais obtidos por substituições na estrutura da estruvita são conhecidos como estruvitas análogas (Ravikumar *et al.* 2010).

De acordo com Ravikumar *et al.* (2010), as principais substituições iônicas que ocorrem são de íons amônio  $\text{NH}_4^+$  por  $\text{K}^+$ ,  $\text{Rb}^+$ ,  $\text{Cs}^+$ ; e dos íons bivalentes  $\text{Mg}^{2+}$  por  $\text{Ca}^{2+}$ ,  $\text{Zn}^{2+}$  e  $\text{Cd}^{2+}$ .

#### 2.1.3.4 Importância global da obtenção de estruvita

De forma geral, a precipitação de estruvita se estabelece como um processo de múltiplo interesse e finalidades, visto que sua produção contribui de maneira positiva na solução de problemáticas globais. A princípio, sua obtenção é geralmente atrelada a utilização de águas residuais como fonte de seus componentes químicos. Logo, a precipitação de estruvita serve como um processo de remoção e recuperação simultânea de fósforo, nitrogênio, magnésio e potássio de efluentes líquidos (Fattah 2004, Fattah *et al.* 2008, Shih *et al.* 2017, Suzuki *et al.* 2007). Esse processo é bastante indicado para águas residuais com nutrientes em concentrações consideráveis, que são agentes de contaminação e que podem ocasionar eutrofização e outras consequências de cunho ambiental (Bendoricchio *et al.* 1993, Capodaglio *et al.* 2003, Carey & Migliaccio 2009, Siciliano *et al.* 2020).

A recuperação e reutilização de nutrientes é uma forma eficaz de reduzir riscos para o meio ambiente e para a sociedade, de modo que o processo permite vantagens em atividades como saneamento e agricultura (Mayer *et al.* 2016, Rittmann *et al.* 2011). Como exemplo, no contexto de saneamento, se tratando da qualidade da água, recuperar elementos como fósforo e nitrogênio combate impactos devastadores da poluição de corpos hídricos, causados principalmente pela fertilização excessiva e pela deterioração proveniente do uso humano diário. Para a agricultura, a capacidade de reciclar o fósforo em função do abastecimento alimentar local ou nacional, minimiza os riscos da futura escassez do elemento, seja pela ausência da fonte natural ou por questões econômicas e interrupções geopolíticas (Mayer *et al.* 2016).



A estruvita é amplamente utilizada para a reciclagem de nutrientes de águas residuais devido a sua capacidade de agregar em um precipitado de pureza relativa, grandes quantidades de fósforo e nitrogênio, contendo apenas vestígios de impurezas (Daneshgar *et al.* 2018, Huygens *et al.* 2019). Levando em consideração sua composição química e propriedades estruturais bem definidas, a estruvita se estabelece como um material de grande interesse para a indústria de fertilizantes. O produto também conhecido por MAP, é um fertilizante de liberação lenta de elevada eficiência e que pode ser comercializável (Münch & Barr 2001, Rahman *et al.* 2014).

Em países nos quais a agroindústria é uma forte atividade, o uso da estruvita contribui na redução do custo do fosfato, sendo capaz de aumentar a produtividade das safras e a segurança alimentar através de uma fonte renovável (Mayer *et al.* 2016). Em muitos países, a dependência de importações de rocha fosfática bem como das matérias-primas secundárias de processamento de fertilizantes fosfatados, ocasionam elevados custos no produto final (Römer & Steingrobe 2018). Em contrapartida, o investimento a médio e longo prazo no desenvolvimento de fertilizantes alternativos como a estruvita, é altamente estimulado para tornar a atividade agrícola menos onerosa, mesmo que atualmente os custos envolvidos no tratamento de efluentes e no uso de reagentes complementares promova um relativo desequilíbrio dessa intenção.

Além disso, a utilização de fertilizantes inorgânicos processados de baixo custo caracterizam-se por apresentar algumas desvantagens. Dentre os prejuízos mais comuns, pode-se destacar a rápida liberação de nutrientes, devido às elevadas taxas de solubilidade, o que contribui no processo de lixiviação do solo; e a presença de metais pesados e/ou resíduos prejudiciais ao sistema solo e às águas subterrâneas (Langergraber & Muellegger 2005). Nesse sentido, a estruvita apresenta-se como um fertilizante de alta efetividade, pois atua com baixa solubilidade, e portanto tem a lenta liberação de nutrientes (Achat *et al.* 2014, Talboys *et al.* 2016), e pode ser produzido com mínima contaminação por metais pesados (Antonini *et al.* 2012).

A baixa solubilidade total da estruvita está vinculada à sua ligeira solubilidade de P em água (1-5%), e elevada solubilidade de P em ácido cítrico (43-51%) (Cabeza *et al.* 2011). Por ser um fertilizante de liberação lenta, a estruvita pode fornecer uma fonte de fósforo de longo prazo para o desenvolvimento de culturas agrícolas. Em comparação com formas prontamente solúveis de P, que apresentam o nutriente de maneira mais limitada, principalmente no

momento mais demandado pelas culturas – crescimento das plantas – (Veneklaas *et al.* 2012), a estruvita condiciona uma melhor eficiência (Withers *et al.* 2014).

Os benefícios da dissolução mais lenta da estruvita, como a menor adsorção de P na solução do solo e menores taxas de liberação de P para o escoamento superficial, implicam na sua utilização para o aumento de produtividade das culturas em favor da menor aplicação de composições fertilizantes. Sendo assim, a produtividade tende a ser mantida ou aumentada com um menor impacto ambiental, sendo economicamente vantajoso para a indústria agrícola e com um *insight* sustentável (Talboys *et al.* 2016).

## 4 MATERIAIS E MÉTODOS

### 4.1 PARTE I CARACTERIZAÇÃO-DIFERENCIAÇÃO DE FOSFATOS AMAZÔNICOS

#### 4.1.1 Materiais

Para esta investigação foram utilizadas seis amostras de rochas fosfáticas, as quais podem ser observadas na Tabela 2, onde estão indicadas as suas procedências e as nomenclaturas adotadas.

Tabela 2- Origem e Código das amostras.

Nome da amostra	Origem	Código
Padrão IPT 18B	Jacupiranga – SP	IPT 18B
Fosfato Ígneo	São Félix do Xingu – PA	IP
Fosfato Intempérico 1	Bonito – PA	WP1
Fosfato Intempérico 2	Bonito – PA	WP2
Fosfato Intempérico 3	Bonito – PA	WP3
Fosfato Biogenético	Carajás – PA	BP

Os materiais de referência IPT 18B e IP são oriundos de fontes ígneas e são utilizados na formulação de fertilizantes químicos. O material de referência IPT 18B (Hama & Zucchini 2011), consiste de uma amostra proveniente de um dos maiores complexos minerais de fosfato do Brasil, onde ocorre a produção de rocha fosfática e seus processados, como ácido fosfórico e superfosfato simples.

As amostras de fosfatos de Bonito-Pará correspondem ao depósito de rochas fosfáticas de origem intempérica, as quais são empregadas na produção de fertilizante termofosfato. As três amostras extraídas deste depósito correspondem às três camadas que compõe o perfil intempérico, sendo estas: WP1 correspondente a camada da base do perfil; WP2 representante da porção intermediária; e WP3 equivalente a camada do topo do perfil.

O fosfato biogenético representa um espeleotema fosfático coletado na Serra dos Carajás-Pará, ressalta-se que esta amostra não representa um depósito fosfático empregado na indústria de fertilizantes, porém, os seus depósitos correlatos, àqueles formados em ilhas oceânicas pela deposição de excrementos de aves, são comumente utilizados na fertilização do solo.

Todas as amostras foram submetidas a pulverização em almofariz de ágata da Retsch, modelo RM 200 e homogeneizadas via pilha alongada, com exceção do material de referência IPT18B, uma vez que este já estava devidamente pulverizado e homogeneizado.

## 4.1.2 Métodos

### 4.1.2.1 Espectroscopia de Infravermelho com Transformadas de Fourier

As investigações espectroscópicas foram realizadas nas regiões do infravermelho próximo – Near-IR (11.000 – 4.000  $\text{cm}^{-1}$ ) e do infravermelho médio – Middle-IR (4.000 – 400  $\text{cm}^{-1}$ ), em um espectrômetro de infravermelho com transformadas de Fourier da Thermo Scientific, Nicolet iS50 FTIR.

Na região Near-IR utilizou-se uma fonte de luz branca com beam splitter de  $\text{CaF}_2$  e detector de PbSe; e na região Middle-IR foi utilizada uma fonte de IR com beam splitter de KBr e detector de KBr DTGS. Todas as medidas foram obtidas com 100 scans e resolução de 8  $\text{cm}^{-1}$ .

A medida na região Near-IR só permite um método de medição, por reflectância difusa (DRIFT- *Diffuse Reflectance Infrared Fourier Transform*), a qual foi empregada. Enquanto na região Middle-IR uma comparação entre os métodos de transmissão, reflectância difusa e total atenuada (ATR- *Attenuated Total Reflectance*) foi realizada.

As análises na região Near-IR foram realizadas pelo método DRIFT com uso de amostra pura e disposta de forma randômica. Para a obtenção das medidas na região Middle-IR pelo método de reflectância difusa (DRIFT), as amostras foram diluídas em uma proporção de 90% de KBr e preenchidas no porta-amostra de forma randômica. Para o método de transmissão, foram preparadas pastilhas prensadas contendo 150 mg de KBr e ~ 2 mg de amostra. No método ATR utilizou-se ~ 9 mg de amostra sem adição de KBr, empregando-se o módulo ATR iS50 com cristal de diamante.

### 4.1.2.2 Caracterização mineralógica por difratometria de raios-X

As medidas foram realizadas em um difratômetro Empyrean da Malvern PANalytical com ânodo de Co ( $K\alpha_1=1.789010 \text{ \AA}$ ), com foco fino longo de 1800W, filtro  $K\beta$  de Fe, detector de área do tipo PIXcel3D-Medpix3  $1 \times 1$  em modo de varredura com uma tensão de 40 kV e corrente de 35 mA, tamanho do passo  $0.0065652^\circ$  em  $2\theta$ , com varredura de  $2^\circ$  a  $110^\circ$ , fenda divergente  $1/4^\circ$  e anti-espalhamento  $1/2^\circ$ , máscara 15 mm e tempo/passo de 20,280s. As medidas foram realizadas empregando-se o método do pó em amostras previamente desaglomeradas e homogeneizadas, com montagem em *backlounding*. A interpretação das respostas foi realizada com o auxílio do *software* X'Pert HighScore Plus também da PANalytical, utilizando os bancos de dados PAN ICSD e PDF2.

#### 4.1.2.3 Análise química elementar por espectrometria de fluorescência de raios-X

A determinação dos elementos maiores e menores das amostras foi realizada empregando-se a técnica de fluorescência de raios-X. Foi utilizado um espectrômetro WDS sequencial, modelo *Axios Minerals* da marca PANalytical, com tubo de raios X cerâmico, ânodo de ródio (Rh) e máximo nível de potência 2,4 KW. As leituras das amostras foram realizadas em disco prensado com 1 g de amostra para 30% de cera; e os resultados foram interpretados com o auxílio do *software SuperQ Manager* também da PANalytical.

Foram realizados testes de perda ao fogo (uma técnica gravimétrica de perda de massa) para todas as amostras, utilizando 1 g de cada amostra submetidas a temperatura constante de 1000 °C por 1 hora em forno mufla.

## 4.2 PARTE II OTIMIZAÇÃO DA SÍNTESE DE ESTRUVITA

### 4.2.1 Materiais

Para a preparação da água residual sintética foram utilizadas soluções estoques contendo os íons envolvidos na síntese:  $\text{PO}_4^{3-}$ ,  $\text{NH}_4^+$ ,  $\text{Mg}^{2+}$ ,  $\text{K}^+$  e  $\text{Ca}^{2+}$ , além de uma solução de NaOH para ajuste de pH. Cada solução estoque foi obtida a partir da dissolução dos compostos (Tabela 3) em água deionizada. As concentrações das soluções foram estimadas de acordo com a perspectiva dos planejamentos experimentais utilizados no estudo (Seção 4.3).

Tabela 3– Reagentes utilizados na composição da água residual e na análise de P

Reagente	Fórmula química	Fabricante
Fosfato de Potássio Monobásico	$\text{KH}_2\text{PO}_4$	Êxodo Científica
Cloreto de Amônio	$\text{NH}_4\text{Cl}$	Neon
Cloreto de Magnésio Hexahidratado	$\text{MgCl}_2 \cdot 6\text{H}_2\text{O}$	Neon
Hidróxido de Sódio	$\text{NaOH}$	Neon
Cloreto de Potássio	$\text{KCl}$	Vetec
Cloreto de Cálcio Anidro	$\text{CaCl}_2$	Vetec

### 4.2.2 Métodos

#### 4.2.2.1 Síntese de estruvita em água residual sintética

O processo de síntese de estruvita foi realizado em um ambiente planejado sob condições favoráveis à sua precipitação em ordem estabelecida nos planejamentos experimentais (Seção 4.3). As sínteses foram realizadas no Laboratório de Análises Químicas do Instituto de Geociências da UFPA.

A princípio, houve o preparo da água residual sintética, a qual foi composta pela mistura em proporções definidas das soluções estoque de Fosfato de potássio, Cloreto de amônio, Cloreto de magnésio hexahidratado, Cloreto de potássio e Cloreto de cálcio. Desse modo, cada mistura elaborada de água residual apresentou um volume final correspondente à 2L, de maneira que os volumes adicionados de cada solução estoque foram estabelecidos de acordo com as concentrações estipuladas para os íons. A aferição do volume final foi realizada com água deionizada.

Para a realização da síntese, a água residual foi submetida à uma agitação constante com o auxílio de um agitador mecânico para fluidos de baixa densidade da marca Fisatom<sup>®</sup>, modelo 711. Durante a etapa de mistura foi realizado o ajuste do pH com a solução de NaOH 1M. Os valores de pH foram verificados com um medidor de pH de bancada da marca Simpla<sup>®</sup>, modelo PH140. Após a agitação, a solução com precipitado foi submetida ao repouso para conseguinte decantação do material. Desse modo, após a etapa de repouso, a solução foi filtrada à vácuo em funil de placa sinterizada com papel de filtro quantitativo Whatman (Ø 150 mm). O material recuperado passou por secagem em estufa à 40 °C durante 48 horas e o sobrenadante foi armazenado e refrigerado para posteriores análises. Os precipitados obtidos pela síntese, após a secagem, foram desaglomerados, homogeneizados, separados em alíquotas e encaminhados para as análises. Todo o processo de síntese está ilustrado, de maneira simplificada na Figura 5.

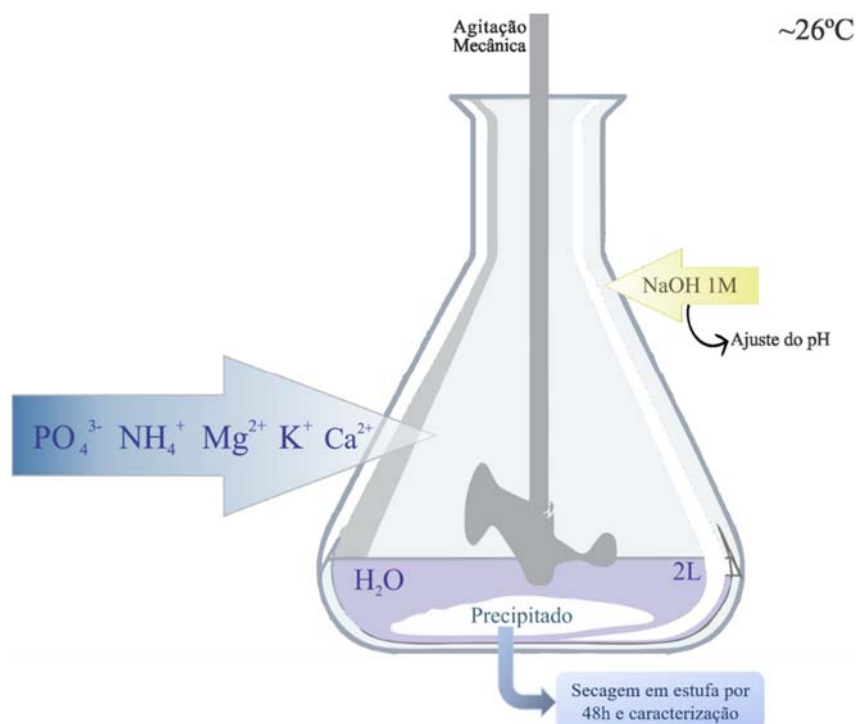


Figura 5 – Esquema simplificado da síntese de estruvita.

É importante ressaltar que variáveis do processo de síntese como a taxa e o tempo de agitação, o tempo de repouso e o pH foram condicionados pelos planejamentos de experimentos utilizados no estudo.

#### 4.2.2.2 Análises

As análises do estudo foram realizadas em diferentes laboratórios, sendo: DRX, FTIR e DSC-TG no Laboratório de Caracterização Mineral (LCM), a Determinação de P no Laboratório de Análises Químicas e DTP no laboratório de Mineralogia e Geoquímica Aplicada (LAMIGA), todos no Instituto de Geociências (IG) da Universidade Federal do Pará (UFPA); as análises de FRX e MEV foram realizadas no Laboratório de Caracterização Tecnológica (LCT) da Universidade de São Paulo (USP).

#### Determinação do fósforo recuperado

A análise do conteúdo de fósforo foi realizada nas soluções sobrenadantes coletadas após a reação de precipitação. As análises foram conduzidas seguindo o método espectrofotométrico azul de molibdênio (“4500-P Phosphorus” 2018), em um espectrofotômetro marca Varian, modelo Cary 50 Probe. Para as análises, foram utilizados 10 mL de cada solução sobrenadante em 20 mL de solução redutora de molibdato de amônio (2%), ácido sulfúrico (3M) e ácido ascórbico (0,1M).

A determinação do conteúdo de fósforo teve por objetivo a obtenção de dados para calcular a taxa de recuperação de fósforo ( $P_{rec}$ ) em cada corrida experimental dos planejamentos realizados. O cálculo da  $P_{rec}$  utilizando os dados de concentração de P foram realizados utilizando a Equação (4):

$$P_{rec} = \frac{C_{P_0} - C_{P_r}}{C_{P_0}} \times 100 \quad (4)$$

onde,  $C_{P_0}$  consiste na concentração inicial de  $PO_4$ -P da água residual sintética; e  $C_{P_r}$  é a concentração de  $PO_4$ -P da solução após a síntese.

#### Difratometria de Raios-X (DRX)

A técnica de difratometria de raios-X foi empregada visando a identificação das fases presentes nos produtos de síntese. O método seguiu as mesmas condições indicadas no item 3.1.2.2, onde foram descritas detalhadamente como as medidas foram tomadas. Um *profile fit*

foi realizado nos difratogramas para padronizar o perfil difratométrico dos produtos com estruvita.

#### Fluorescência de Raios-X (FRX)

A análise química elementar dos produtos de síntese foi realizada em um espectrômetro de fluorescência de raios-X modelo *Zetium* da Malvern PANalytical, na calibração STD-1 (*Standatless*), relativa à análise sem padrões dos elementos químicos entre o flúor e o urânio. As amostras foram preparadas sob a forma de pastilhas prensadas e os valores foram normalizados a 100%.

#### Calorimetria Exploratória Diferencial (DSC) e Termogravimetria (TG)

As medidas de DSC-TG foram realizadas em um termoanalisador NETZSCH modelo STA 449F3 Júpiter, com analisador térmico simultâneo da NETStanton Redcrof Ltda e forno cilíndrico vertical de platina. Foi utilizada uma faixa de temperatura entre 25°C e 1000°C em atmosfera de nitrogênio com fluxo de 50 mL/min. A taxa de aquecimento empregada foi de 5°C/min, tendo-se um cadinho de platina como referência. Foram utilizadas ~10 mg de amostra. As entalpias de degradação dos produtos foram medidas através do DSC com fluxo de calor. Essa técnica permite relacionar, proporcionalmente, a área de um pico com a variação de entalpia através de um fator de calibração dependente da temperatura. O fator de calibração foi determinado com as seguintes substâncias e respectivos pontos de fusão: In (156.6 °C), Sn (231.9 °C), Bi (271.4 °C), Zn (416.6 °C), Al (660.6 °C) e Au (1064.4 °C). A variação de entalpia nos picos ( $\Delta H$ ) é determinada pela Equação 5, e suas respostas são dadas em J.g<sup>-1</sup>. A técnica consiste em estabelecer a razão entre a área do pico e as mudanças na entalpia usando uma temperatura dependente do fator de calibração (Paz et al. 2016).

$$\Delta H = \pm \frac{A}{mK} = \frac{1}{mK} \int_{t_{initial}}^{t_{final}} [\text{fluxo de calor } (t) - \text{linha da base interpolada } (t)] dt \quad (5)$$

Onde:  $A$  é a área do pico,  $m$  (g) é massa da amostra, e  $K$  é uma constante empírica relativa à sensibilidade do sensor.

#### Espectroscopia de Infravermelho com Transformadas de Fourier (FTIR)

As análises de FTIR foram utilizadas para determinar os grupos funcionais presentes nas amostras estudadas a partir suas respectivas vibrações na região do infravermelho. Os dados espectrais foram obtidos na região do infravermelho médio (MIR-*middle infrared*), com fonte



de IR, *beam splitter* de KBr e detector de KBr DTGS. Todas as medidas foram realizadas sob o modo de transmissão em pastilhas de KBr (proporção: 2 mg de amostra/150 mg de KBr), e tomadas a 100 scans, com resolução espectral de  $4 \text{ cm}^{-1}$ . A aquisição e tratamento dos dados foram realizados com o auxílio do *software* OMINIC.

#### Distribuição do Tamanho de Partículas (DTP)

As análises de distribuição do tamanho de partículas foram realizadas em um granulômetro por difração a laser ANALYSETTE 22 MicroTec Plus. As amostras foram dispersas em água, com medidas tomadas a 100 scans, obscuração do feixe de 15%, com intervalo de tamanho medido entre  $0,08 - 2000,00 \mu\text{m}$ , com respostas calculadas pelo modelo de Mie.

#### Microscopia Eletrônica de Varredura (MEV)

As análises morfológicas foram realizadas a fim de identificar as estruturas e as texturas dos produtos de síntese. As micrografias foram obtidas através de um microscópio eletrônico de varredura marca Thermo Fisher Scientific, modelo Quanta 650 FEG. As análises foram tomadas utilizando elétrons retroespalhados e elétrons secundários, com voltagem de aceleração constante de 15.0 kV e distância de trabalho  $\sim 14 \text{ mm}$ .

### **4.2.3 Planejamento experimental e modelagem estatística**

Essa etapa da pesquisa foi baseada em uma metodologia de planejamento experimental sequencial. Inicialmente, um planejamento Plackett Burman foi aplicado com o objetivo de identificar e estimar os fatores significativos dentro do processo de síntese. Após serem estabelecidos os fatores que não apresentaram relativa influência, esses foram fixados e um novo planejamento de segunda ordem com matriz de Doehlert foi realizado a fim de se determinar os pontos ótimos dos fatores realmente significativos a partir de modelos de regressão utilizando metodologia de superfície de respostas (RSM) e função desejabilidade.

Todos os experimentos foram realizados de forma randomizada e seguidos pela determinação de resíduos ajustados (obedecendo aos pressupostos de independência, aleatoriedade, homocedasticidade e normalidade) e testes ANOVA com intervalo de confiança de 95%. A análise estatística dos dados foi realizada com o programa Statistica®.

### 3.2.3.1 Planejamento Plackett Burman

O planejamento experimental Plackett Burman, foi utilizado a fim de estabelecer a triagem dos fatores estudados neste processo de síntese. O planejamento consistiu em um PB-12 com 8 fatores independentes testados em dois níveis, resultando em 12 corridas experimentais. A matriz de experimentos do planejamento é mostrada na Tabela 4 com variáveis codificadas.

Tabela 4-Planejamento PB-12 com fatores codificados

Experimento*	Fatores Codificados								Resposta
	X <sub>1</sub>	X <sub>2</sub>	X <sub>3</sub>	X <sub>4</sub>	X <sub>5</sub>	X <sub>6</sub>	X <sub>7</sub>	X <sub>8</sub>	P <sub>rec</sub> (%)
1 <sup>(6)</sup>	1	-1	1	-1	-1	-1	1	1	
2 <sup>(1)</sup>	1	1	-1	1	-1	-1	-1	1	
3 <sup>(4)</sup>	-1	1	1	-1	1	-1	-1	-1	
4 <sup>(12)</sup>	1	-1	1	1	-1	1	-1	-1	
5 <sup>(10)</sup>	1	1	-1	1	1	-1	1	-1	
6 <sup>(3)</sup>	1	1	1	-1	1	1	-1	1	
7 <sup>(7)</sup>	-1	1	1	1	-1	1	1	-1	
8 <sup>(11)</sup>	-1	-1	1	1	1	-1	1	1	
9 <sup>(9)</sup>	-1	-1	-1	1	1	1	-1	1	
10 <sup>(5)</sup>	1	-1	-1	-1	1	1	1	-1	
11 <sup>(2)</sup>	-1	1	-1	-1	-1	1	1	1	
12 <sup>(8)</sup>	-1	-1	-1	-1	-1	-1	-1	-1	

\* Ordem dos experimentos

Os fatores avaliados, bem como as faixas consideradas nesse planejamento foram selecionadas a partir de dados de processo reportados por diversos autores. A escolha dos fatores foi pautada no arcabouço teórico e metodológico que destacaram importantes aspectos físico-químicos para o processo de síntese de estruvita. Os fatores de processo foram: concentração inicial de fósforo, pH da água residual sintética, razões molares iniciais NH<sub>4</sub>/PO<sub>4</sub>, Mg/PO<sub>4</sub> e K/PO<sub>4</sub>, presença de Ca, tempo e a taxa de agitação. As descrições dessas variáveis e os seus respectivos valores são mostrados na Tabela 5.

A triagem dos fatores através do planejamento PB-12 foi estabelecida a partir da taxa de recuperação de fósforo – P<sub>rec</sub> (%) – que foi considerada como a resposta do planejamento em conjunto com a análise qualitativa das fases formadas nos produtos de síntese. A análise das fases por DRX avaliou a formação de estruvita como resposta positiva em detrimento da formação de outras fases ou a não formação de material cristalino.

Tabela 5-Fatores e níveis do planejamento PB-12

Fatores codificados	Fatores originais	Níveis	
		-1	1
X <sub>1</sub>	Concentração de fósforo (mg/L)	78	310
X <sub>2</sub>	pH	9	11
X <sub>3</sub>	N:P	1	3
X <sub>4</sub>	Mg:P	1	2,5
X <sub>5</sub>	K:P	1	2
X <sub>6</sub>	Presença de Ca (mg/L)	0	100
X <sub>7</sub>	Tempo total (Min)	15	50
X <sub>8</sub>	Taxa de agitação (RPM)	100	300

### 3.2.3.2 Planejamento Matriz de Doehlert

Para se determinar os pontos ótimos de síntese foi necessário a aplicação de um planejamento experimental de segunda ordem. Desse modo, levando-se em consideração os fatores significativos observados através do PB-12 juntamente com a determinação da região experimental, um planejamento em Matriz de Doehlert para três fatores foi implementado. Os fatores estudados foram: pH ( $X_1$ ), razão N/P ( $X_2$ ) e a concentração inicial de fósforo ( $X_3$ ). A Tabela 6 mostra o planejamento completo com os fatores codificados e reais. Portanto, foram realizadas 15 corridas experimentais, considerando os três fatores independentes e três repetições no ponto central. Duas respostas foram utilizadas nesse planejamento: a taxa de recuperação de fósforo –  $P_{rec}$  (%) e a entalpia do pico endotérmico de decomposição da estruvita -  $\Delta H$  ( $J.g^{-1}$ ) com metodologia adaptada de Meira (2020).

Os fatores codificados foram transformados nas variáveis reais de acordo com a Equação 6.

$$X_i = \left( \frac{U_i - \bar{U}_i}{\Delta U_i} \right) \times \alpha \quad (6)$$

Onde  $X_i$  é o valor codificado do fator;  $U_i$  é o valor real do fator;  $\bar{U}_i$  é o valor do ponto central dentro da faixa experimental;  $\Delta U_i$  é a faixa de variação do fator  $i$  e  $\alpha$  é o limite de valor codificado para cada valor.

O método de síntese de estruvita foi otimizado segundo:

- (a) Análise dos efeitos principais e interações dos fatores de acordo com as respostas experimentais do planejamento em Matriz de Doehlert;
- (b) Regressão linear por mínimos quadrados para os fatores com efeitos significativos e geração de modelos estatísticos de predição;
- (c) Aplicação da função desejabilidade para a otimização simultânea.

Tabela 6-Matriz de Doehlert para o experimento com fatores codificados e valores experimentais

Run*	Valores experimentais			Fatores Codificados			Respostas	
	pH	N/P	P (mg/L)	X <sub>1</sub>	X <sub>2</sub>	X <sub>3</sub>	P-Rec (%)	$\Delta H$ (J.g <sup>-1</sup> )
1 <sup>(4)</sup>	11	2,5	155	1	0	0		
2 <sup>(2)</sup>	10,5	4	155	0,5	0,866	0		
3 <sup>(9)</sup>	10,5	3	250	0,5	0,289	0,817		
4 <sup>(5)</sup>	9	2,5	155	-1	0	0		
5 <sup>(8)</sup>	9,5	1	155	-0,5	-0,866	0		
6 <sup>(10)</sup>	9,5	2	60	-0,5	-0,289	-0,817		
7 <sup>(7)</sup>	10,5	1	155	0,5	-0,866	0		
8 <sup>(12)</sup>	10,5	2	60	0,5	-0,289	-0,817		
9 <sup>(11)</sup>	9,5	4	155	-0,5	0,866	0		
10 <sup>(15)</sup>	10	3,5	60	0	0,577	-0,817		
11 <sup>(3)</sup>	9,5	3	250	-0,5	0,289	0,817		
12 <sup>(1)</sup>	10	1,5	250	0	-0,577	0,817		
13 <sup>(6)</sup>	10	2,5	155	0	0	0		
14 <sup>(14)</sup>	10	2,5	155	0	0	0		
15 <sup>(13)</sup>	10	2,5	155	0	0	0		

\*Ordem dos experimentos

Os demais fatores utilizados na síntese e que não foram significativas na etapa de triagem tiveram seus valores fixados para todos os experimentos nesta segunda fase do estudo. Desse modo, a razão Mg/P foi fixada em 1 e a K/P foi igual a 2, o tempo de síntese foi fixado em 35 minutos e a agitação em 200 rpm e não houve a adição de Ca.

## 5 RESULTADOS E DISCUSSÃO

### 5.1 ARTIGO 01

Spectrochimica Acta Part A: Molecular and Biomolecular Spectroscopy 251 (2021) 119476



Contents lists available at ScienceDirect

## Spectrochimica Acta Part A: Molecular and Biomolecular Spectroscopy

journal homepage: [www.elsevier.com/locate/saa](http://www.elsevier.com/locate/saa)



## FTIR spectral signatures of amazon inorganic phosphates: Igneous, weathering, and biogenetic origin



P.V. Campos<sup>a,\*</sup>, A.R.L. Albuquerque<sup>a</sup>, R.S. Angélica<sup>a</sup>, S.P.A. Paz<sup>a,b</sup>

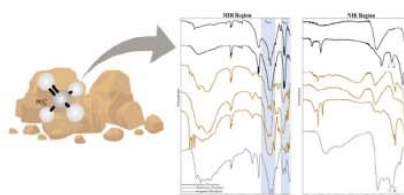
<sup>a</sup> Programa de Pós-Graduação em Geologia e Geoquímica, Universidade Federal do Pará, Belém, PA 66075-110, Brazil

<sup>b</sup> Programa de Pós-Graduação em Engenharia de Recursos Naturais da Amazônia, Universidade Federal do Pará, Belém, PA 66075-110, Brazil

### HIGHLIGHTS

- Amazonian inorganic phosphates from different geological origins were investigated.
- Spectral FTIR information about phosphates are listed in a database.
- Differentiation of phosphate genesis according to spectral patterns.
- Practicality in the interpretation of analytical data in the phosphate industry.

### GRAPHICAL ABSTRACT



### ARTICLE INFO

#### Article history:

Received 22 October 2020

Received in revised form 9 January 2021

Accepted 10 January 2021

Available online 18 January 2021

#### Keywords:

Amazonian phosphates

Database

FTIR

Genetic differentiation

### ABSTRACT

The characterization of phosphates is generally hampered by the variability of their sources, the complexity of the mineralogical assemblies and/or the thermochemical transformations undergone. Fourier transform infrared (FTIR) spectroscopy can characterize and differentiate phosphates in a practical and efficient way. In this sense, in order to differentiate phosphates from different Amazonian deposits and establish a spectral database, initially small because it is starting, six samples of phosphate rocks were analyzed by FTIR spectroscopy in the near-IR and middle-IR regions using the transmittance, attenuated reflectance, and diffuse reflectance methods. X-ray diffraction and X-ray fluorescence spectroscopy were also used as complementary analyses. The IR results revealed that the transmittance and diffuse reflectance methods are the most suitable for the analysis of phosphate materials, and they should be used together whenever possible. The identification of the  $\text{PO}_4$  bands, as well as of the  $(\text{CO}_3)^{2-}$ ,  $\text{Al}_2\text{OH}$ , and  $\text{NH}_4$  bands, allowed the differentiation of the phosphate materials according to their geological source and the establishment of a database of the studied materials by both the transmittance and diffuse reflectance methods.

© 2021 Elsevier B.V. All rights reserved.

### 1. Introduction

The chemical element phosphorus is distributed in the Earth's crust in the ionic form of orthophosphate ( $\text{PO}_4^{3-}$ ), as well as in variations such as acid orthophosphate anions ( $\text{HPO}_4^{2-}$  and  $\text{H}_2\text{PO}_4^-$ ), which commonly exist in the form of phosphate minerals, among which the following stand out: apatite,  $\text{Ca}_5(\text{PO}_4)_3(\text{F},\text{OH},\text{Cl})$ ; lazulite,

$(\text{Mg},\text{Fe})\text{Al}_2(\text{PO}_4)_2(\text{OH})_2$ ; and monazite,  $(\text{Ce},\text{La},\text{Nd},\text{Th})\text{PO}_4$  [1–3]. Phosphorus is simply the element responsible for the production of chemical energy in plant development (growth, flowering, and fruit production) and therefore it is indispensably required in the cultivation of agricultural and forest soils [3]. Its ionic expression form of orthophosphate is also referred to as inorganic phosphate, which is commonly expressed in the results of chemical analyses in the form of phosphorus pentoxide ( $\text{P}_2\text{O}_5$ ) [2]. While, organic phosphate is phosphate in monoester or diester form (C-O-P bonds) existing in the molecules of adenosine triphosphate (ATP),

\* Corresponding author.

E-mail address: [pvcamps97@gmail.com](mailto:pvcamps97@gmail.com) (P.V. Campos).

DNA, and RNA, and in the form of organic polyphosphates and phosphonates [4–6].

Plants use inorganic phosphate to produce organic compounds necessary for life. The cycle begins with the leaching of the phosphate mineral and the release of the  $(\text{PO}_4^{3-})$  anion into the soil, which is absorbed by plant roots and transported to cells, which use it to store and transport energy in the form of ATP; thereafter, phosphorus is incorporated into the consumer trophic chain. Phosphorus is returned to the soil through droppings and the death of food chain components. That is, since phosphorus makes up biomass, with the death of plants and animals this element returns to the soil through the action of decomposers, which use biomass as food [7]. In the soil, organic phosphorus can be adsorbed, precipitated, and/or remineralized; thus, phosphorus moves in a cycle [5,7–9].

During rock weathering in the surface environment, some phosphorus leaches out of the system in the water leaving the soil surface or percolating to the water table [10]. Once it reaches a water body, it is incorporated into the aquatic trophic chain or accumulates in bottom sediments, where it cannot be used until the trophic chain can reincorporate it and start a new cycle [8,9]. From the orthophosphate flow that circulates with the movement of water, new conformations are generated through ionic combinations [10,11]. These associations occur in the form of minerals (more than 460 species), which in turn make up rocks [11].

Phosphate rocks are formed in different geological environments and may be of igneous, sedimentary, metamorphic, biogenetic, or weathering origin [2,12]. Sedimentary phosphate deposits correspond to approximately 75% of all mineral resources, and the sum of igneous, metamorphic and weathering deposits corresponds to ~ 22%, while deposits of biogenetic origin (guanos), which are derived from the interaction of rocks with bird and bat droppings, correspond to approximately 3% of phosphate sources [12,13]. Minerals of the apatite group are predominant phosphates both in igneous and sedimentary phosphate rocks. The apatite  $\text{Ca}_5(\text{F,Cl,OH})(\text{PO}_4)_3$  is essentially a calcium phosphate that has isomorphic transformations according to its environment of origin, and can commonly be called fluorapatite, chlorapatite, or hydroxypapatite, depending on the ionic concentrations of the  $\text{F}^-$ ,  $\text{Cl}^-$ , and  $\text{OH}^-$  ions.  $\text{Ca}^{2+}$  can also be replaced by other bivalent cations, and the  $(\text{PO}_4)^{3-}$  radical can be partially replaced by other anions, thus forming other minerals of the apatite group [11,14]. In deposits of sedimentary origin, apatite crystals usually occur associated with calcite, dolomite, clay minerals, and iron oxyhydroxides, such as goethite and hematite. In these deposits, the carbonate-apatite  $\text{Ca}_5(\text{PO}_4, \text{CO}_3)_3(\text{OH,F})$  and francolite or carbonate-fluorapatite  $\text{Ca}_5(\text{PO}_4, \text{CO}_3)_3(\text{F,OH})$  varieties predominate and are usually found in cryptocrystalline masses called colophane [14]. Another cryptocrystalline mass of calcium phosphate from sedimentary processes is phosphorite, which consists of an amorphous variation of apatite and has deposits with high phosphorus concentrations [11,14].

Phosphate deposits are classified as iron-aluminum phosphate (Fe-Al-P), calcium-iron-aluminum phosphate (Ca-Fe-Al-P), and calcium phosphates (Ca-P). These three classes constitute a natural weathering sequence of phosphate rock deposits, in which the calcium phosphate represents the matrix rock and stable forms of iron-aluminum phosphates such as crandallite  $\text{CaAl}_3(\text{PO}_4)_2(\text{OH})_5 \cdot \text{H}_2\text{O}$  and vivianite  $\text{Fe}_3(\text{PO}_4)_3 \cdot 8\text{H}_2\text{O}$  represent the most advanced weathering stage [13].

Faced with a chemical characterization of phosphate materials, the instrumental analytical technique known as infrared (IR) spectroscopy has become indispensable. However, solid databases that gather spectroscopic data about agricultural phosphates are of limited worth, as these data exist in a dispersed and, in most cases,

nonuniform manner. IR spectroscopy is a technique that can generate spectral graphical responses that relate the vibrational wavenumber and the absorbance of IR radiation from the interaction of electromagnetic IR radiation with matter [15]. Due to its simplicity, speed, and relatively low cost, this technique has become one of the most important in the characterization of materials, becoming widely spread in the identification and quantification of organic compounds and, less commonly, in inorganic materials [16–18]. Fourier transform infrared (FTIR) spectrometers were introduced in the 1970 s and replaced instruments with dispersive IR systems. This led to a large increase in the sensitivity and resolution of spectra, as well as a reduction in analysis time [19]. As FTIR spectrometers advanced, measurements performed under the transmission (TRM) method improved with the emergence of reflectance analysis methods [20]. Thus, different IR analytical methods came into existence, which are chosen according to the nature and state of the sample, as well as the spectral region of interest [21].

Transmission analyses are characterized by using small amounts of samples diluted in KBr pellets, which commonly require adequate preparation [22]. Measurements by diffuse reflectance (diffuse reflectance infrared Fourier transform, DRIFT) and attenuated reflectance (attenuated total reflectance, ATR) are well known for their practicality and for their low interference originating from sample preparation. However, some limitations associated with instrumentation can be observed in these modes of analysis, such as destabilizations relevant to the signal/noise ratio generated by attenuated total reflectance and interference effects (Restrahlens effects) related to the particle size and to the IR wavelength in the diffuse reflectance method [17,22,23].

One of the main characteristics of IR spectroscopy is the identification of organic and inorganic chemical compounds, which makes it a widely used tool in the differentiation of mineral species with similar internal structures (isomorphic minerals) and, consequently, similar analytical standards. This is observed in some isomorphic minerals of the phosphate group, whose identification and differentiation by X-ray diffraction is hampered because they have the same diffractometric pattern [24,25].

In recent years, even with its increase in phosphate production for agribusiness, Brazil remains a major global importer of fertilizers. Regional prospecting studies were conducted throughout the territory by the Brazilian Geological Survey to delimit areas with potential for phosphate exploitation and thus reducing Brazil's dependence on importing this mineral input [26]. In such prospective studies, chemical analyses of P and other chemical elements remain the main mineral exploration tool, combined with other mineralogical characterization techniques, especially X-ray diffraction. There is no information available on the use of IR spectroscopy as an auxiliary analytical technique in mineral prospecting projects of this nature.

In this context, different phosphates from the Amazon region were investigated in comparison with a reference phosphate material, with the objective of contributing to the establishment of an IR spectral database for phosphates, initially small because it is starting (six samples). The absorption bands corresponding to the phosphate bonds were evaluated, as were their variations according to the analysis methods (transmission, diffuse reflectance, and attenuated reflectance) and the near-IR (NIR) and middle-IR (MIR) spectral regions.

## 2. Materials and methods

### 2.1. Materials

Six samples of phosphate rocks were used in this study, whose origin and nomenclature are shown in Table 1.

The reference material IPT 18B and the sample IP are from igneous sources and used in the formulation of chemical fertilizers. The IPT 18B reference material [27] corresponds to a sample from one of the largest phosphate mineral complexes in Brazil, known as the Jacupiranga alkaline complex, located in the southeastern part of São Paulo state, where phosphate rock and its processed products, as phosphoric acid and simple superphosphate, are produced. The Jacupiranga complex consists of alkaline and ultrabasic rocks with associated carbonatite manifestations, which constitute a phosphate deposit of magmatic affiliation. The sample IP was obtained from São Félix do Xingú, a region located in center-south of Pará state, in the context of the Central Amazon Province of the Amazonian Craton. The IP sample is associated with carbonatite rocks intruded in sedimentary vulcan sequences of the Iriri group. This phosphate is still undergoing prospecting studies for mining.

The phosphate samples from Bonito, northeast of Pará state, correspond to the deposition of phosphate rocks of weathering origin, which are used in the production of thermophosphate fertilizer. The three samples extracted from this deposit correspond to the three layers that make up the weathering profile, namely, WP1, corresponding to the profile base layer; WP2, representative of the intermediate portion; and WP3, equivalent to the top layer of the profile. This phosphate deposit corresponds to a mature and complete lateritic profile formed, possibly, from sedimentary rocks enriched with primary phosphorus from the Parnaíba Basin [28].

The biogenic phosphate (BP) represents a phosphate speleothem collected in Serra dos Carajás, Southeast of Pará State. This material was formed by the interaction of products from the bat decomposition with the iron caves host rocks, such as lateritic crusts and jaspilite saprolites [24]. This sample does not represent a phosphate deposit used in the fertilizer industry, but its related deposits, which are formed in oceanic islands by the deposition of bird droppings, are commonly used in soil fertilization.

All samples were pulverized in a Retsch RM 200 agate mortar and homogenized using the elongated pile method, except for the two samples IPT18B and IP, as they were already properly pulverized and homogenized.

## 2.2. Methods

The spectroscopic investigations were performed in the NIR (11,000–4,000  $\text{cm}^{-1}$ ) and MIR (4,000–400  $\text{cm}^{-1}$ ) regions in a Nicolet iS50 FTIR spectrometer from Thermo Scientific. In the NIR region, a white light source, a  $\text{CaF}_2$  beam splitter, and a PbSe detector were used. In the MIR region, an IR source, KBr beam splitter, and KBr DTGS detector were used. All measurements were obtained with 100 scans at 8  $\text{cm}^{-1}$  resolution. Only one measurement method can be used in the NIR region, diffuse reflectance (DRIFT), which was used. In the MIR region, the Transmission, DRIFT, and ATR methods were compared.

The analyses in the NIR region were performed by the DRIFT method using a pure sample randomly arranged. To obtain the measurements in the MIR region by the DRIFT method, the samples

were mixed with KBr in a 10% sample/90% KBr weight ratio and randomly filled into the sample holder. For the Transmission method, pressed tablets containing 150 mg of KBr and ~ 2 mg of sample were prepared. In the ATR method, ~9 mg of sample was used without the addition of KBr, using the built-in diamond ATR module (iS50 ATR).

For the complementary mineralogical and chemical analyses, the following techniques were used:

**X-ray diffractometry** was performed with a Malvern PANalytical Empyrean diffractometer with a Co anode ( $K\alpha_1 = 1.790 \text{ \AA}$ ), Fe K $\beta$  filter, 40 kV voltage, 35 mA current, step size of 0.0065652° in 2 $\theta$ , scanning from 3° to 111°, 1/4° divergent slit, 1/2° anti-scattering slit, 15-mm mask, and time/step of 20.280 s.

**X-ray fluorescence spectrometry (XRF)** using an Axios Minerals WDS sequential spectrometer from Malvern PANalytical, with a Rh anode and power of 2.4 KW. The measurements were performed in tablets pressed with 1 g of sample, with a final concentration of 30% wax. To obtain the loss on ignition (LOI) values, 1 g of each sample was calcined in a muffle furnace at 1000 °C for 1 h.

All the above analyses were performed in triplicate.

## 3. Results and discussion

### 3.1. Chemical and mineralogical composition

#### 3.1.1. Igneous phosphates

The igneous phosphates (IP and IPT 18B), although from different regions, had similar chemical and mineralogical compositions (Table 2 and Fig. 1). Both samples consisted predominantly of P and Ca. In the IP sample, these constituents were essentially related to apatite, while in the IPT 18B sample, in addition to apatite, there were carbonates, calcite ( $\text{Ca}(\text{CO}_3)$ ), and dolomite ( $\text{CaMg}(\text{CO}_3)_2$ ), conferring an increase in the LOI percentage over the sample without carbonates (IP).

LOI values also refer to the hydroxyl constituents of the hydroxyapatite variety that are present together with fluoroapatite, which is corroborated by the levels of F in the samples. According to the diffractometric pattern, the apatite group crystallizes in the hexagonal system and is found in the spatial group P 6 $_3$ /m. The apatite group is a rare example of a mineral group with solid anion solutions, which, depending on the predominance of fluorine, chlorine, or hydroxyl, can be established as fluorapatite, chlorapatite, or hydroxyapatite, respectively [29].

The IPT 18B sample also contained mica ( $\text{K}(\text{Mg,Fe})_3(\text{OH})_2\text{AlSi}_3\text{O}_{10}$ ) and although its basal plane (001) showed high intensity, the low Si and Al levels (Table 2) indicated low concentrations of this mineral. The marked intensity of the (001) plane was attributed to the preferential orientation effect.

#### 3.1.2. Weathering phosphates

The samples of weathering origin also had similar chemical (Table 3) and mineralogical compositions (Fig. 2), even though they were from different layers of the same deposit. These samples consisted mostly of aluminum phosphate minerals, thus conferring high levels of P and Al.

These aluminum phosphates occurred in the form of crandallite-goyazite, woodhouseite-svanbergite, and wardite ( $\text{NaAl}_3(\text{PO}_4)_2(\text{OH})_4 \cdot 2\text{H}_2\text{O}$ ), the latter being present only in sample WP3 (Fig. 2). Similar to the apatite group, these minerals represent solid solutions with a high capacity for complete ion exchange, with Ca distributed in the crandallite ( $\text{CaAl}_3(\text{PO}_4)_2(\text{OH})_5 \cdot \text{H}_2\text{O}$ ) and woodhouseite ( $\text{CaAl}_3(\text{PO}_4)(\text{SO}_4)(\text{OH})_6$ ) phases and Sr present in the goyazite ( $\text{SrAl}_3(\text{PO}_4)(\text{PO}_3\text{OH})(\text{OH})_6$ ) and svanbergite ( $\text{SrAl}_3(\text{PO}_4)(\text{SO}_4)(\text{OH})_6$ ) structures [28,30–32].

**Table 1**  
Phosphate samples and their origins.

Sample name	Origin	Code
Standard IPT 18B	Jacupiranga, São Paulo	IPT 18B
Igneous Phosphate	São Félix do Xingú, Pará	IP
Weathering Phosphate 1	Bonito, Pará	WP1
Weathering Phosphate 2	Bonito, Pará	WP2
Weathering Phosphate 3	Bonito, Pará	WP3
Biogenetic Phosphate	Carajás, Pará	BP

**Table 2**  
Chemical composition of igneous phosphates obtained by XRF.

Samples	Constituent (%)											LOI
	P <sub>2</sub> O <sub>5</sub>	CaO	F	Fe <sub>2</sub> O <sub>3</sub>	SiO <sub>2</sub>	Al <sub>2</sub> O <sub>3</sub>	MgO	SrO	K <sub>2</sub> O	Na <sub>2</sub> O	MnO	
IP	36.8	56	2.8	0.9	0.5	0.8	< 0.1	–	< 0.1	–	0.1	2.0
IPT 18B	32.4	55.4	0.9	0.3	1.6	0.6	2.1	0.6	0.3	0.1	< 0.1	5.6

LOI: loss on ignition at 1000 °C; <0.1: elements below the limit of quantification; -: undetected elements.

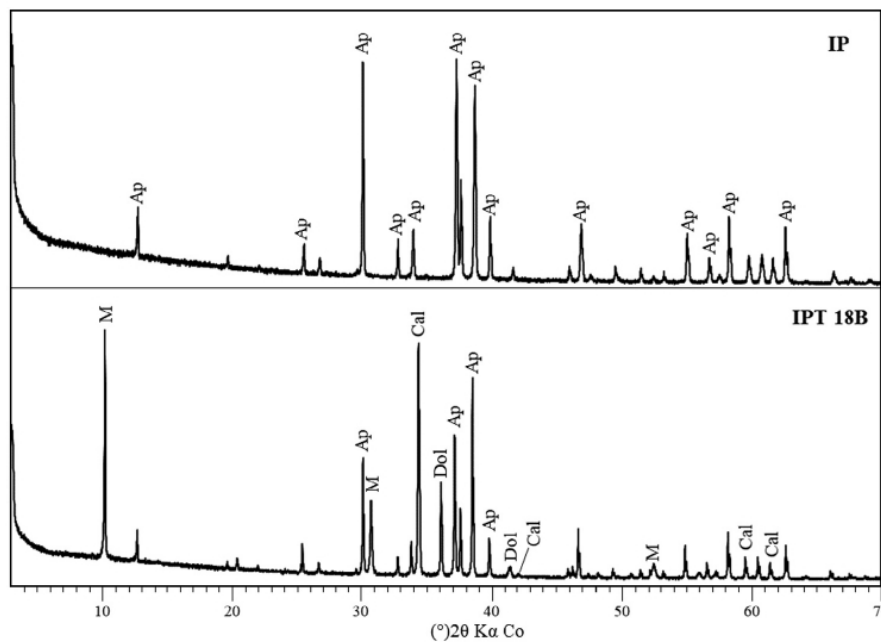


**Fig. 1.** Mineralogical composition of igneous phosphates (Ap: apatite; Cal: calcite; Dol: dolomite; M: mica).

**Table 3**  
Chemical composition of weathering phosphates obtained by XRF.

Samples	Constituent (%)										LOI
	P <sub>2</sub> O <sub>5</sub>	Al <sub>2</sub> O <sub>3</sub>	SiO <sub>2</sub>	CaO	SrO	Fe <sub>2</sub> O <sub>3</sub>	TiO <sub>2</sub>	SO <sub>3</sub>	Na <sub>2</sub> O	K <sub>2</sub> O	
WP1	16.9	22.8	23.9	5.2	3.6	9.0	1.5	1.9	0.2	–	14.6
WP2	24.5	28.9	4.4	8.3	6.7	3.5	2.8	3.2	0.1	–	17.4
WP3	13.5	33.5	30.4	1.4	1.3	2.3	0.7	0.4	1.8	0.2	14.6

(LOI) loss on ignition at 1000 °C; (–) undetected elements.

In this deposit, crandallite-goyazite was the main phosphorus mineral, followed by the woodhouseite-svanbergite phases. These minerals were more highly concentrated in sample WP2, thus representing the main mining ore raw material for the production of thermophosphate fertilizer [28]. These minerals are known as minerals APS (aluminum-phosphate-sulfate), and belong to the solid solution alunite-jarosite, which in turn are established in the crust through different environmental conditions, mainly from weathering [33]. According Costa et al., (2016) [28], among the APS minerals there is the alunite supergroup, where crandallite and woodhouseite groups are embedded, so that the crandallite group together with its crandallite-goyazite solid solution present the most common minerals, mainly in lateritic formations.

In the WP3 sample, along with aluminum phosphate minerals, kaolinite and quartz were present, which conferred an enrichment of Si and, to a lesser degree, of Al. The weathering phosphates also had as accessory minerals anatase on all samples and muscovite mica only at the WP3 sample, as determined by the presence of

Ti and K in the chemical analyses (Table 3) and by the low-intensity peaks in the X-ray diffractograms (Fig. 2).

### 3.1.3. Biogenic phosphate

BP, described by Albuquerque et al., (2018) [24] as a phosphate speleothem formed in iron caves in the Carajás region of Pará, has high P and Fe levels (Table 4) and is directly related to the presence of iron phosphate minerals. These compounds occur predominantly in the form of spheniscidite (Fe<sub>2</sub>(NH<sub>4</sub>)(OH)(PO<sub>4</sub>)<sub>2</sub>(H<sub>2</sub>O)<sub>2</sub>) as well as strengite (FePO<sub>4</sub>·2H<sub>2</sub>O) (Fig. 3). In addition to these minerals, biogenic phosphate has quartz crystals as an accessory phase. Spheniscidite and strengite result from the interaction of iron rocks with the phosphate product of the biogenetic alteration of bat droppings (guano) [24].



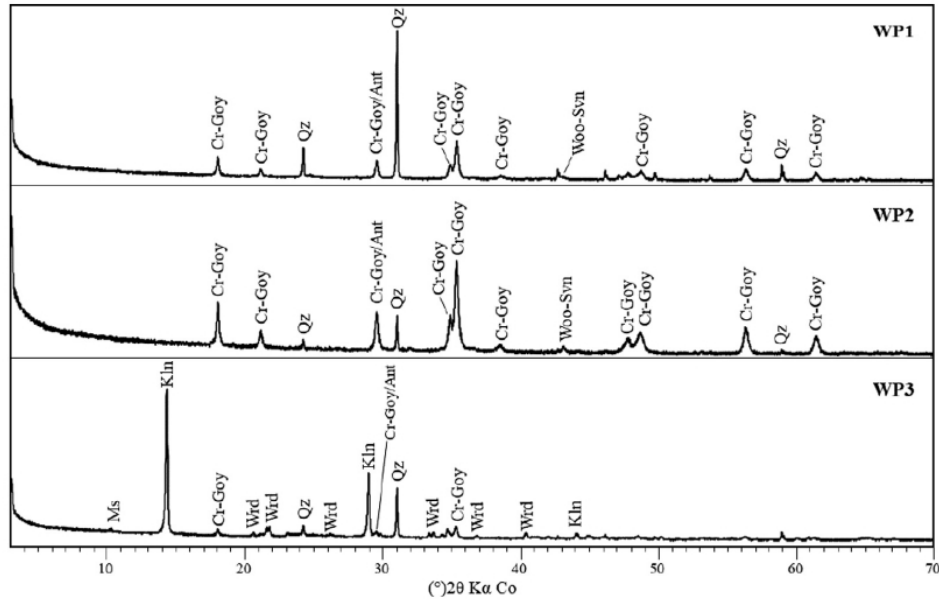


**Fig. 2.** Mineralogical composition of weathering phosphates (Cr-Goy: crandallite-goyazite; Woo-Svn: woodhouseite-svanbergite; Wrđ: wardite; Qz: quartz; Kln: kaolinite; Ant: anatase; Ms: muscovite).

**Table 4**  
Chemical composition of biogenetic phosphate obtained by XRF.

Sample	Constituent (%)								
	P <sub>2</sub> O <sub>5</sub>	Fe <sub>2</sub> O <sub>3</sub>	SiO <sub>2</sub>	K <sub>2</sub> O	Al <sub>2</sub> O <sub>3</sub>	MgO	ZnO	TiO <sub>2</sub>	LOI
BP	33.5	44.4	0.8	1.0	0.4	0.2	0.2	0.1	19.0

(LOI) loss on ignition at 1000 °C.

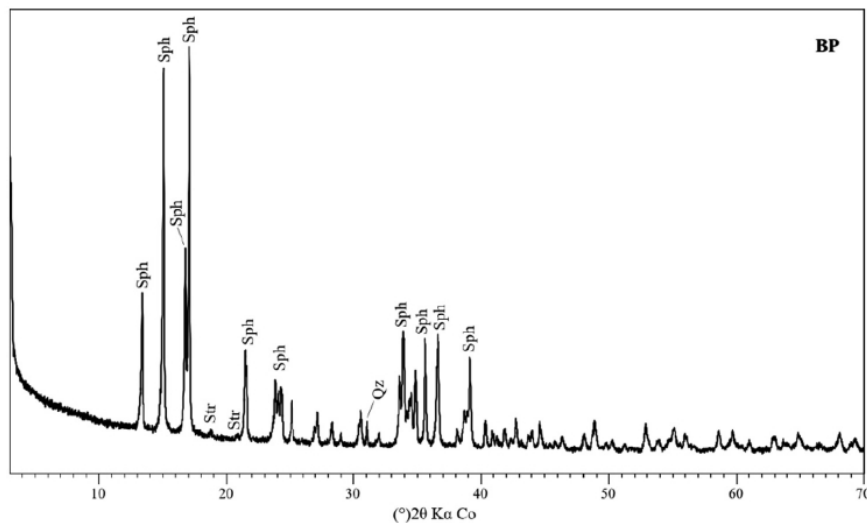


**Fig. 3.** Mineralogical composition of biogenetic phosphate (Sph: spheniscidite; Str: strengite; Qz: quartz).

### 3.2. FTIR

The sets of spectra for the MIR region, obtained using the Transmission, ATR, and DRIFT methods, as well as the spectral responses in the NIR region obtained by DRIFT, are presented in the following sections according to the method of analysis and their genetic sources.

#### 3.2.1. MIR region

**3.2.1.1. Comparison between analysis methods.** The comparison of the methods used in the analyses in the MIR region of phosphates of different origins is shown in Fig. 4. This comparison allowed us to select the most appropriate technique for each material.

The spectra obtained by the ATR method showed the greatest differences in both the intensity and the position of the bands. In

the spectral region below  $1500\text{ cm}^{-1}$ , slight band displacements and suppressions were observed, while in the region between  $3700$  and  $3100\text{ cm}^{-1}$ , there was attenuation of the absorption bands attributed to the presence of OH and  $\text{H}_2\text{O}$ .

The Transmission and DRIFT analyses showed the greatest similarities, with more intense absorption bands and better resolution. In these two methods, the bands of the water molecules were also

accentuated, probably due to the absorption promoted by the use of KBr (Fig. 4).

Thus, given the suppression and attenuation of the absorption bands observed with the ATR method, the identification of the functional groups of the phosphate samples was based here on the spectra obtained either by the Transmission or by the DRIFT method.

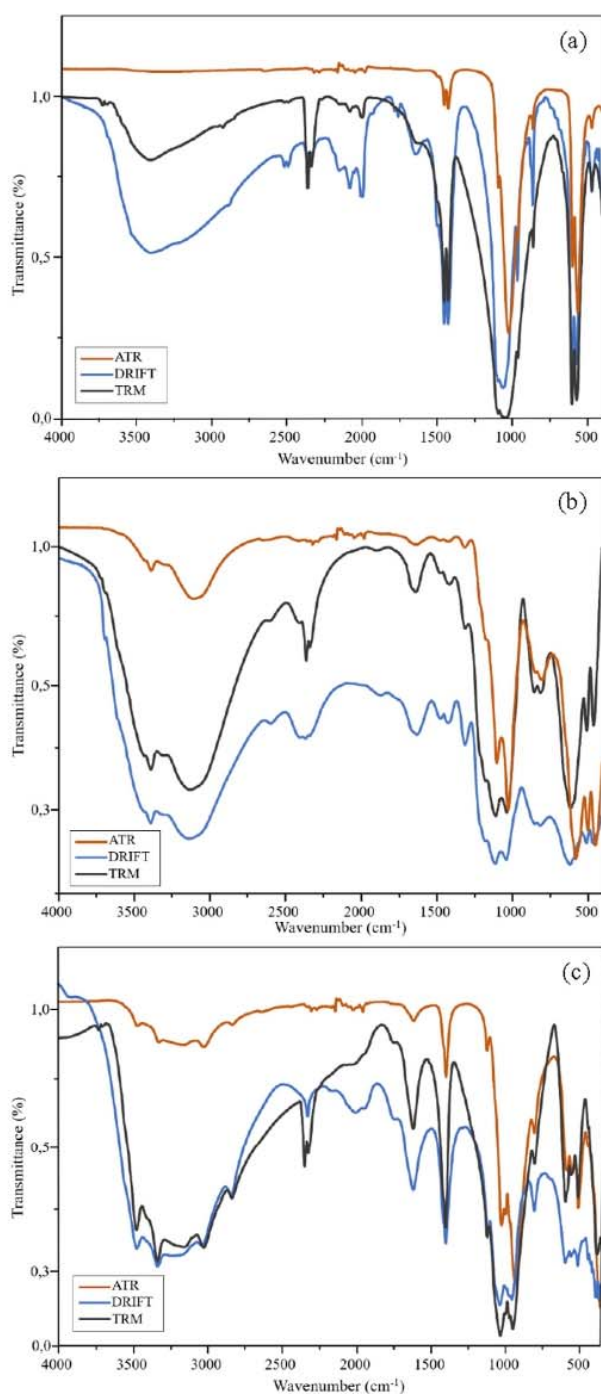


Fig. 4. Infrared spectra of (a) IP, (b) WP2, and (c) BP obtained by ATR, DRIFT, and TRM.

3.2.1.2. *Structural dynamics of phosphates.* All IR spectra of the phosphate materials showed bands assigned to phosphate ion ( $\text{PO}_4^{3-}$ ), characteristically identified between the  $1200\text{--}984\text{ cm}^{-1}$  and  $634\text{--}450\text{ cm}^{-1}$  regions [25,34–50]. A more detailed interpretation of the spectra according to the analytical method is shown in the supplementary material. It is important to note that ( $\text{PO}_4^{3-}$ ) ions usually have two types of vibrations induced by IR radiation: bending deformational vibrations of the O–P–O fragment ( $\delta$ ) and asymmetric stretching vibrations of the P–O bond ( $\nu_{as}$ ). For solid materials, vibrations that are theoretically IR-inactive can also be visualized in the generated spectra [25]. Thus, bending and stretching vibrations were also observed both in the symmetric and asymmetric modes in the spectra obtained for the studied phosphate materials.

The IR spectra obtained for the igneous phosphate samples (Fig. 5) showed absorption bands in the spectral range from  $1182$  to  $1005\text{ cm}^{-1}$ , which were mostly attributed to the asymmetric stretching vibrations of the P–O bond. The bands observed in the  $634\text{--}539\text{ cm}^{-1}$  and  $516\text{--}451\text{ cm}^{-1}$  regions were related to the deformation vibrations in the plane of the O–P–O bond, which were symmetric deformation in the first region and asymmetric deformation in the second.

In addition to the absorption bands corresponding to the  $\text{PO}_4$  functional group in the igneous phosphates (Fig. 5), a set of bands attributed to the carbonate ion ( $\text{CO}_3^{2-}$ ) was present in the  $1458\text{--}1427\text{ cm}^{-1}$  and  $\sim 870\text{ cm}^{-1}$  regions [25,34,36,42,48,51]. The twin bands in the  $1458\text{--}1427\text{ cm}^{-1}$  region, with more symmetrical

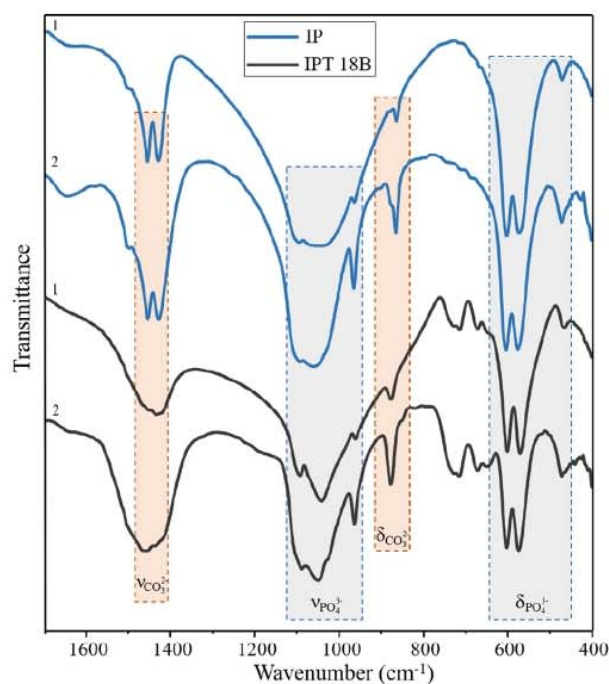
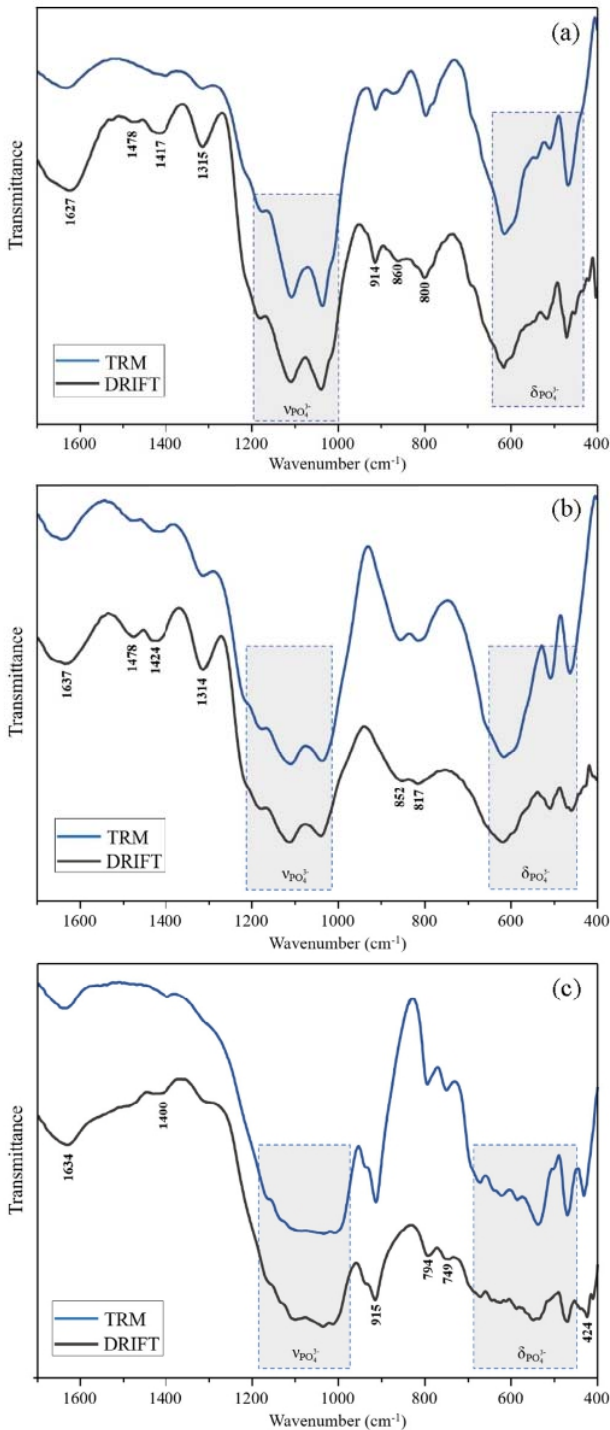
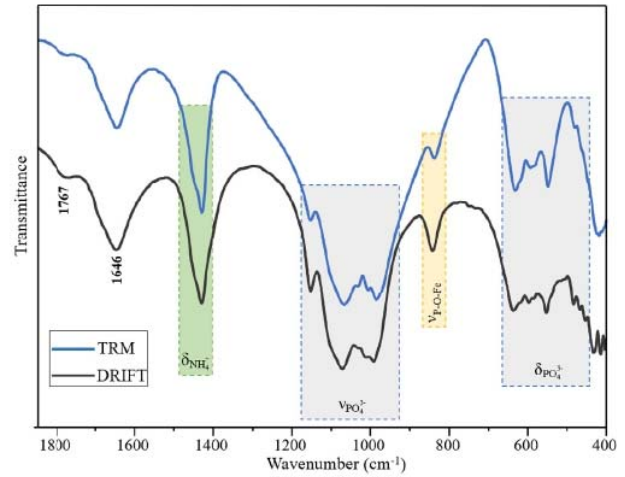


Fig. 5. Infrared spectra of igneous phosphates in the  $1700\text{--}400\text{ cm}^{-1}$  region: (1) Spectra obtained by the TRM method; (2) spectra obtained by the DRIFT method.



**Fig. 6.** Infrared spectra of weathering phosphates in the 1700–400 cm<sup>-1</sup> region: (a) WP1, (b) WP2, and (c) WP3.

and defined shapes in the IP sample and wider in the IPT 18B sample, corresponded to the asymmetric stretching vibrations of the C–O bond. In turn, the band at 870 cm<sup>-1</sup>, which was more intense with the DRIFT method, was attributed to the symmetric deformation vibrations of the C–O–C bond. In the IPT 18B phosphate, two absorption bands were also identified at 717 and 672 cm<sup>-1</sup>, which were attributed to the asymmetric deformation vibrations of the C–O–C bond [34]. The presence of bands indicative of the (CO<sub>3</sub>)<sup>2-</sup>



**Fig. 7.** Infrared spectra of biogenetic phosphate in the 1900–400 cm<sup>-1</sup> region.

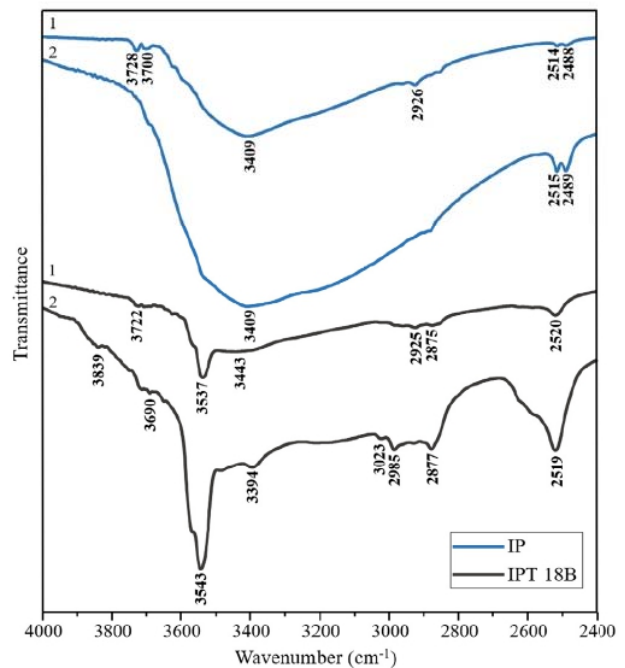


**Fig. 8.** Infrared spectra of igneous phosphates in the 4000–2400 cm<sup>-1</sup> region obtained by the TRM (1) and DRIFT methods (2).

ion in igneous phosphates was associated with bonds with calcium in the structure of apatite, as well as in the structures of calcite and dolomite, which were present in the phosphate standard.

Because the weathering phosphate samples contained a broad mineralogical assemblage, they showed greater band overlapping, including in the 1200–1009 cm<sup>-1</sup> and 625–452 cm<sup>-1</sup> regions corresponding to the stretching and deformation bands of the phosphate group, respectively (Fig. 6). Despite their greater spectral complexity, it was possible to highlight some important attributes, such as the presence of bands related to stretching (672 cm<sup>-1</sup>, 588 cm<sup>-1</sup>, ~470 cm<sup>-1</sup> and ~460 cm<sup>-1</sup>) and deformation vibrations (~1180 cm<sup>-1</sup>, ~1040 cm<sup>-1</sup>, and 800 cm<sup>-1</sup>) vibrations of the bonds of the Al<sub>2</sub>OH structure; and the single band at ~620 cm<sup>-1</sup> was

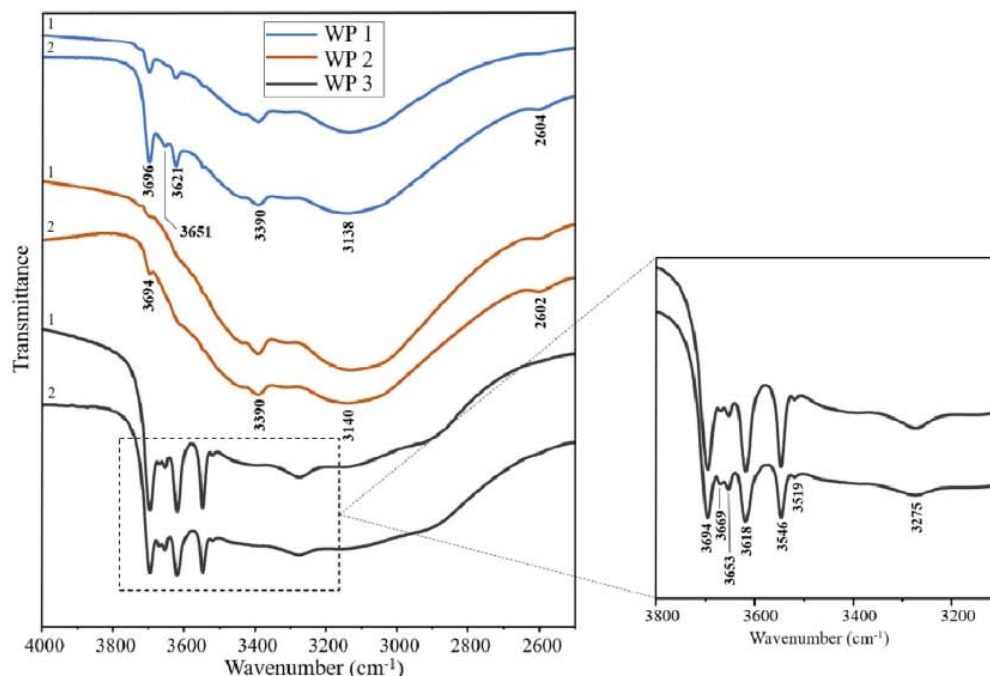


**Fig. 9.** Infrared spectra of weathering phosphates in the 4000–2400  $\text{cm}^{-1}$  region obtained by the TRM (1) and DRIFT methods (2). Highlighted bands correspond to the OH molecules of the kaolinite structure.

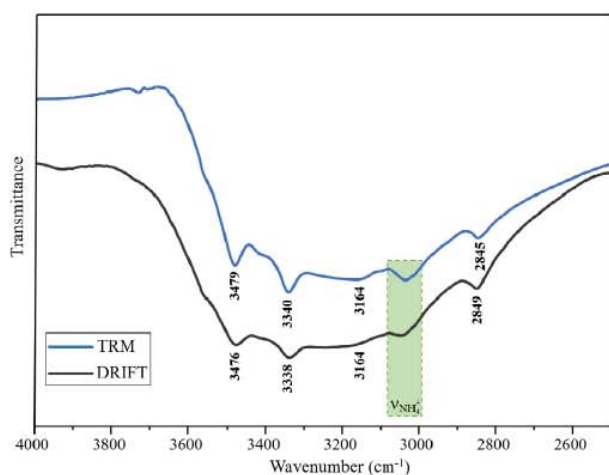


**Fig. 10.** Infrared spectra of biogenetic phosphate in the 4000–2500  $\text{cm}^{-1}$  region.

the product of the stretching of the bonds of the  $\text{Al}(\text{O}/\text{OH})_6$  structure [52–57]. The presence of groups with Al in their composition was consistent with the structures of aluminum phosphate minerals such as crandallite-goyazite, woodhouseite, wardite and also clay mineral kaolinite.

The presence of quartz was indicated by the stretching vibration bands of the Si–O bond and by the deformation vibration bands of the Si–O–Si fragment. These bands were also observed in the region where the bands corresponding to the phosphate and aluminate groups occurred, in the 1120–1000  $\text{cm}^{-1}$ , 540  $\text{cm}^{-1}$ , and 470  $\text{cm}^{-1}$  regions [36,58–61]. The bands corresponding to  $\text{SiO}_2$  together with those of the aluminous groups in the WH3 sample were also associated with the presence of kaolinite (Fig. 6).

As in the igneous phosphates, the same process of association of the  $(\text{CO}_3)^{2-}$  ion to some mineral structures occurred in the weathering phosphates, because the asymmetric stretching bands of the C–O bond that appeared in the 1478–1400  $\text{cm}^{-1}$  region were related to the presence of Ca in the structures of crandallite and woodhouseite [53,56].

As can be observed in Fig. 7, the infrared spectra of the biogenetic phosphate sample, in addition to showing the phosphate bands that occurred in the 1152–984  $\text{cm}^{-1}$  region representing stretching vibrations and the 634–465  $\text{cm}^{-1}$  region representing deformation vibrations, there was also a stretching vibration band corresponding to the N–H bond in the 3045–3033  $\text{cm}^{-1}$  region (Fig. 10), as well as a deformation band in the plane of the H–N–N bond at 1428  $\text{cm}^{-1}$  (Fig. 7), both related to the  $\text{NH}_4$  molecule [62]. In addition, a deformation vibration band corresponding to the Al–OH–Fe bond was observed at  $\sim 840$   $\text{cm}^{-1}$  [63].

As seen in Figs. 8, 9, and 10, in the spectral region above 1600  $\text{cm}^{-1}$ , there were mostly absorption bands related to hydroxyl and water molecules. Deformation bands were observed in the 2146–1630  $\text{cm}^{-1}$  interval, corresponding to the H–O–H bond, while there were stretching vibration bands corresponding to structural or surface O–H in the 3700–3110  $\text{cm}^{-1}$  region (Figs. 8–10) [34,36,43,45–47,61]. More specifically, in the WP3 sample (Fig. 9), the bands between 3700 and 3520  $\text{cm}^{-1}$  were directly related to the OH molecules present in the octahedral layers of kaolinite [17,21].

### 3.2.2. NIR region

Overtone and stretching/deformation combination bands of the fundamental mode region are usually formed in the NIR region, which can theoretically be calculated from the wavenumbers of the bands generated in the MIR region [17,64]. For this reason, the assignment of functional groups becomes quite difficult, even if there is a lower band overlapping different groups on either side. Data regarding the assignment of bands in the NIR region to inor-

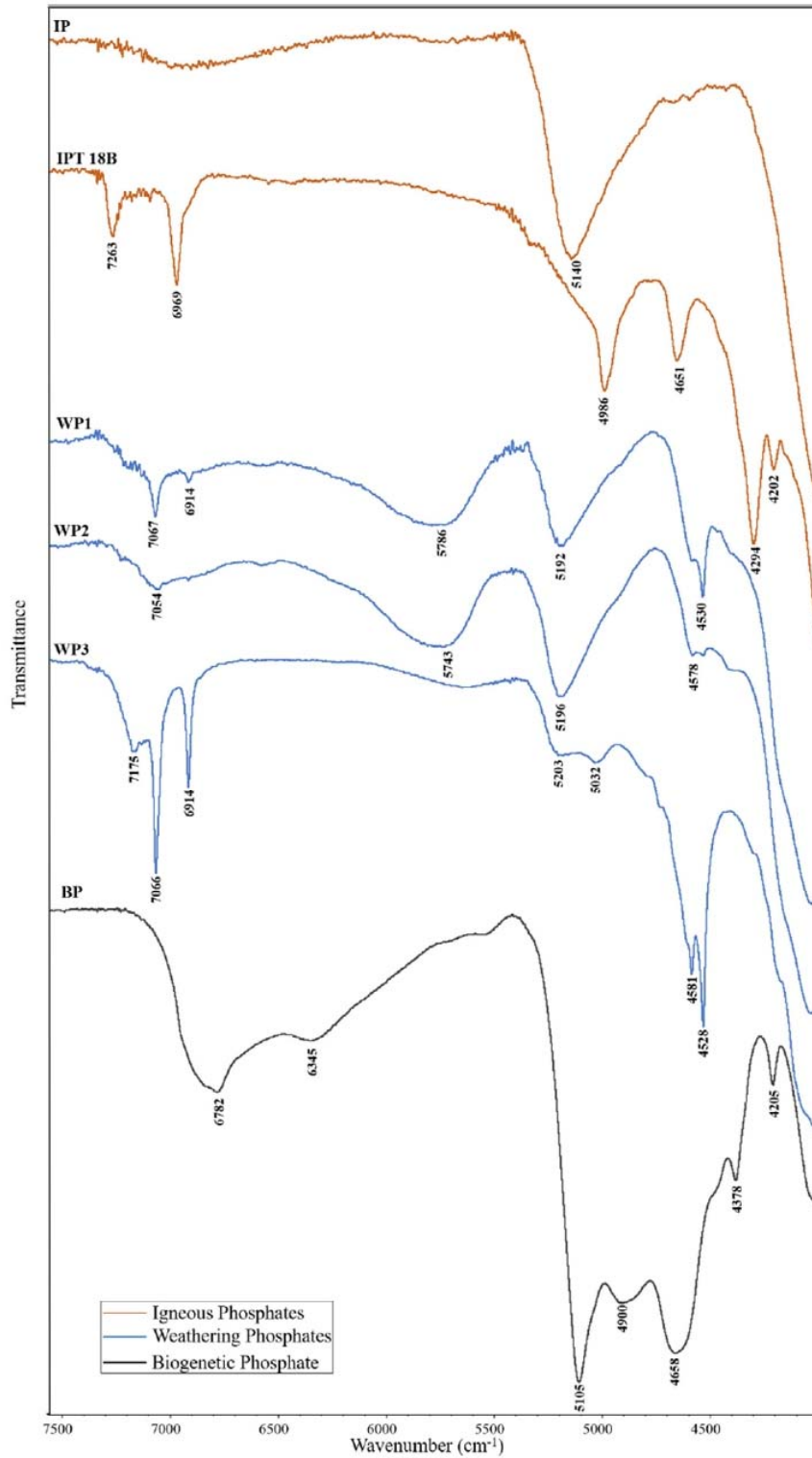
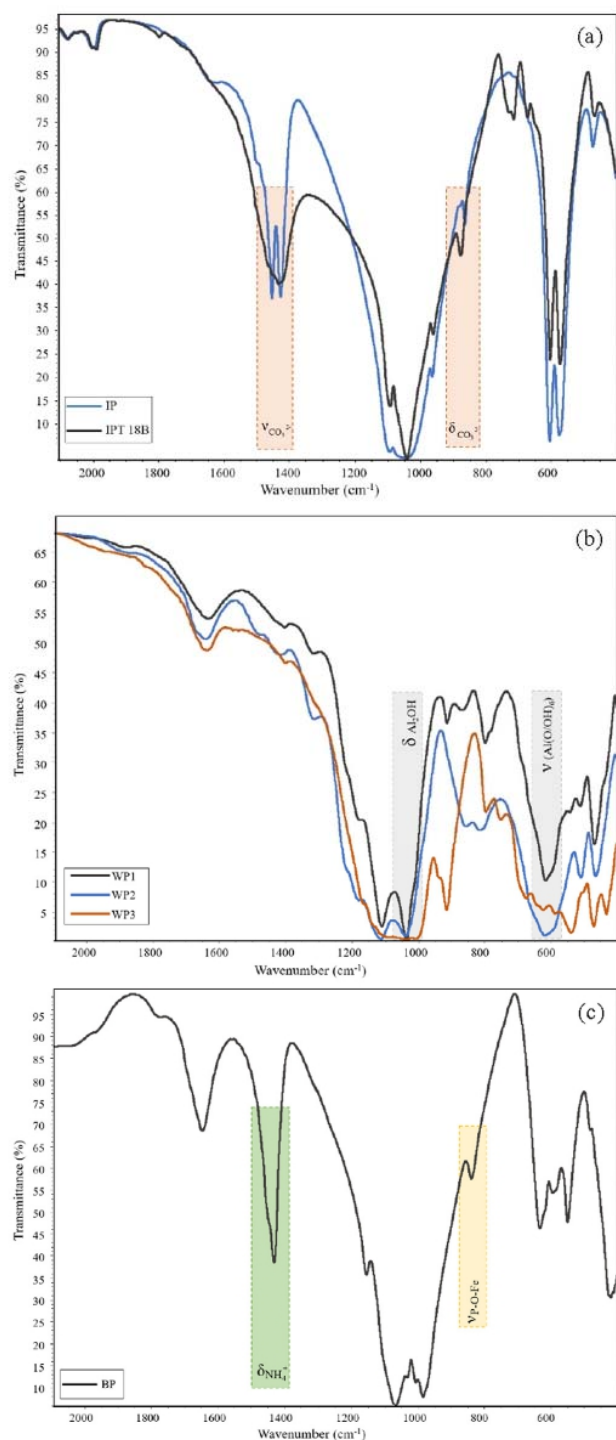


Fig. 11. Comparison of the infrared spectra of igneous, weathering, and biogenetic phosphates in the NIR region.

ganic compounds are quite limited. In the case of phosphate materials, these data are scarce due to the weak dipole moment of the P–O bond [65].

Despite the difficulty of obtaining bands characteristic of the phosphate group, in the IPT 18B and BP samples, there were combination bands ( $\nu + \delta$ ) of the surface P–OH bond, which were



**Fig. 12.** Differentiation of the infrared spectra of igneous phosphates (a), weathering phosphates (b), and biogenetic phosphate (c).

observed in the 4651 cm<sup>-1</sup> region in the IPT 18B sample and at 4657 cm<sup>-1</sup> in the spectrum of the BP sample [66,67]. In IPT 18B, this combination of vibration modes is related to the structure of apatite, possibly to its hydroxyapatite isomorphous variation. In the case of BP, this combination band is consistent with the spheniscidite structural framework.

As in the MIR region, the bands assigned to the OH molecules were easily defined and identified in the NIR spectral region (Fig. 11). The bands attributed to the first overtone of the OH stretching vibration ( $2\nu_{\text{OH}}$ ) were observed in all phosphate materials with bands between 7270 and 6340 cm<sup>-1</sup>, which indicated the presence of structural OH [17,67,68]. In the region close to 5200 cm<sup>-1</sup>, the samples showed stretching and deformation combination bands ( $\nu_{\text{OH}} + \delta_{\text{OH}}$ ) of surface water molecules [17,66,67], with the exception of IPT. In addition, the weathering phosphates showed bands related to the combination of the stretching vibrations of OH with the deformation vibrations of the Al<sub>2</sub>OH group ( $\nu_{\text{OH}} + \delta_{\text{Al(OH)}}$ ) in the regions close to 4580 cm<sup>-1</sup> and 4530 cm<sup>-1</sup> [17]. The presence of the Al<sub>2</sub>OH group can also be indicated by bands close to 7067 cm<sup>-1</sup>, which were observed in the aluminum phosphate samples [68]. In the WP3 sample, these bands may have been related to both the structure of the aluminum phosphate minerals and the structure of kaolinite.

### 3.2.3. Differentiation of phosphate materials by IR

Based on the spectral data obtained in the MIR region together with the compositional and structural information for each phosphate material, it was possible to differentiate them according to origin. This differentiation was mainly based on the spectral bands related to functional groups bound or not to phosphate minerals, as well as the spectral profile obtained for each genetic origin (Fig. 12).

Igneous phosphates were differentiated by their simple composition, marked mainly by phosphate and carbonate bands. Their spectra, in addition to showing similarity in the positions of the absorption bands, were similar due to their profiles, which showed narrow and sharp phosphate bands. In turn, the spectra of weathering phosphates showed less intense and broader bands, possibly attributed to the overlapping of bands related to different functional groups of both phosphate minerals and silicates. The weathering phosphate materials could also be differentiated both by the presence of SiO bands and of Al<sub>2</sub>OH bands, the latter being present in the MIR and NIR regions. Similar to igneous phosphates, biogenetic phosphate, although formed in a supergenic environment, had an IR spectrum with sharp and narrow bands both for the phosphate group and for the NH<sub>4</sub>, FeO, and FePO<sub>4</sub> bands. These compounds are the main components that make biogenetic phosphate different from other genetic groups.

## 4. Conclusions

FTIR analysis allowed the differentiation of Amazonian phosphates according to their geological origin through the definition of the main bands of the PO<sub>4</sub> group in the MIR region and some bands with the OH group in the NIR region.

The identification of other functional groups interconnected or not to phosphate minerals also contributed to the genetic differentiation of the studied materials, with (CO<sub>3</sub>)<sup>2-</sup> bands being characteristic of igneous phosphates, Al<sub>2</sub>OH and SiO bands specific to weathering phosphates, and NH<sub>4</sub> bands and components bound to Fe related to biogenetic phosphates.

The establishment of the characteristic regions of the stretching and bending vibration bands of PO<sub>4</sub>, as well as of the other functional groups, also contributed to the establishment of a database of phosphate materials from the Amazon region using transmittance and diffuse reflectance analytical methods.

The comparison of the FTIR analysis methods in the MIR region also made it possible to establish the best modes of analysis of solid phosphate compounds. The transmittance or diffuse reflectance method is recommended, and whenever possible, the two

methods should be applied together, complementing spectral responses.

### CRedit authorship contribution statement

**P.V. Campos:** Conceptualization, Methodology, Validation, Investigation, Data curation, Formal analysis, Visualization, Writing - original draft, Writing - review & editing. **A.R.L. Albuquerque:** Conceptualization, Methodology, Investigation, Writing - review & editing, Visualization. **R.S. Angélica:** Conceptualization, Methodology, Resources, Funding acquisition. **S.P.A. Paz:** Conceptualization, Validation, Resources, Supervision, Funding acquisition, Project administration.

### Declaration of Competing Interest

The authors declare that they have no known competing financial interests or personal relationships that could have appeared to influence the work reported in this paper.

### Acknowledgments

The authors thank the Brazilian agency CNPq (Conselho Nacional de Desenvolvimento Científico e Tecnológico) for the following grants: master's scholarship to the first author (131133/2019-5), doctorate scholarship to the second author (140101/2019-5), and funding support (MCT/CNPq/Universal No. 28/2018, 429756/2018-6). We also thank the Pró-Reitoria de Pesquisa e Pós-Graduação – Universidade Federal do Pará (PROPESP/UFPA) for funding support (EDITAL PAPQ No. 01/2020). We thank Phosfaz Fertilizantes for support with the weathering phosphate samples. We also thank the Graduate Program in Geology and Geochemistry of UFPA (PPGG/UFPA) for the use of its laboratories and the staff of the Laboratory of Mineral Characterization (LCM/UFPA).

### Appendix A. Supplementary data

Supplementary data to this article can be found online at <https://doi.org/10.1016/j.saa.2021.119476>.

### References

- [1] J.P. Atfield, Phosphate Anions, *Encycl. Mater. Sci. Technol.* (Second Ed. (1974) 1–6.
- [2] P. Van Straaten, *Agrogeology: The use of rocks for crops*, Enviroquest, Toronto, 2007.
- [3] R.L. Zimdahl, Phosphorus, in: *Six Chem. That Chang. Agric.*, Elsevier, 2015: pp. 73–88. DOI: 10.1016/B978-0-12-800561-3.00005-5.
- [4] A. Angert, T. Weiner, S. Mazeh, F. Tamburini, E. Frossard, S.M. Bernasconi, M. Stemberg, Seasonal variability of soil phosphate stable oxygen isotopes in rainfall manipulation experiments, *Geochim. Cosmochim. Acta* 75 (2011) 4216–4227, <https://doi.org/10.1016/j.gca.2011.05.002>.
- [5] E.K. Bünemann, Assessment of gross and net mineralization rates of soil organic phosphorus - A review, *Soil Biol. Biochem.* 89 (2015) 82–98, <https://doi.org/10.1016/j.soilbio.2015.06.026>.
- [6] L.M. Huang, X.X. Jia, G.L. Zhang, M.A. Shao, Soil organic phosphorus transformation during ecosystem development: A review, *Plant Soil* 417 (2017) 17–42, <https://doi.org/10.1007/s11104-017-3240-y>.
- [7] D.M. Nash, P.M. Haygarth, B.L. Turner, L.M. Condron, R.W. McDowell, A.E. Richardson, M. Watkins, M.W. Heaven, Using organic phosphorus to sustain pasture productivity: A perspective, *Geoderma* 221–222 (2014) 11–19, <https://doi.org/10.1016/j.geoderma.2013.12.004>.
- [8] L.M. Condron, B.L. Turner, B.J. Cade-Menun, Chemistry and Dynamics of Soil Organic Phosphorus (2015) 87–121, <https://doi.org/10.2134/agronmonogr46.c4>.
- [9] M.D. Mullen, *Phosphorus in Soils—Biological Interactions*, 2nd ed., Elsevier Inc., 2019. DOI: 10.1016/B978-0-12-409548-9.11992-x.
- [10] K.C. Ruttanberg, Phosphorus Cycle Encycl, *Ocean Sci.* (2001) 2149–2162, <https://doi.org/10.1006/rwos.2001.0277>.
- [11] S.K. Haldar, J. Tišljarić, *Basic Mineralogy* (2014), <https://doi.org/10.1016/B978-0-12-408133-8.00002-x>.
- [12] Van Straaten, *Rocks for Crops: Agrominerals of sub-Saharan Africa*, 2002.
- [13] P. Ptáček, Phosphate Rocks in, *Apatites Their Synth. Analog. - Synth. Struct. Prop. Appl.*, InTech (2016) 13, <https://doi.org/10.5772/62214>.
- [14] S.A. Dar, K.F. Khan, *Sedimentary: Phosphates*, Elsevier Inc., 2017. DOI: 10.1016/B978-0-12-409548-9.10509-3.
- [15] F. van der Meer, Near-infrared laboratory spectroscopy of mineral chemistry: A review, *Int. J. Appl. Earth Obs. Geoinf.* 65 (2018) 71–78, <https://doi.org/10.1016/j.jag.2017.10.004>.
- [16] J.T. Klopogge, *Infrared and raman spectroscopy of minerals and inorganic materials*, 3rd ed., Elsevier Ltd., 2016. DOI: 10.1016/B978-0-12-409547-2.12154-7.
- [17] J. Madejová, P. Komadel, Baseline studies of the clay minerals society source clays: Infrared methods, *Clays Clay Miner.* 49 (2001) 410–432, <https://doi.org/10.1346/CCMN.2001.0490508>.
- [18] Z. Xu, B.C. Cornilsen, D.C. Popko, B. Wei, W.D. Pennington, J.R. Wood, Quantitative Mineral Analysis By FTIR Spectroscopy, *Internet J. Vib. Spectrosc.* 5 (2001) 1–11. [www.ijvs.com](http://www.ijvs.com).
- [19] L. Rintoul, H. Panayiotou, S. Kokot, G. George, G. Cash, R. Frost, T. Bui, P. Fredericks, Fourier transform infrared spectrometry: A versatile technique for real world samples, *Analyst.* 123 (1998) 571–577, <https://doi.org/10.1039/a707111f>.
- [20] P.R. Griffiths, Fourier transform infrared spectrometry, *Science* (80-.). 222 (1983) 297–302. DOI: 10.1126/science.6623077.
- [21] J. Madejová, FTIR techniques in clay mineral studies, *Vib. Spectrosc.* 31 (2003) 1–10, [https://doi.org/10.1016/S0924-2031\(02\)00065-6](https://doi.org/10.1016/S0924-2031(02)00065-6).
- [22] S.S. Palayangoda, Q.P. Nguyen, An ATR-FTIR procedure for quantitative analysis of mineral constituents and kerogen in oil shale, *Oil Shale.* 29 (2012) 344–356, <https://doi.org/10.3176/oil.2012.4.05>.
- [23] R.L. Frost, U. Jonansson, Combination bands in the infrared spectroscopy of kaolins - A drift spectroscopic study, *Clays Clay Miner.* 46 (1998) 466–477, <https://doi.org/10.1346/CCMN.1998.0460411>.
- [24] A.R.L. Albuquerque, R.S. Angélica, D.F. Gonçalves, S.P.A. Paz, Phosphate speleothems in caves developed in iron ores and laterites of the carajás mineral province (Brazil) and a new occurrence of spheniscidite, *Int. J. Speleol.* 47 (2018) 53–67, <https://doi.org/10.5038/1827-806X.47.1.2135>.
- [25] W. Jastrzbski, M. Sitarz, M. Rokita, K. Bułat, Infrared spectroscopy of different phosphates structures, *Spectrochim. Acta - Part A Mol. Biomol. Spectrosc.* 79 (2011) 722–727, <https://doi.org/10.1016/j.saa.2010.08.044>.
- [26] M.B. Abram, I.C. Bahiense, C.G. Porto, R.S.C. de Brito, *Projeto Fosfato Brasil - Parte 1*, Inf. Recur. Minerais, Série Insumos Minerais Para a Agric. 13 (2011) 524.
- [27] P. Hama, R. Zucchini, Certificado De Material De Referência No 1908-103, (2011) 1–3.
- [28] M.L. da Costa, A.S. Leite, H. Pöllmann, A laterite-hosted APS deposit in the Amazon region, Brazil: The physical-chemical regime and environment of formation, *J. Geochemical Explor.* 170 (2016) 107–124, <https://doi.org/10.1016/j.gexplo.2016.08.015>.
- [29] J.M. Hughes, J.F. Rakovan, Structurally robust, chemically diverse: Apatite and apatite supergroup minerals, *Elements.* 11 (2015) 165–170, <https://doi.org/10.2113/gselements.11.3.165>.
- [30] H.G. Dill, A. Fricke, K.H. Henning, The origin of Ba- and REE-bearing aluminium-phosphate-sulphate minerals from the Lohrheim kaolinitic clay deposit (Rheinisches Schiefergebirge, Germany), *Appl. Clay Sci.* 10 (1995) 231–245, [https://doi.org/10.1016/0169-1317\(95\)00023-W](https://doi.org/10.1016/0169-1317(95)00023-W).
- [31] T. Kato, Further refinement of the goyazite structure, *Mineral. J.* 13 (1987) 390–396, <https://doi.org/10.2465/minerj.13.390>.
- [32] M.C.M. de Toledo, Os fosfatos aluminosos da série da crandallita - uma revisão, *Rev. Do Inst. Geológico.* 20 (1999) 49–63, <https://doi.org/10.5935/0100-929x.19990005>.
- [33] H.G. Dill, The geology of aluminum phosphate and sulphates of the alunite group minerals: A review, *Earth Sci. Rev.* 53 (2001) 35–93, [https://doi.org/10.1016/S0012-8252\(00\)00035-0](https://doi.org/10.1016/S0012-8252(00)00035-0).
- [34] A. Antonakos, E. Liarokapis, T. Leventouri, Micro-Raman and FTIR studies of synthetic and natural apatites, *Biomaterials* 28 (2007) 3043–3054, <https://doi.org/10.1016/j.biomaterials.2007.02.028>.
- [35] Ş. Marincea, D.Ş.D. Georgeta, D. Gabriel, *Mineralogical Data on the Bat Guano Deposit From Gura Ponicevei Cave (Almaj Mountains, Romania)*, *Romanian J. of Earth Sci.* 8 (2004) 126–129.
- [36] A. Minjigmaa, G. Oyun-Erdene, T. Zolzaya, B. Davaabal, J. Amgalan, J. Temuujin, Phosphorus fertilizer prepared from natural Burenkhaan phosphorite (Mongolia) by a mechanical activation, *Geosystem Eng.* 19 (2016) 119–124, <https://doi.org/10.1080/12269328.2015.1137501>.
- [37] M. Rokita, A. Brozek, M. Handke, Phospho-silicate and silicate layers modified by hydroxyapatite particles, *J. Mol. Struct.* 744–747 (2005) 589–595, <https://doi.org/10.1016/j.molstruc.2005.01.060>.
- [38] F.N. Shi, A. Moreira dos Santos, L. Cunha-Silva, B.F.O. Costa, J. Klinowski, F.A. Almeida Paz, V.S. Amaral, J. Rocha, T. Trindade, Synthesis, structure and magnetic behaviour of mixed metal leucophosphate, *J. Solid State Chem.* 181 (2008) 1330–1336, <https://doi.org/10.1016/j.jssc.2008.02.027>.
- [39] S.V. Stefanovsky, O.I. Stefanovsky, M.B. Remizov, E.A. Belanova, P.V. Kozlov, Y.S. Glazkova, A.V. Sobolev, I.A. Presniakov, S.N. Kalmykov, B.F. Myasoedov, FTIR and Mössbauer spectroscopic study of sodium-aluminum-iron phosphate glassy materials for high level waste immobilization, *J. Nucl. Mater.* 466 (2015) 142–149, <https://doi.org/10.1016/j.jnucmat.2015.06.007>.
- [40] S.V. Stefanovsky, O.I. Stefanovsky, M.I. Kadyko, I.A. Presniakov, B.F. Myasoedov, The effect of Fe<sub>2</sub>O<sub>3</sub> substitution for Al<sub>2</sub>O<sub>3</sub> on the phase composition and

- structure of sodium-aluminum-iron phosphate glasses, *J. Non. Cryst. Solids*. 425 (2015) 138–145, <https://doi.org/10.1016/j.jnoncrysol.2015.05.039>.
- [41] P. Stoch, A. Stoch, M. Ciecinska, I. Krakowiak, M. Sitarz, Structure of phosphate and iron-phosphate glasses by DFT calculations and FTIR/Raman spectroscopy, *J. Non. Cryst. Solids*. 450 (2016) 48–60, <https://doi.org/10.1016/j.jnoncrysol.2016.07.027>.
- [42] M. Veiderma, R. Knubovets, K. Tõnsuaadu, Structural properties of apatites from Finland studied by FTIR spectroscopy, *Bull. Geol. Soc. Finl.* 70 (1998) 69–75, <https://doi.org/10.17741/bgsf/70.1-2.005>.
- [43] N. Clavier, A. Mesbah, S. Szenknect, N. Dacheux, Monazite, rhabdophane, xenotime & churchite: Vibrational spectroscopy of gadolinium phosphate polymorphs, *Spectrochim. Acta - Part A Mol. Biomol. Spectrosc.* 205 (2018) 85–94, <https://doi.org/10.1016/j.saa.2018.07.016>.
- [44] T. Du, X. Niu, Z. Li, P. Li, Q. Feng, Y. Fan, Crosslinking induces high mineralization of apatite minerals on collagen fibers, *Int. J. Biol. Macromol.* 113 (2018) 450–457, <https://doi.org/10.1016/j.ijbiomac.2018.02.136>.
- [45] D.-G. Dumitras, S. Marincea, A.-M. Fransolet, Brushite in the bat guano deposit from the “dry” Cioclovina Cave (Sureanu Mountains, Romania), *Neues Jahrb. Für Mineral. - Abhandlungen*. 180 (2004) 45–64, <https://doi.org/10.1127/0077-7757/2004/0180-0045>.
- [46] R.L. Frost, S.J. Palmer, R.E. Pogson, Raman spectroscopy of newberyite Mg(PO<sub>3</sub>H)<sub>3</sub>·3H<sub>2</sub>O: A cave mineral, *Spectrochim. Acta - Part A Mol. Biomol. Spectrosc.* 79 (2011) 1149–1153, <https://doi.org/10.1016/j.saa.2011.04.035>.
- [47] R.L. Frost, Y. Xi, S.J. Palmer, G.J. Millar, K. Tan, R.E. Pogson, Vibrational spectroscopy of synthetic stercoite H(NH<sub>4</sub>)<sub>2</sub>(NaPO<sub>3</sub>)<sub>4</sub>·4H<sub>2</sub>O - A comparison with the natural cave mineral, *Spectrochim. Acta - Part A Mol. Biomol. Spectrosc.* 84 (2011) 269–274, <https://doi.org/10.1016/j.saa.2011.09.040>.
- [48] M. Karimi, M.R. Ramsheh, S.M. Ahmadi, M.R. Madani, M. Shamsi, R. Reshadi, F. Lotfi, Reline-assisted green and facile synthesis of fluorapatite nanoparticles, *Mater. Sci. Eng., C* 77 (2017) 121–128, <https://doi.org/10.1016/j.msec.2017.03.217>.
- [49] A. Kumaresh, R. Arun Kumar, Structural, spectroscopic, and nonlinear optical investigations on a novel nonlinear optical crystal: Hippuric acid doped ammonium di hydrogen phosphate (HAADP), *Spectrochim. Acta - Part A Mol. Biomol. Spectrosc.* 121 (2014) 346–349, <https://doi.org/10.1016/j.saa.2013.10.117>.
- [50] S. Marincea, D.G. Dumitras, G. Diaconu, E. Bilal, Hydroxylapatite, brushite and ardealite in the bat guano deposit from Peștera Mare de la Merești, Pârșani Mountains, Romania, *Neues Jahrb. Für Mineral. Monatshefte*. 10 (2004) 464–488, <https://doi.org/10.1127/0028-3649/2004/2004-0464>.
- [51] N. Pleshko, A. Boskey, R. Mendelsohn, Novel infrared spectroscopic method for the determination of crystallinity of hydroxyapatite minerals, *Biophys. J.* 60 (1991) 786–793, [https://doi.org/10.1016/S0006-3495\(91\)82113-0](https://doi.org/10.1016/S0006-3495(91)82113-0).
- [52] D.K. Breiting, G. Brehm, J. Mohr, D. Colognesi, S.F. Parker, A. Stolle, T.H. Pimpl, R.G. Schwab, Vibrational spectra of synthetic crandallite-type minerals - Optical and inelastic neutron scattering spectra, *J. Raman Spectrosc.* 37 (2006) 208–216, <https://doi.org/10.1002/jrs.1444>.
- [53] P. Fischer, R. Pöthig, B. Gücker, M. Venohr, Phosphorus saturation and superficial fertilizer application as key parameters to assess the risk of diffuse phosphorus losses from agricultural soils in Brazil, *Sci. Total Environ.* 630 (2018) 1515–1527, <https://doi.org/10.1016/j.scitotenv.2018.02.070>.
- [54] R.L. Frost, R. Scholz, A. López, C. Lana, Y. Xi, A Raman and infrared spectroscopic analysis of the phosphate mineral wardite NaAl<sub>3</sub>(PO<sub>4</sub>)<sub>2</sub>(OH)<sub>4</sub>·2(H<sub>2</sub>O) from Brazil, *Spectrochim. Acta - Part A Mol. Biomol. Spectrosc.* 126 (2014) 164–169, <https://doi.org/10.1016/j.saa.2014.02.007>.
- [55] R.L. Frost, Y. Xi, A vibrational spectroscopic study of the phosphate mineral Wardite NaAl<sub>3</sub>(PO<sub>4</sub>)<sub>2</sub>(OH)<sub>4</sub>·2(H<sub>2</sub>O), *Spectrochim. Acta - Part A Mol. Biomol. Spectrosc.* 93 (2012) 155–163, <https://doi.org/10.1016/j.saa.2012.02.103>.
- [56] R.L. Frost, Y. Xi, S.J. Palmer, Molecular structure of the mineral woodhouseite CaAl<sub>3</sub>(PO<sub>4</sub>)<sub>2</sub>·5H<sub>2</sub>O, *J. Mol. Struct.* 1001 (2011) 56–61, <https://doi.org/10.1016/j.molstruc.2011.06.017>.
- [57] R.L. Frost, Y. Xi, S.J. Palmer, R. Pogson, Vibrational spectroscopic analysis of the mineral crandallite CaAl<sub>3</sub>(PO<sub>4</sub>)<sub>2</sub>(OH)<sub>5</sub>·(H<sub>2</sub>O) from the Jenolan Caves, Australia, *Spectrochim. Acta - Part A Mol. Biomol. Spectrosc.* 82 (2011) 461–466, <https://doi.org/10.1016/j.saa.2011.07.078>.
- [58] D. Bougeard, K.S. Smimov, E. Geidel, Vibrational spectra and structure of kaolinite: A computer simulation study, *J. Phys. Chem. B* 104 (2000) 9210–9217, <https://doi.org/10.1021/jp0013255>.
- [59] S. Bouhazma, S. Chajri, S. Herradi, M. Khaldi, A. El Hachadi, B. El Bali, M. Lachkar, Effect of P, Na, Mg, and Ag content on the in vitro bioactivity, wettability and mechanical strength of sol-gel glasses, *J. Phys. Conf. Ser.* 984 (2018), <https://doi.org/10.1088/1742-6596/984/1/012012>.
- [60] W. Salama, Paleoenvironmental significance of aluminum phosphate-sulfate minerals in the upper Cretaceous ooidal ironstones, E-NE Aswan area, southern Egypt, *Int. J. Earth Sci.* 103 (2014) 1621–1639, <https://doi.org/10.1007/s00531-014-1027-4>.
- [61] W. Salama, M. El Aref, R. Gaupp, Spectroscopic characterization of iron ores formed in different geological environments using FTIR, XPS, Mössbauer spectroscopy and thermoanalyses, *Spectrochim. Acta - Part A Mol. Biomol. Spectrosc.* 136 (2015) 1816–1826, <https://doi.org/10.1016/j.saa.2014.10.090>.
- [62] J. Pironon, M. Pelletier, P. De Donato, R. Mosser-Ruck, Characterization of smectite and illite by FTIR spectroscopy of interlayer NH<sub>4</sub><sup>+</sup> cations, *Clay Miner.* 38 (2003) 201–211, <https://doi.org/10.1180/0009855033820089>.
- [63] R.L. Frost, Y. Xi, R. Scholz, A vibrational spectroscopic study of the phosphate mineral cyrilovite Na(Fe<sup>3+</sup>)<sub>3</sub>(PO<sub>4</sub>)<sub>2</sub>(OH)<sub>4</sub>·2(H<sub>2</sub>O) and in comparison with wardite, *Spectrochim. Acta - Part A Mol. Biomol. Spectrosc.* 108 (2013) 244–250, <https://doi.org/10.1016/j.saa.2013.02.007>.
- [64] H. Siesler, Y. Ozaki, S. Kawata, H. Heise, *Near-infrared spectroscopy Principles, instruments, applications* (2002).
- [65] C. Roberts, J. Workman, J. III, D. Malley, P. Martin, E. Ben-Dor, Application in Analysis of Soils, in: *Near-Infrared Spectrosc. Agric.*, 2004. DOI: 10.2134/agronmonogr44.c26.
- [66] T. Ishikawa, M. Wakamura, S. Kondo, Surface Characterization of Calcium Hydroxylapatite by Fourier Transform Infrared Spectroscopy, *Langmuir* 5 (1989) 140–144, <https://doi.org/10.1021/la00085a025>.
- [67] J. Kolmas, D. Marek, W. Kolodziejcki, Near-Infrared (NIR) Spectroscopy of Synthetic Hydroxyapatites and Human Dental Tissues, *Appl. Spectrosc.* 69 (2015) 902–912, <https://doi.org/10.1366/14-07720>.
- [68] E.T. Stathopoulou, V. Psycharis, G.D. Chryssikos, V. Gionis, G. Theodorou, Bone diagenesis: New data from infrared spectroscopy and X-ray diffraction, *Palaeogeogr. Palaeoclimatol. Palaeoecol.* 266 (2008) 168–174, <https://doi.org/10.1016/j.palaeo.2008.03.022>.



## 5.2 ARTIGO 02

**Chemical Engineering Journal**  
**A SEQUENTIAL PLACKETT-BURMAN AND DOEHLERT DESIGN TO OPTIMIZE  
 STRUVITE PRECIPITATION FOR PHOSPHORUS RECOVERY FROM  
 WASTEWATER AIMING FERTILIZER PRODUCTION**  
 --Manuscript Draft--

<b>Manuscript Number:</b>	
<b>Article Type:</b>	Research Paper
<b>Section/Category:</b>	Environmental Chemical Engineering
<b>Keywords:</b>	DOE; Phosphates; Phosphorous recovery; Optimization; Struvite; Combined responses
<b>Corresponding Author:</b>	Paulo Victor Campos, Engineer UFPA: Universidade Federal do Para Belém, Pará BRAZIL
<b>First Author:</b>	Paulo Victor Campos, Engineer
<b>Order of Authors:</b>	Paulo Victor Campos, Engineer Rômulo Simões Angélica, PhD in Mineralogy and Geochemistry Lênio José Guerreiro Faria, PhD in Chemistry Engineering Simone Patrícia Aranha Paz, PhD in Mineral Engineering

**Abstract**

The precipitation of struvite from wastewater is a potential alternative for the recovery of nutrients, especially phosphorus, which is an essential macronutrient for agriculture but can be harmful to the environment when improperly disposed of in water bodies. In addition, struvite has elements of great added value for agricultural activity (P, N, and Mg) and is therefore considered a sustainable alternative fertilizer. In its formation process, several intervening physicochemical factors may be responsible for the production yield levels. Optimization processes can help to define and direct the factors that truly matter for precipitation. In this context, a sequential design of experiments (DOE) methodology was applied to select and optimize the main struvite precipitation factors in wastewater. Initially, a screening was performed with eight factors with the aid of Plackett-Burman design, and the factors with a real influence on the process were identified. Then, a Doehlert design was used for optimization by applying the response surface methodology and the desirability function. The results were used to identify the optimal points of the pH (10.2), N/P ratio ( $\geq 4$ ), and initial phosphorus concentration (183.5 mg/L); these values had a greater effect on phosphorus recovery and the production of struvite, which was confirmed through thermochemical analysis of the decomposition of its structure by differential scanning calorimeter - glass transition temperature (DSC-TG) and phase identification by X-ray diffraction (XRD). The determination

of the best synthesis conditions is an enormous contribution to the control of the process because these conditions lead to better yields and higher levels of phosphorus recovery.

**Keywords:** DOE, Phosphates, Phosphorous recovery, Optimization, Struvite, Combined responses

## 1 Introduction

Phosphorus is a nutrient of great relevance and one of the most essential elements, if not the most essential, for all living organisms on planet Earth [1–3]. Due to its high reactivity, phosphorus is available on Earth's crust in the ionic form of orthophosphate ( $\text{PO}_4^{3-}$ ), which is characteristically distributed as phosphate minerals. Its biological importance is based on the constitution of genetic material in the form of monoesters or diesters (C-O-P bonds) that exist in the molecules of adenosine triphosphate (ATP), DNA, and RNA as well as its role in the production of chemical energy that ensures the development of living beings, especially plants. Plants fundamentally depend on phosphorus for the vital functions of growth, flowering, and fruit production, and they transform inorganic phosphorus from minerals present in the soil into organic phosphorus [3].

During the phosphorus cycle, phosphate ions are leached from phosphate rocks, released into the soil, and then absorbed through the roots of plants. This activity constitutes one of the final stages of the geochemical phosphorus subcycle. In the biological subcycle, plants synthesize phosphate by transforming it into an energetic and structural component [4]. Phosphorus, now in the form of a molecular constituent of living beings, follows the trophic chain as it is consumed and transferred among organisms, which in turn release phosphorus through excrement and/or death. Thus, phosphorus returns to the soil by the action of decomposers and can participate in several reactions that make it available again to plants or that immobilize it in microbial biomass [3–6].

In the biological subcycle, phosphorus naturally follows its course; some of it is kept in the soil solution and some of it is transported to water bodies. However, the excessive human consumption of phosphate resources and the large deposition of urban and industrial wastes negatively drive the accumulation of this element in water bodies [7–9]. Phosphorus bioaccumulation poses a certain threat to the ecological environment and can cause several environmental problems, such as the eutrophication of rivers and lakes [7–12].

Sustainable actions to address the phosphorus cycle have been debated for decades because in addition to the numerous losses and immobilizations during its cycle, its main source, which has a geological origin, is a finite and nonrenewable resource [13]. Temporal estimates show that existing phosphate reserves will be depleted in the next 50-100 years [13,14]; more optimistic forecasts estimate that these sources will last for approximately 100-400 years, given technological advances and the possible exploitation of new stocks [15,16]. This impact is due to the increasing exponential growth of the world population and increasing demands for food. Food production is in turn conditioned by the global agricultural market, which depends on fertile soils, pesticides, and favorable edaphoclimatic conditions [13,17,18]. In this global context, strategies for using phosphate resources are required, and the search for alternative and sustainable sources is necessary. Strategies for the recovery and/or recycling of phosphorus from wastewater (domestic and industrial sewage) have been shown to be viable and promising, with the reclaimed phosphorus being used for fertilizer.

Different wastewater technologies for phosphorus recovery have been developed and researched [19,20]. Many of these technologies are based on the physicochemical process of precipitation [21,22] and produce calcium and magnesium inorganic phosphates [20]. Among the precipitation products, magnesium ammonium phosphate hexahydrate, or struvite ( $MgNH_4PO_4 \cdot 6H_2O$ ), is notable, which is a mineral that has a large added value. Its orthorhombic crystal structure consists of equimolar chemical proportions of the ions  $PO_4^{3-}$ ,  $NH_4^+$  and  $Mg^{2+}$  [23–25], all of which are plant nutrients. Struvite is characterized as a qualitatively slow-release fertilizer with a low solubility and a low metal content [26]. The physicochemical properties that permeate the crystallization of struvite are conditioned mainly by the pH, the concentration and proportion of ionic components, and the presence of impurities [24,27]. Several other compounds tend to coprecipitate with struvite, and the formation of calcium phosphates (brushite, amorphous calcium phosphate) and other magnesium phosphates (bobierrite and brucite), in addition to similar struvites, which are generated through different isomorphic substitutions in the structure of the solid solution, is possible [25,28,29].

Many methods to develop and/or optimize the struvite precipitation process have been proposed. Certain statistical tools and methodologies are key to this goal. Kumar and Pal (2013) [30] studied the optimal concentrations of ammonium, phosphate, and magnesium ions during the precipitation and recovery of struvite from raw wastewater from a coke plant and developed a hybrid process by proposing a regression model considering the removal of  $NH_4-N$  as a response. Optimal parameters of struvite synthesis were also stipulated by Capdevielle et al. (2013) [31], who investigated the effects of the mixing rate, temperature and Ca, Mg, and N

concentrations on the precipitation of struvite from synthetic wastewater. Daneshgar et al. (2019) [32] investigated the effects of the pH, the presence of calcium, and the concentration of nitrogen on the efficiency of phosphorus recovery through struvite precipitation by applying chemical modeling together with the response surface methodology (RSM). The RSM was also used by Thant Zin and Kim (2019) [33], who promoted the optimization of struvite production from food processing wastewater and sewage sludge ash as a function of variations in the pH and N and Mg concentrations.

Statistical methods can be used to investigate the effects of the variables that affect a process and quantitatively determine the efficiency factors to thereby optimize the process to make it economically feasible. Multivariate experimental designs are tools that have a high efficacy for optimization and enable the simultaneous evaluation of several factors by using reduced amounts of experiments. The applicability of these designs is conditioned by the process responses, which enables the detection of significant effects, the determination of optimal regions, the generation of adjusted optimization models and the analysis of optimal points with combined responses if the process has more than one response variable [32]. In addition, experimental designs are the basis for the application of the RSM, which can be used to determine the impact of variations in the degrees of freedom of the factors at the optimal points [32,34].

Experimental designs are widely disseminated and commonly used for the optimization of various processes. The precipitation of struvite from wastewater has been a recent target in experimental designs aiming to identify the best production conditions given the various physicochemical reaction factors that can affect the process and its purpose of use [32,35]. Some studies have used Box-Behnken or central composite designs to evaluate the impact of some reduced variables and to optimize the synthesis process through responses such as phosphorus recovery [32], the mean particle size of precipitated struvite [36], and the removal of ammonium [30].

Screening designs such as the Plackett-Burman and second-order designs in a Doehlert matrix are rare in studies on the optimization of struvite synthesis. The principle of the Plackett-Burman experimental design is the investigation of factors influencing the process, which can be fixed or eliminated when used in other designs [34,37]. The Doehlert matrix consists of a multivariate design that is highly effective in generating second-order models. This design shows a uniform distribution of points within an experimental interval, with several unequal levels proportional to the importance of each variable. In addition, the Doehlert design requires a smaller number of experiments compared to other types of design, such as the central

composite design and the Box-Behnken design, which also have a high degree of efficiency [38,39].

In this context, this study aimed to identify the best conditions for struvite precipitation through the recovery and recycling of nutrients from wastewater. Thus, a sequential experimental design methodology was applied to determine the factors affecting the process through a Plackett-Burman design and to optimize the synthesis through a Doehlert matrix design together with the RSM and the desirability function, which enabled the establishment of an optimized experimental area, regression models for the synthesis, and identification of the optimal points for struvite precipitation with combined responses. In addition to using designs that are uncommon in studies on struvite production, this study also aimed to investigate the structure of the precipitated material, the details of the phases formed, and the combination of phosphorus recovery and the thermochemical results of the degradation of the struvite structure from enthalpy variations as second-order design responses.

## **2 Materials and methods**

### **2.1 Synthetic wastewater preparation and synthesis of struvite**

The synthesis of artificial wastewater was conducted in a simple reaction system. Solutions of  $K_2HPO_4$ ,  $NH_4Cl$ ,  $MgCl_2 \cdot 6H_2O$ ,  $KCl$ , and  $CaCl_2$  with deionized water were used to prepare the synthetic wastewater in 2.5 L reactors at room temperature ( $26 \text{ }^\circ\text{C} \pm 1 \text{ }^\circ\text{C}$ ). Sodium hydroxide (NaOH) 1 M was used during the synthesis to adjust the pH. The input stoichiometry of the solutions was established according to each experimental design applied, and the pH of the reaction medium, the agitation rate, and the reaction time were also defined.

After the precipitation reaction, the solution was filtered in a vacuum separation process with quantitative filters (150 mm). The material obtained was dried in an oven at  $40 \text{ }^\circ\text{C}$  for 48 h. After drying, the material was deagglomerated, homogenized, and subjected to phase analysis by powder X-ray Diffractometry (XRD).

### **2.2 Analytical methods**

#### **2.2.1 Phosphorus recovery**

The phosphorus content in the supernatant solutions was analyzed using the molybdenum blue spectrophotometric method. The phosphorus content was determined by calculating the phosphorus recovery rate ( $P_{rec}$ ) of the experimental runs. The calculation of  $P_{rec}$  using the P concentration data was performed using Eq. (1):

$$P_{rec} = \frac{C_{P_0} - C_{P_r}}{C_{P_0}} \times 100 \quad (1)$$

where  $C_{P_0}$  is the initial  $PO_4$ -P concentration of the synthetic wastewater, and  $C_{P_r}$  is the  $PO_4$ -P concentration of the solution after synthesis.

### 2.2.2 Phases analysis

The phase analysis of the products obtained by precipitation was performed in a Malvern PANalytical Empyrean diffractometer with a Co anode ( $K\alpha_1 = 1.789010 \text{ \AA}$ ), with 1800 W long fine focus, an Fe  $K\beta$  filter, a PIXcel3D-Medpix3 area detector  $1 \times 1$  in scanning mode with a voltage of 40 kV and a current of 35 mA, a step size of  $0.0065652^\circ$  in  $2\theta$ , with scanning from  $2^\circ$  to  $110^\circ$ , a divergent slit at  $1/4^\circ$ , and antiscattering at  $1/2^\circ$ , a 10 mm mask, and a time step of 19.266 s. The results were interpreted using X'Pert HighScore Plus software version 4.9, from PANalytical, using the COD database [40]. A profile fit (pseudo-Voigt function) was performed on the diffractograms to standardize the diffractometric profile of the products with struvite.

### 2.2.3 Elementary chemical analysis

The elemental chemical analysis of the synthesis products was performed in a Malvern PANalytical Zetium X-ray fluorescence spectrometer in the STD-1 calibration (Standardless) relative to the nonstandard analysis of the chemical elements between fluoride and uranium. The samples were prepared in the form of pressed pellets, and the values were normalized to 100%.

### 2.2.4 Thermal analysis

The differential scanning calorimeter - glass transition temperature (DSC-TG) measurements were performed in a NETZSCH thermal analyzer model STA 449F3 Jupiter with a simultaneous thermal analyzer from Stanton Redcroft and a platinum vertical cylindrical oven. A temperature range between 25 °C and 1000 °C was used in a nitrogen atmosphere with a flow rate of 50 mL/min. The heating rate was 5 °C/min, with a platinum crucible as a reference. Approximately 10 mg of sample were used. The enthalpies of product degradation were measured by using the DSC with heat flux. This technique enables the area of a peak and the enthalpy variation to be proportionally related through a temperature-dependent (2) calibration factor. The calibration factor was determined using the following substances and respective melting points: In (156.6 °C), Sn (231.9 °C), Bi (271.4 °C), Zn (416.6 °C), Al (660.6 °C), and Au (1064.4 °C). The enthalpy variation at the peaks ( $\Delta H$ ) was determined by Eq. 2, and the responses are presented in  $J.g^{-1}$ .

$$\Delta H = \pm \frac{A}{mK} = \frac{1}{mK} \int_{t_{initial}}^{t_{final}} [heat\ flux(t) - interpolated\ baseline(t)] dt$$

where  $A$  is the peak area,  $m$  (g) is the sample mass, and  $K$  is an empirical constant relative to the sensor sensitivity.

### 2.2.5 Particle size distribution

The particle size distribution analyses were performed in a granulometer using an ANALYSETTE 22 MicroTec Plus laser diffraction instrument. The samples were dispersed in water, the measurements were taken with 100 scans, a beam obscuration of 15%, and size intervals between 0.08 and 2000.00  $\mu m$ , and the responses were calculated using the Mie model.

### 2.2.6 Fourier transform infrared spectroscopy

The Fourier transform infrared spectroscopy (FTIR) measurements were performed in an infrared spectrometer with Thermo Scientific Fourier transform, model Nicolet iS50 FTIR. The spectral data were in the mid-infrared (MIR) region, with an IR source, a KBr beam splitter, and a DTGS KBr detector. All measurements were performed under the transmission mode with KBr pellets (ratio: 2 mg of sample/150 mg of KBr), and 100 scans were taken with a spectral resolution of 4  $cm^{-1}$ .

### 2.2.7 Scanning electron microscopy

Morphological analyses were performed to identify the structures and textures of the synthesis products. Micrographs were obtained using a Thermo Fisher Scientific Quanta 650 FEG scanning electron microscope. The analyses were performed using backscattered and secondary electrons, with a constant acceleration voltage of 15.0 kV and a working distance of ~ 14 mm.

### 2.3 Experimental design and statistical modeling

This study was based on a sequential experimental design methodology. In the first stage, a Plackett-Burman design was applied to identify and estimate the significant factors within the synthesis process. In the second stage, after establishing the values of the factors that did not show significance, a second-order design with a Doehlert matrix was performed to determine the optimal points of the factors from the regression models using the RSM and the desirability function.

All experiments were performed randomly. The residuals of the experimental values and the values obtained by the multiple regression models (which obeyed the assumptions of independence, randomness, homoscedasticity, and normality of the residuals) were compared, and analysis of variance (ANOVA) tests were performed with a confidence level of 95%. Statistical analysis of the data was performed using the outputs generated by Statistica® software version 13.1.

#### 2.3.1 Plackett-Burman design

The Plackett-Burman experimental design was used to screen the variables studied in this synthesis process. This type of design is used to screen a large number of factors, which can affect the responses in the analysis of a process of interest [34]. The design consisted of a PB-12 with 8 independent factors tested at two levels, which resulted in 12 experimental runs (see section 3.1). The factors evaluated in this design, as well as their levels, were selected from process data reported by several authors. The choice of factors was based on the theoretical and methodological framework, which highlighted important physicochemical aspects of the struvite synthesis process. The process factors studied, with their respective units and codes, were the initial phosphorus concentration ( $\text{mg}\cdot\text{L}^{-1}$ ,  $X_1$ ), the pH of the synthetic wastewater ( $X_2$ ), the initial molar ratios ( $\text{NH}_4/\text{PO}_4$ ,  $X_3$ ;  $\text{Mg}/\text{PO}_4$ ,  $X_4$ ; and  $\text{K}/\text{PO}_4$ ,  $X_5$ ), the presence of Ca ( $X_6$ ), the time (min,  $X_7$ ), and the agitation rate (rpm,  $X_8$ ).



The screening of the parameters through the PB-12 design was established based on the phosphorus recovery rate “P<sub>rec</sub> (%)”, which was considered to be the design response variable, and the qualitative analysis of the phases formed in the synthesis products. The XRD analysis of the phases was performed to evaluate the formation of struvite as a positive response compared to the formation of other phases or the nonformation of crystalline material.

### 2.3.2 Doehlert Matrix design

By considering the selection of significant factors for the phosphorus recovery rate response, it was possible to establish a second-order design for the optimization of the synthesis based on the first-order experimental design. Thus, a Doehlert design for three factors was used, and the response variables were the phosphorus recovery rate “P<sub>rec</sub> (%)” and the enthalpy of the endothermic peak of struvite decomposition “ΔH (J.g<sup>-1</sup>)”.

In this design, the total experimental domain was determined through a minimum number of experiments, which was related to the number of factors considered in the study. As a simplified representation,  $k$  factors determine the number of experiments based on the formula  $k^2 + k + 1$  by economically planning the ideal number of experimental runs.

In this step, the effects of three factors were investigated: the pH ( $U_1$ ), the N/P ratio ( $U_2$ ), and the P concentration ( $U_3$ ), which were related to the variables coded according to Eq. 3.

$$X_i = \left( \frac{U_i - \bar{U}_i}{\Delta U_i} \right) \quad (3)$$

where  $X_i$  is the coded value of the variable;  $U_i$  is the actual value of the variable;  $\bar{U}_i$  is the center point value within the experimental range (Eq. 4); and  $\Delta U_i$  is the range of variation of factor  $i$  (Eq. 5).

$$\bar{U}_i = \frac{\text{Upper limit of } (U_i) + \text{Lower limit of } (U_i)}{2} \quad (4)$$

$$\Delta U_i = \frac{\text{Upper limit of } (U_i) - \text{Lower limit of } (U_i)}{2\alpha_i} \quad (5)$$

where  $\alpha_i$  is the coded limit value for each factor.

The experimental domain is shown in Table 1. The design matrix is detailed in section 3.2.

**Table 1.** Factors and experimental domain.

Coded factor ( $X_i$ )	Factor	Experimental field		$\bar{U}_i$	$\Delta U_i$
		Lower limit	Upper limit		
$X_1$	$U_1$ : pH	9	11	10	0.5
$X_2$	$U_2$ : N/P	1	4	2.5	0.5
$X_3$	$U_3$ : $P_{\text{initial}}$ (mg/L)	60	250	155	95

### 3 Results and discussion

#### 3.1 Plackett-Burman design

A PB-12 design was performed to determine the factors affecting the synthesis of struvite. The experimental matrix with coded and actual factors for the response ( $P_{\text{rec}}$ ) is detailed in Table 2.

Table 2. PB-12 design matrix.

Run*	Natural units								Coded units								Response
	$X_1$	$X_2$	$X_3$	$X_4$	$X_5$	$X_6$	$X_7$	$X_8$	$X_1$	$X_2$	$X_3$	$X_4$	$X_5$	$X_6$	$X_7$	$X_8$	$P_{\text{rec}}$ (%)
1 <sup>(6)</sup>	310	9	3	1	1	no	50	300	1	-1	1	-1	-1	-1	1	1	56.8
2 <sup>(1)</sup>	310	11	1	2.5	1	no	15	300	1	1	-1	1	-1	-1	-1	1	90.3
3 <sup>(4)</sup>	78	11	3	1	2	no	15	100	-1	1	1	-1	1	-1	-1	-1	63.3
4 <sup>(12)</sup>	310	9	3	2.5	1	yes	15	100	1	-1	1	1	-1	1	-1	-1	98.2
5 <sup>(10)</sup>	310	11	1	2.5	2	no	50	100	1	1	-1	1	1	-1	1	-1	86.1
6 <sup>(3)</sup>	310	11	3	1	2	yes	15	300	1	1	1	-1	1	1	-1	1	99.4
7 <sup>(7)</sup>	78	11	3	2.5	1	yes	50	100	-1	1	1	1	-1	1	1	-1	98.3
8 <sup>(11)</sup>	78	9	3	2.5	2	no	50	300	-1	-1	1	1	1	-1	1	1	42.8
9 <sup>(9)</sup>	78	9	1	2.5	2	yes	15	300	-1	-1	-1	1	1	1	-1	1	95.3
10 <sup>(5)</sup>	310	9	1	1	2	yes	50	100	1	-1	-1	-1	1	1	1	-1	89.2
11 <sup>(2)</sup>	78	11	1	1	1	yes	50	300	-1	1	-1	-1	-1	1	1	1	96.9
12 <sup>(8)</sup>	78	9	1	1	1	no	15	100	-1	-1	-1	-1	-1	-1	-1	-1	71.1

\* The numbers in parentheses indicate the order of the experiments

##### 3.1.1 Product characterization

Fig. 1 shows the phase characterization of the products obtained through the Plackett-Burman design experiments. Six experimental runs showed struvite formation (Fig. 1a). Among them, race numbers 8 and 12 stand out because they presented better yields regarding the intensity of the main peak of struvite ( $d_{111} = 4.25 \text{ \AA}$ ) in the refined (Fit Profile) diffractometric pattern (Table 3). In runs 1, 3, 8, and 12, the peaks related to the crystalline planes (002), (012), and (004) of the struvite structure showed a high relative intensity, which can be explained by the preferred orientation of the crystals. The material obtained in experiment no. 3, in addition to containing struvite as the main phase, also showed the formation of its isomorphous potassium analog (K-struvite), which is corroborated by the slight displacements in the struvite peaks (Fig. 1a). These displacements occur as a function of the unit cell contraction due to the replacement

of  $\text{NH}_4^+$  ions (1.40 Å) with  $\text{K}^+$  (1.33 Å) [41,42]. The presence of a struvite analog in sample no. 3 is related to the concentration of  $\text{K}^+$  ions in the wastewater, which was slightly higher than the proportion of the ammonium concentration (Table 2); this result is consistent with the substitutions in the unit cell. In addition, the radius of the cation affects the stability of the structure, which consequently increases with larger cations [43]. Therefore, more struvite than K-struvite was formed due to the structural stability provided by the  $\text{NH}_4^+$  ion compared to the stability provided by  $\text{K}^+$ .

The synthesis products obtained in experiments 4 and 10 also formed struvite as a single phase (Fig. 1a); however, the phase in both experiments showed low intensity peaks (Table 3), indicating a low conversion. This low conversion into struvite was due to the presence of  $\text{Ca}^{2+}$  in the wastewater from these runs, which “competes” with  $\text{Mg}^{2+}$  and is responsible for the formation of amorphous calcium phosphate (ACP) as a coprecipitated material. In supersaturated and alkaline media with high pH values and in the presence of Ca, P, and Mg, the coprecipitation of ACP with other calcium phosphate compounds may be common [28,44,45].

**Table 3.** *Diffractometric* data of struvite: d111 (4.25 Å).

Run	FWHM*	Intensity (cts)	Area (cts.°2 $\theta$ )
1	0.094	747.89	77.1
3	0.107	940.62	104.4
4	0.095	485.22	41.3
8	0.098	1668.9	174.6
10	0.0867	248.02	15.9
12	0.131	1740.5	200.2

\* Full width at half maximum

The diffractograms of the other experiments (Fig. 1b) show the formation of undesired phases in the process, such as brucite (Runs 2, 5, and 7) and bobierrite (Runs 2 and 5), as well as the formation of amorphous material (Runs 6, 9, and 11). The precipitation of the brucite and bobierrite phases had a direct correlation with the high Mg/P ratio and the more alkaline medium (pH 11). In the experiments in which there was an absence of crystalline phases, the formation of ACP was assumed to be due to the presence of calcium in solution with a lower supersaturation ratio, given the proportions of Mg (Runs 6 and 11) and/or ammonium (Run 9) at the lower levels. The presence of other competitive ions strongly affects the struvite formation process.

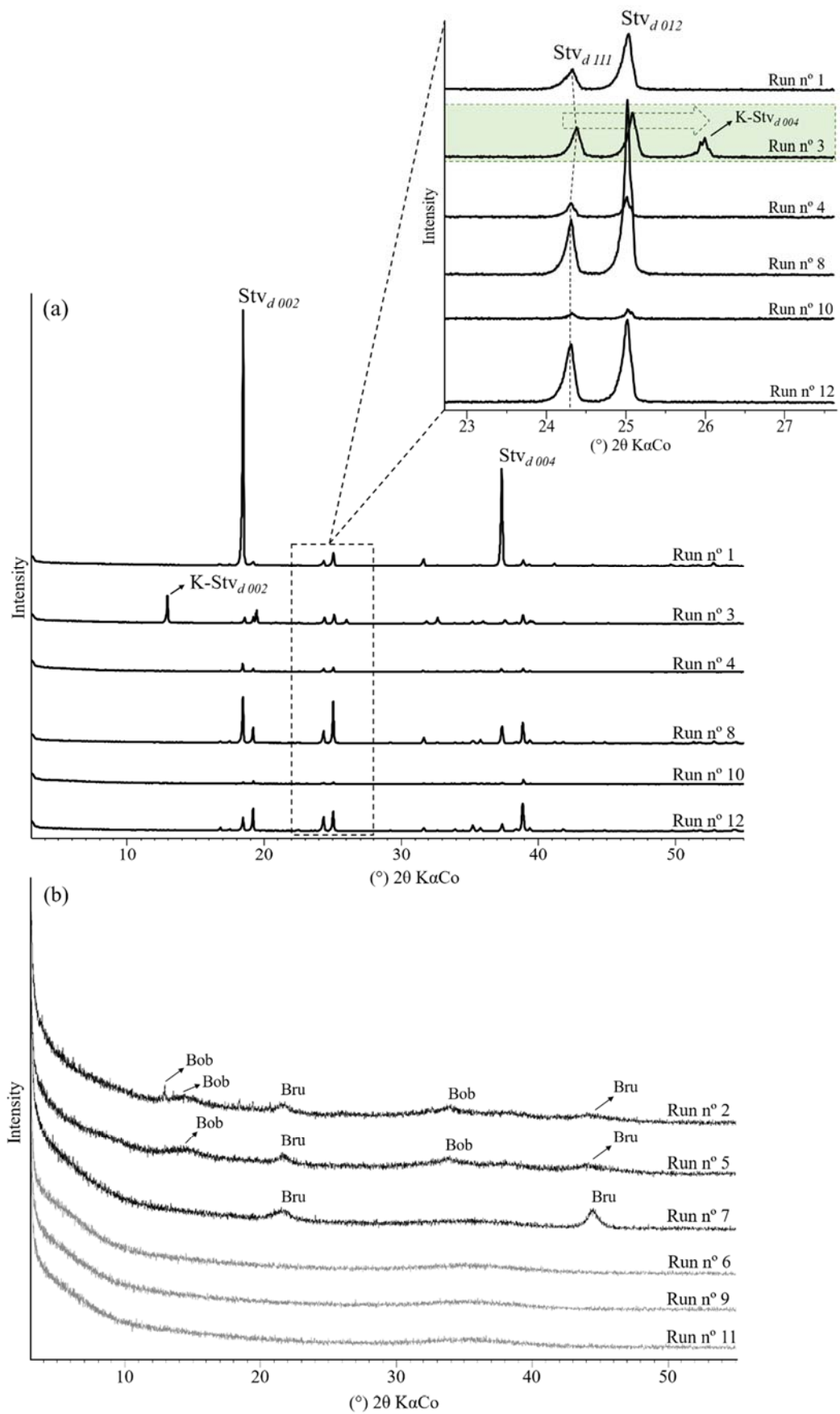


**Fig. 1.** Diffractometric patterns of the precipitates obtained according to the experimental Plackett-Burman design. (a) Runs 1, 3, 4, 8, 10, and 12. (b) Runs 2, 5, 6, 7, 9, and 11. Abbreviations: Stv: struvite; K-Stv: K-struvite; Bob: Bobierite; Bru: brucite.

### 3.1.2 Analysis of the main effects and interactions

In conjunction with the phase analysis from the diffractograms of the PB-12 design experiments, a statistical analysis using the phosphorus recovery rate ( $P_{rec}$ ) was performed. The phosphorus recovery values obtained after the synthesis process using PB-12 are shown in Table 2.

Most tests showed phosphorus recovery rates above 70%, which indicates a high efficiency in the synthesis process. However, according to the analysis of the phases in the products, not all experiments were efficient for the formation of struvite. From the runs with phosphorus recovery rates higher than 90% (Runs 2, 4, 6, 7, 9, and 11), only experiment 4 showed struvite formation, but the peak intensity was reduced (Fig. 1). The product of experimental run 10 showed a similar behavior, with a low conversion into struvite even with a high phosphorus recovery rate (89.2%). Only in experiment 12 was observed a high conversion into struvite with a high phosphorus recovery rate (71.1%). The products with a high phosphorus recovery rate and without the presence of struvite correspond to those with the formation of amorphous calcium phosphate, which is more favorable than struvite when calcium is present in the reaction medium.

Table 4 shows the statistical analysis of the main effects of the operational factors evaluated in the PB-12 design for the phosphorus recovery rate response. The response data were subjected to a regression analysis to evaluate the  $p$ -value with a confidence level of 95%. The analysis of the results showed that only the initial phosphorus concentration ( $X_1$ ), the pH ( $X_2$ ), the molar ratio N/P ( $X_3$ ), and the presence of Ca ( $X_6$ ) were statistically significant for the response. The greatest effect of the  $X_6$  factor in Table 4 is because calcium reacts in the formation of calcium phosphate, which in this context is established as ACP. In this sense, this factor is comparatively the most significant and positive factor, but it is undesirable because it unfavorably affects the formation of struvite.

The analysis of the values of the  $p$  descriptive level and the F statistics contained in Table 4 allows us to conclude that the factors  $X_4$ ,  $X_5$ ,  $X_7$ , and  $X_8$  were not statistically significant in the phosphorus recovery.

**Table 4.** Analysis of the main effects of the PB-12 design variables.

Factor	Effect	Std. Error	<i>p</i> -value	F-value
P concentration (X <sub>1</sub> )	8.6768	2.590749	0.044087*	11.2168
pH (X <sub>2</sub> )	13.4928	2.590749	0.013760*	27.1239
N/P (X <sub>3</sub> )	-11.6635	2.590749	0.020466*	20.2679
Mg/P (X <sub>4</sub> )	5.7361	2.590749	0.113670	4.9021
K/P (X <sub>5</sub> )	-5.9252	2.590749	0.106244	5.2306
Ca (X <sub>6</sub> )	27.8429	2.590749	0.001723*	115.4989
Time (X <sub>7</sub> )	-7.9125	2.590749	0.055248	9.3277
Mixing rate (X <sub>8</sub> )	-4.1363	2.590749	0.208642	2.5490

\**p* < 0.05 (Statistically significant values)

### 3.2 Doehlert design

Based on the results obtained from the Plackett-Burman design, a second-order experimental design (Doehlert design) was performed with the statistically significant factors. The other factors that were not influential had their values fixed, considering the economic constraints of the synthesis: Mg/P ratio = 1/1, K/P ratio = 2/1, absence of calcium, time = 30 min, and mixing rate = 200 rpm. Table 5 shows the matrix of experiments used.

**Table 5.** Doehlert experiment matrix and response  $P_{rec}$  (%).

Run *	Natural units			Coded units			Response
	pH	N/P	P <sub>initial</sub>	X <sub>1</sub>	X <sub>2</sub>	X <sub>3</sub>	P <sub>rec</sub> (%)
1 <sup>(4)</sup>	11	2.5	155	1	0	0	55.9
2 <sup>(2)</sup>	10.5	4	155	0.5	0.866	0	74.8
3 <sup>(9)</sup>	10.5	3	250	0.5	0.289	0.817	74.7
4 <sup>(5)</sup>	9	2.5	155	-1	0	0	41.5
5 <sup>(8)</sup>	9.5	1	155	-0.5	-0.866	0	35.8
6 <sup>(10)</sup>	9.5	2	60	-0.5	-0.289	-0.817	30.2
7 <sup>(7)</sup>	10.5	1	155	0.5	-0.866	0	52.3
8 <sup>(12)</sup>	10.5	2	60	0.5	-0.289	-0.817	31.6
9 <sup>(11)</sup>	9.5	4	155	-0.5	0.866	0	65.8
10 <sup>(15)</sup>	10	3.5	60	0	0.577	-0.817	51.5
11 <sup>(3)</sup>	9.5	3	250	-0.5	0.289	0.817	67.9
12 <sup>(1)</sup>	10	1.5	250	0	-0.577	0.817	65.6
13 <sup>(6)</sup>	10	2.5	155	0	0	0	64.1
14 <sup>(14)</sup>	10	2.5	155	0	0	0	67.4
15 <sup>(13)</sup>	10	2.5	155	0	0	0	63.2

\* The numbers in parentheses indicate the order of the experiments

### 3.2.1 Analysis of the response: phosphorus recovery

The phosphorus recovery results for each test of the Doehlert matrix are shown in Table 5. The variation in the recovery rate was established in a range of values between 30 and 75%. Similar recovery rates have been found in other studies on the production of struvite from wastewater. Crutchick and Garrido (2011) [46] obtained struvite crystallization with a phosphorus recovery efficacy of 64% for industrial wastewater and 60% for synthetic wastewater. In the present study, it is noteworthy that all research was conducted using synthetic wastewater.

Experimental runs 2 and 3 showed the best  $P_{rec}$  responses: 74.8 and 74.7%, respectively. These results can be explained by the relationship between the relatively higher pH value and the higher N/P ratios [2]. The lowest phosphorus recovery rates were observed in experiments 5, 6, and 8, with values close to 30%. These lower recoveries may have been related to the low concentrations of  $NH_4$  and P (Table 5).

### 3.2.2 Product characterization

The diffractograms in Fig. 2 show the phase analysis of some of the products obtained through the Doehlert design. All experiments presented struvite as the main phase. In some cases, struvite analogs were also formed (Runs 1, 7, and 8). The formed struvite analog acts as a compensatory phase and is not detrimental to the synthesis objective because it has K in its composition, which is a highly valuable nutrient [47], and it contributes to the recovery of phosphorus from wastewater for use as a slow-release fertilizer.

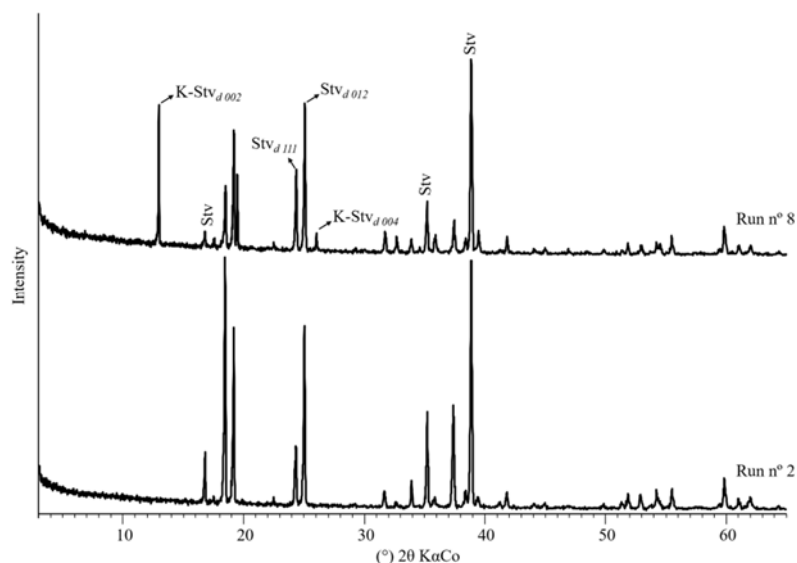


**Fig. 2.** XRD patterns of the products obtained in experiments 2 and 8 according to the Doehlert Matrix design. Abbreviations: Stv: struvite; K-Stv: K-struvite.

Due to the formation of struvite as the main phase in all the samples, the adopted experimental region constituted the optimal synthesis region (thermodynamically stable region for struvite). This fact is corroborated by the elemental chemical analysis of the products, which quantitatively shows the presence of the elements that make up the struvite (Table 6). The high values of P in the products expressed by  $P_2O_5$  varied between 46 and 51%, while the values of Mg expressed by MgO were between 25.4 and 30.2%, and the values of ammonium + hydroxyls expressed by the loss on ignition were between 5.2 and 19.1%. The variations in the loss on ignition levels were mainly due to the formation of K-struvite in some experimental runs, which is confirmed both by the phase analysis and by the  $K_2O$  values, which increased at the expense of the loss on ignition values in runs 1, 7, and 8. This increase was due to the isomorphic substitutions between  $K^+$  and  $NH_4^+$  that occur in the struvite structure.

**Table 6.** Chemical composition of the Doehlert design products by XRF.

Components	Runs												
	1	2	3	4	5	6	7	8	9	10	11	12	13
$P_2O_5$	46.3	48.2	48	51	50.2	49.7	49	48.3	51	49.8	50.7	47.8	49.9
MgO	30.1	25.5	25.4	26.8	26.2	26.1	30.2	27.2	27.1	26.4	27	25.6	26.1
$K_2O$	12.8	9.48	9.21	3.49	10.2	5.79	15.3	12.4	2.63	6.05	3.45	10.6	8.53
LOI	10.4	16.8	17	18.6	13.3	18.3	5.2	11.7	19.1	17.6	18.8	15.9	15.4

(LOI) loss on ignition at 1000 °C

The FTIR chemical analysis of the functional groups showed a great similarity in the responses of the products obtained. Fig. 3 shows the results of experimental runs 3 and 7, and the bands characteristic of struvite are exposed.

Wide, asymmetric, and well-structured bands were observed in the region between 3500 and 2300  $cm^{-1}$ . These bands are attributed to the vibrations of asymmetric stretching of the  $OH^-$  group and vibrations of symmetric and asymmetric stretching of the N–H bond of the  $NH_4^+$  group (Fig. 4) [42,48]. These bands have wide and asymmetric shapes due to the forces of the hydrogen bonds in the struvite structure, mainly those attributed to water molecules, and the possible overlapping of bands caused by the presence of various functional groups [48]. The bands located in the ranges of 3500 to 3000  $cm^{-1}$  are characteristic of the stretching vibrations of the H-O-H molecules of crystallization water, while the bands observed at the wavelength  $\sim 2360$   $cm^{-1}$  are attributed to the stretching vibrations of the H-O-H of the crystallization water molecules cluster [48–50]. Deformational vibrations of the flexion mode of the H-O-H molecule refer to the bands present between 1680 and 1600  $cm^{-1}$  [48,51]. A band positioned at  $\sim 760$   $cm^{-1}$  indicates vibrations related to weak H bonds between water molecules.



The infrared spectra also show two bands characteristic of the  $\text{NH}_4^+$  functional group. The band close to  $1475\text{ cm}^{-1}$  is attributed to the deformation vibrations in the plane of the H–N–H bond, while the band located in the region between  $905$  and  $895\text{ cm}^{-1}$  can be attributed to the H bond of the ammonium-water interaction [52] and/or the deformation vibration of the O–H fragment bound to  $\text{Mg}^{2+}$  [49]. The ionic group  $(\text{PO}_4)^{3-}$  was identified through the bands that are attributed to the strong asymmetric stretching vibrations of the P–O bond ( $\sim 1005\text{ cm}^{-1}$ ), the symmetrical deformation vibrations in the plane of the O – P – O bond ( $\sim 570\text{ cm}^{-1}$ ), and the asymmetric strain vibrations in the plane of the O – P – O bond ( $\sim 460\text{ cm}^{-1}$ ) [48,51–53]. The formation of small bands at positions  $\sim 436\text{ cm}^{-1}$  and  $\sim 690\text{ cm}^{-1}$  can be attributed to the vibrations of metal-oxygen (Mg–O) bonds [49,53,54].

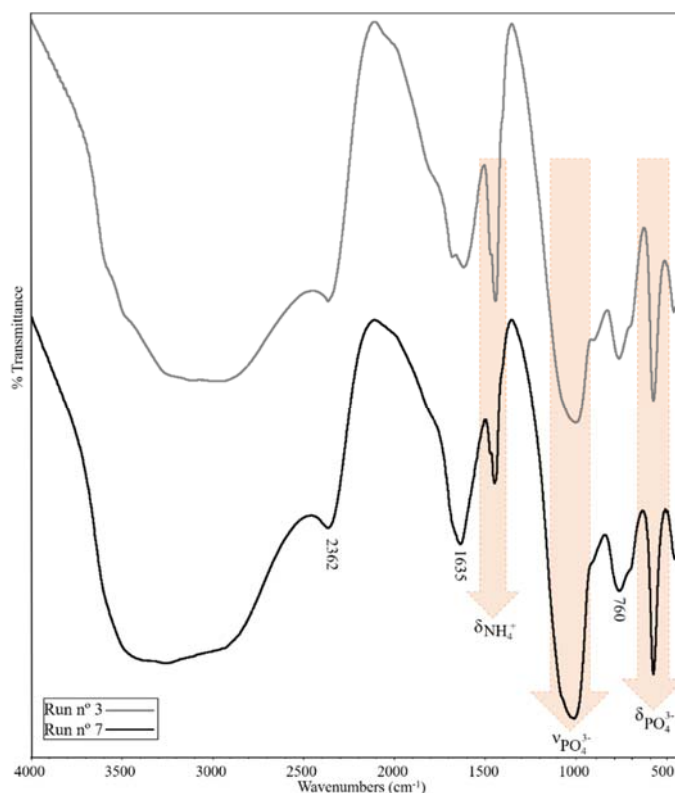
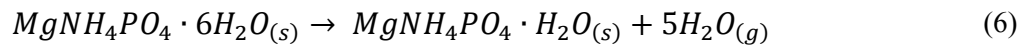


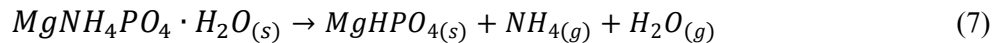
**Fig. 3.** Infrared spectra obtained for experiments 3 and 7 according to the Doehlert Matrix design

The products obtained in the Doehlert experiments also showed very similar thermal behaviors and were divided into three thermal response groups. Fig. 4 shows the DSC-TG representative curves of the three groups: group 1, which corresponds to runs 1, 7, and 8 and contains struvite and the struvite analog, as represented by run 1 in Fig. 4a; group 2, which corresponds to runs 2, 5, 12, 13, and 15 and contains struvite alone, as represented by run 2 in Fig. 4b; and group 3, which corresponds to runs 3, 4, 6, 9, 10, 11, and 14 and contains struvite alone, but with a difference in the content of the events in relation to group 2, as represented by run 6 in Fig. 4c.

Struvite undergoes decomposition at low temperatures (above 40 °C) and is affected by the heating rate [55]. Thus, by using a heating rate of 5 °C/min, the first decomposition events in the DSC curves appeared between 55.6 and 105 °C. The endothermic peaks at ~ 60 °C were observed only in the samples of group 1, which correspond to the presence of the struvite analog, while the endothermic event at ~ 100 °C occurred markedly in all samples because it corresponds to the presence of struvite in all products. This event (single, double, or even multiple) corresponds to the collapse of the struvite family structure, and the simultaneous loss of ammonia with the loss of structural water [56,57]. When the water loss precedes the loss of ammonia, an intermediate monohydrate crystalline phase called dittmarite ( $MgNH_4PO_4 \cdot H_2O$ ) is formed, as shown in Eq. 6.



The TG curves (Fig. 4) show that the main mass loss occurred between 50 and 110 °C. However, the curves are constant only at ~ 300 °C, because struvite shows significant water loss above 60 °C and is completely transformed into dittmarite at approximately 100 °C. Thus, the dittmarite is then thermally stable between 90 °C and 230 °C and completely dehydrated at ~ 300 °C. Heating above 300 °C transforms the dittmarite into an amorphous phase, Eq. 7 [57,58]. The mass loss values were between 40 and 51.5% (Table 7), thus corroborating the consecutive losses of water and ammonia. Similar values were observed by Frost et al. (2004) [55], who found mass losses of ~ 42% during struvite decomposition. For those products considered to have a high conversion into struvite (Runs no. 2 and no. 3), the values obtained can be considered equal to the theoretically predicted value of 51.42%; 44.08% corresponds to water loss, while 7.34% represents the loss of  $NH_4$  [55].



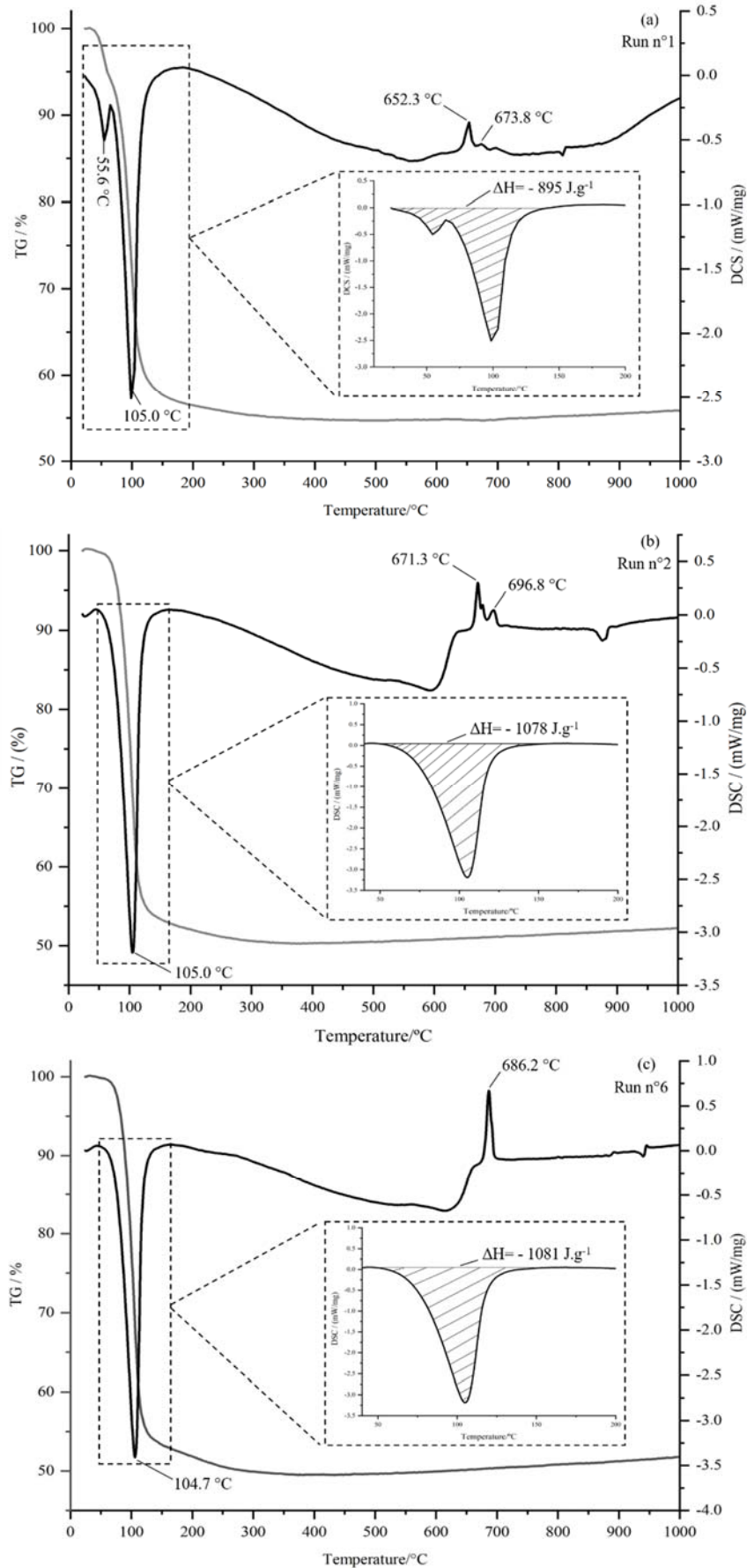
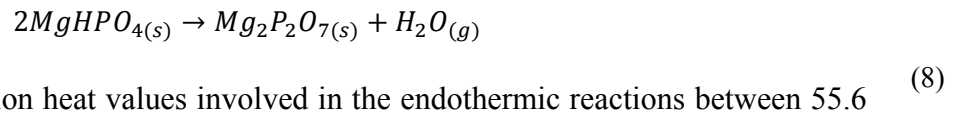


**Fig. 4.** DSC-TG curves of the products obtained in runs (a) no. 1 – group 1, (b) no. 2 – group 2, and (c) no. 6 – group 3.

Exothermic peaks at ~ 650-720 °C were also observed in the DSC curves. Group 1 (Fig. 4a) is marked by the presence of a multiple event with a low formation energy; group 2 (Fig. 4b) also presented a multiple event in this region but with higher energies; and group 3 (Fig. 4c) presented a simple event with a higher formation energy. These exothermic events represent the phase transformation of the material structure, in which the amorphous phase is transformed into the crystalline form of magnesium pyrophosphate ( $Mg_2P_2O_7$ ) (Eq. 8) [42,57–59].



The reaction heat values involved in the endothermic reactions between 55.6 and 105 °C are highlighted in Fig. 4 ( $\Delta H = - A.m^{-1}.K^{-1}$ , see also Eq. 2), for the representatives of the three groups observed, and Table 7 shows the values for all products. The products of group 1 had the lowest enthalpy values (823-918 J.g<sup>-1</sup>), which can be explained by the fact that the corresponding precipitates consist of both struvite and the struvite analog, so that the amount of ammonia is lower when compared to the amount of ammonia in “true” struvites; this is due to the replacement of  $NH_4^+$  with  $K^+$  in the solid solution. Thus, the other two groups of products with similar thermal profiles, with only “true” struvite, presented enthalpies of decomposition higher than 1015 J.g<sup>-1</sup>.

**Table 7.** Losses of mass and enthalpies of decomposition of the products obtained in the Doehlert design.

Run	$\Delta m$ (%)	$\Delta H$ (J.g <sup>-1</sup> )
1	44.07	895
2	47.98	1078
3	48.60	1029
4	49.94	1103
5	44.96	1057
6	48.20	1081
7	41.07	823
8	43.66	918
9	49.65	1061
10	48.81	1076
11	49.29	1015
12	47.87	1054
13	47.21	1076
14	50.70	1051
15	51.46	1071

The particle size distribution was similar for most products, i.e., a very fine material but with well-developed particles. Product no. 2 (Fig. 5a) had a D90 of 22 μm; it was the finest

product and had two modes, the smallest of which represented the population of ultrafines (D10 of 5  $\mu\text{m}$ ). The other products had D90 values between 80 and 130  $\mu\text{m}$ , as can be observed for product no. 7 in Fig. 5b, a result similar to that of the other products.

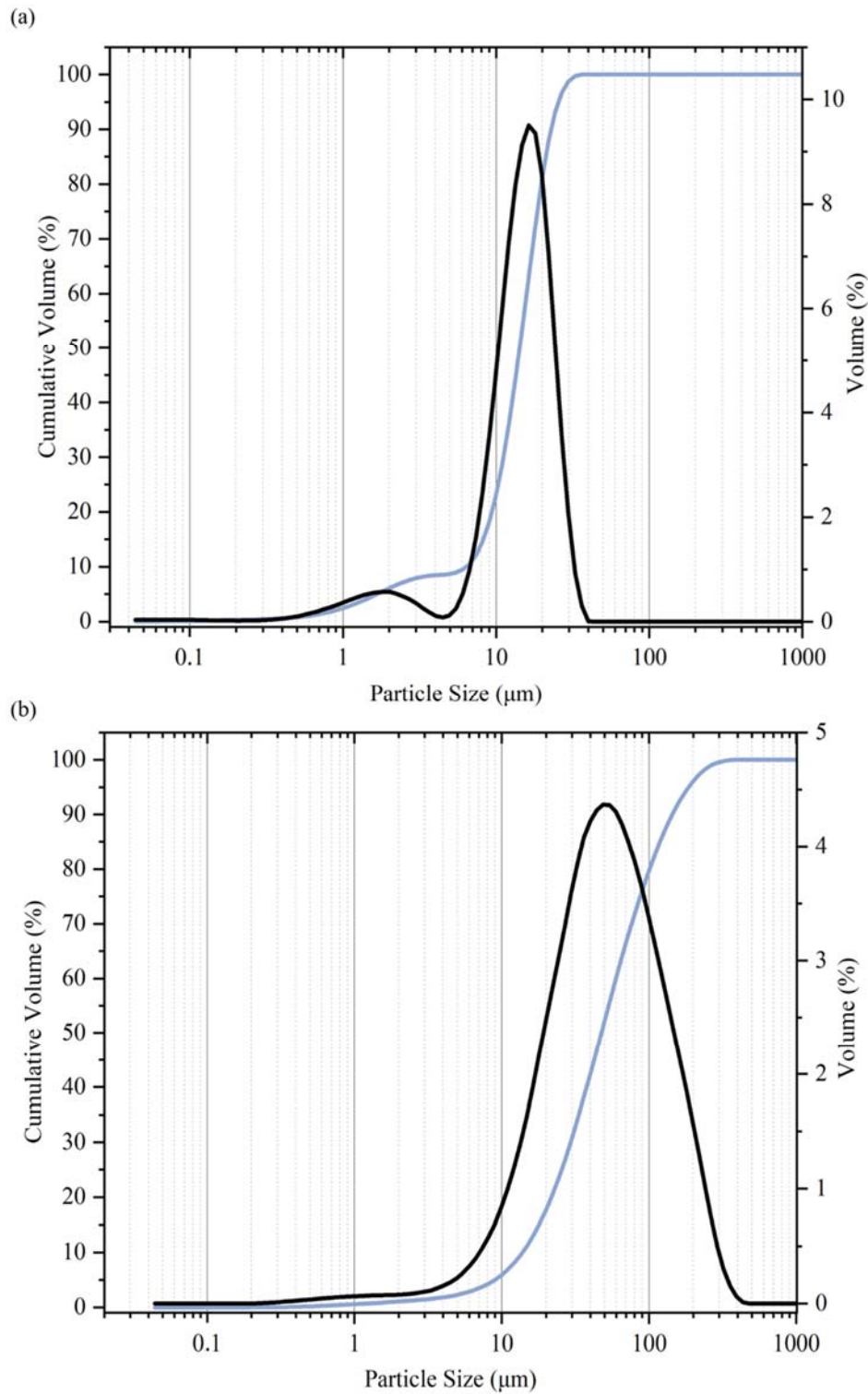


**Fig. 5.** Particle size distributions: (a) Run 2, (b) Run 7.

The mean diameter was 16.3  $\mu\text{m}$  for product no. 2, and it was between 48.7 and 53.8  $\mu\text{m}$  for the other products. Similar results for particle sizes were found by Kozik et al. (2013) [60], who noted mean particle diameter values between 12.6 and 50.2  $\mu\text{m}$ . The aforementioned authors attributed the particle size variations to variations in the pH and mixing time. Thus, by establishing a fixed mixing time, there were no major changes in the particle diameter of the products obtained in the design.

The morphology of the products is shown in the micrographs of Fig. 6 a-c (run 2) and d-f (run 7). In the analyzed products, crystals characteristic of the struvite orthorhombic structure were formed, which confirms the analysis of the obtained phases. Most crystals had simple needle-shaped morphologies. Some crystals presented their morphology as X-shaped twin crystals with dendritic growth (Fig. 6b) and as larger crystals with faceted structures (Fig. 6f). These changes in morphology may be due to the structural remnants caused by transitions during synthesis [2]. The crystals formed in the product of run 7, which has struvite and K-struvite, did not show large differences when compared to the crystals formed in run 2, in which only struvite was found. This finding explains why there is no structural change between the phases, with only an ionic change occurring at the  $\text{NH}_4^+$  site [61].

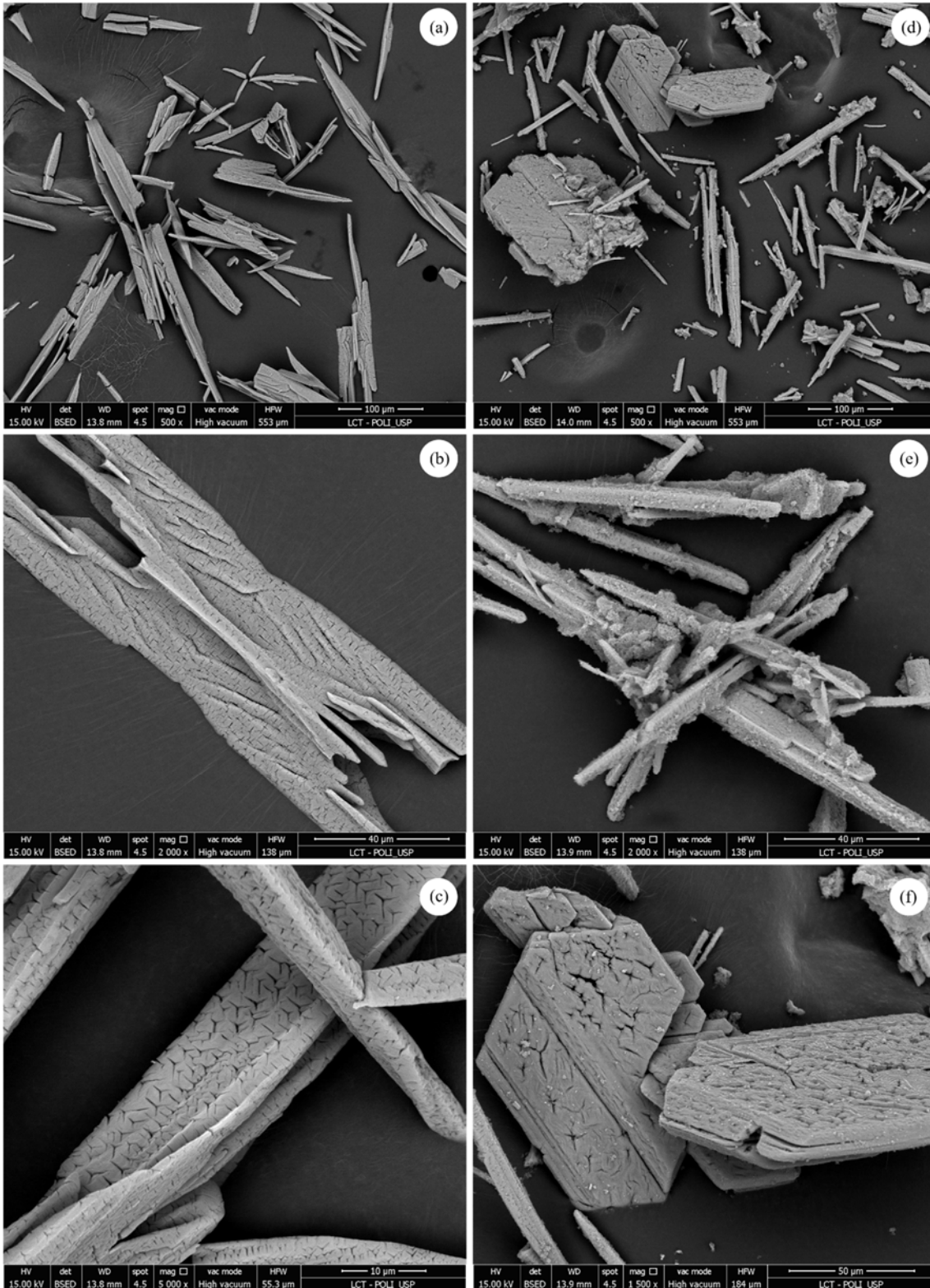


**Fig. 6.** Micrographs of the products obtained by precipitation. (a) - (c): Run 2; (d) - (f): Run 7.

### 3.3.3 Statistical modeling and analysis

The recovery of phosphorus from wastewater through precipitation processes and struvite crystallization is sometimes a joint process that depends on the physicochemical

conditions. Thus, a statistical analysis involving the factors screened in the PB-12 design was performed with a second-order design. The pH ( $X_1$ ), the molar ratio N/P ( $X_2$ ), and the initial P concentration ( $X_3$ ) were then analyzed in a three-factor Doehlert matrix (Table 5), and the responses were the recovery rate of P ( $P_{rec}$ ) and the enthalpy of the endothermic peak of struvite decomposition ( $\Delta H$ ). Investigations of the individual and combined effects of the factors were performed using Statistica software. The coefficients of the second-order regression models for both responses were determined, and the response surfaces and contour lines were obtained to analyze the functional relationships between the levels and the responses and to perform a simultaneous optimization by applying the desirability function within the stipulated experimental domain.

Table 8 shows the ANOVA of the Doehlert design for the two responses.

**Table 8.** ANOVA results for the of operational variables in each response variable

Source	df	Phosphorus recovery				Enthalpy variation			
		SS	MS	F	<i>p</i>	SS	MS	F	<i>p</i>
$X_1$	1	240.816	240.816	24.2438	0.004383*	9.77544	9.775444	237.4597	0.004185*
$X_1^2$	1	320.330	320.330	32.2488	0.002358*	1.40460	1.404598	34.1197	0.028080*
$X_2$	1	917.223	917.223	92.3400	0.000207*	4.12160	4.121599	100.1196	0.009841*
$X_2^2$	1	29.149	29.149	2.9345	0.147379	1.13150	1.131497	27.4857	0.034510*
$X_3$	1	1497.589	1497.589	150.7674	0.000063*	0.02976	0.029760	0.7229	0.484741
$X_3^2$	1	181.562	181.562	18.2785	0.007899*	0.17769	0.177691	4.3164	0.173343
$X_1 X_2$	1	14.000	14.000	1.4094	0.288475	4.17581	4.175813	101.4365	0.009715*
$X_1 X_3$	1	14.130	14.130	1.4225	0.286501	0.46436	0.464363	11.2801	0.078372
$X_2 X_3$	1	25.573	25.573	2.5745	0.169502	0.82189	0.821890	19.9649	0.046614*
Lack of fit	3	39.406	13.135	2.5606	0.293257	0.68841	0.229471	5.5742	0.155876
Pure error	2	10.259				0.08233	0.041167		
Total	14	3190.441				23.96243			

(df) degree of freedom, (SS) sum of square, (MS) mean square, (F) Fischer test, (p) significance probability  
\* $p < 0.05$  (Statistically significant values)

The phosphorus recovery results indicate that all the factors studied in the linear forms, together with the quadratic forms of the terms  $X_1$  (pH) and  $X_3$  (P concentration), were significant ( $p < 0.05$ ) and should therefore be considered in the elaboration of the model. In addition, none of the interactions between the factors were significant, indicating that, for the high phosphorus recovery rates, the factors act in isolation, without the dependence of one in relation to the others, however, each factor is individually important for obtaining better yields in the process as a whole. Regarding the thermal decomposition of struvite, the pH ( $X_1$ ), the



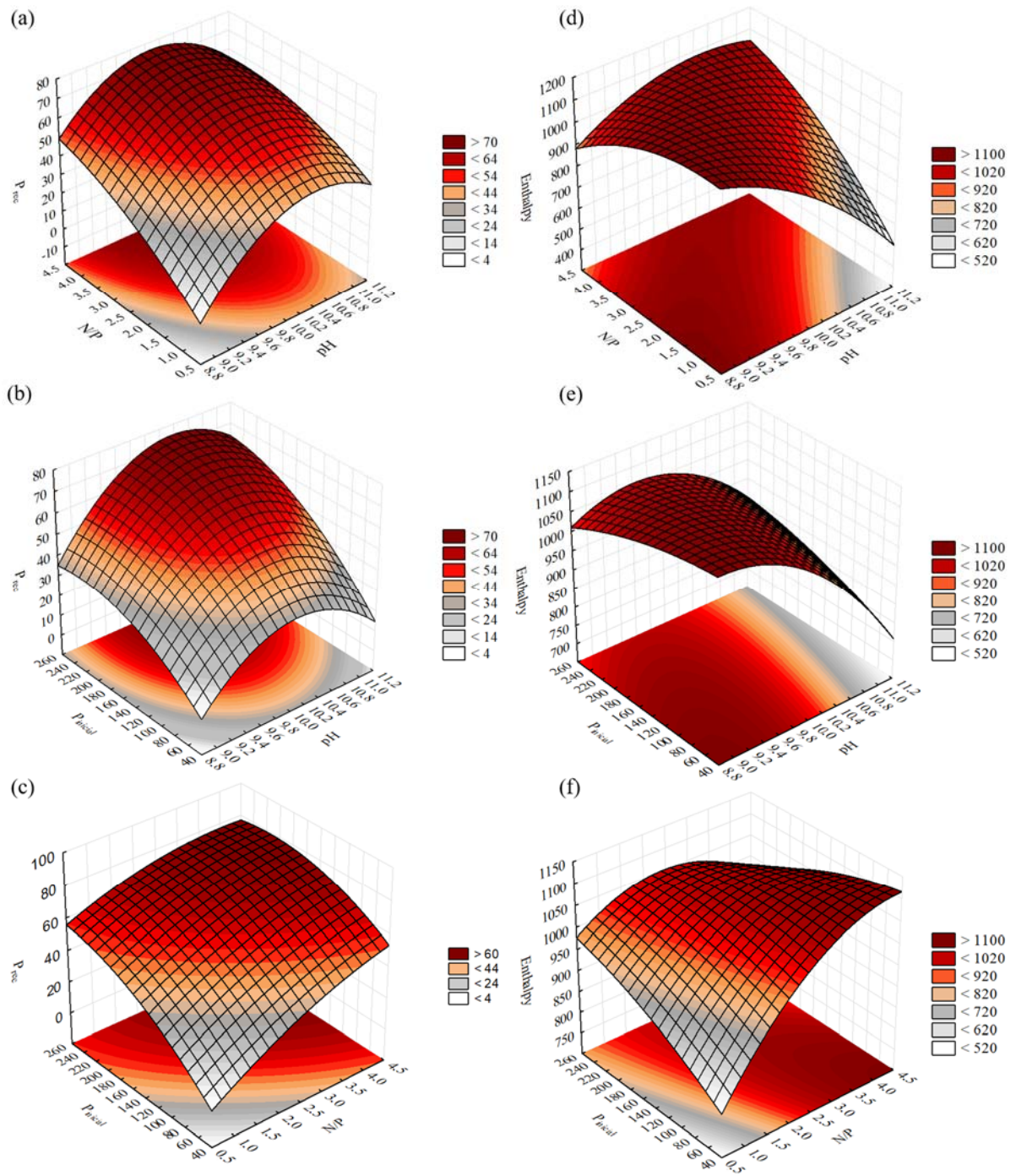
N/P ratio ( $X_2$ ), their respective second-order effects ( $X_1^2$  and  $X_2^2$ ), and the interactions between the pH and the ratio N/P ( $X_1 X_2$ ) and between the N/P ratio and the initial P concentration ( $X_2 X_3$ ) were significant. The P concentration was a noninfluential factor in its independent ( $X_3$ ) and quadratic ( $X_3^2$ ) forms; in addition, its interaction with pH ( $X_1 X_3$ ) was also not statistically significant.

Table 8 shows that the regression models proposed for both the phosphorus recovery and enthalpy variation responses did not lack fit and that their respective coefficients of multiple determination,  $R^2 = 0.985$  and  $R^2 = 0.968$ , were able to explain more than 96% of the experimental variabilities. Thus, the fitted models obtained for  $P_{rec}$  (Eq. 9) and  $\Delta H$  (Eq. 10) can predict the formation of struvite with the desired quality because, as indicated by the values of the coefficients of determination, the correlation between the experimental values and those predicted by the models is significant for both responses.

$$P_{rec} = 64.94 + 7.76X_1 - 8.17X_1^2 + 26.23X_2 + 31.60X_3 - 15.56X_3^2 \quad (9)$$

$$\Delta H = (32.65 - 1.56X_1 - 0.54X_1^2 + 1.76X_2 - 1.46X_2^2 + 2.04X_1X_2 - 1.65X_2X_3)^2 \quad (10)$$

The response surfaces of the effects of the pH ( $X_1$ ), the N/P ratio ( $X_2$ ), and the initial P concentration ( $X_3$ ) on phosphorus recovery and the enthalpy of decomposition are shown in Fig. 7. Greater phosphorus recoveries were obtained for a pH close to 10, N/P ratios equal to or greater than 4, and a P concentration equal to 250 mg/L, as shown in Fig. 7 a-c. The values determined for the pH and the N/P ratio are consistent with the results of other optimization studies on phosphorus recovery, which have shown that the pH should be higher than 9.5, and the N/P ratio should be above 2 [31,32]. The response surface graphs in Fig. 7 d-f show that for greater enthalpies of the endothermic peak indicative of struvite decomposition, the synthesis conditions should include pH values between 9 and 10, N/P ratios greater than 2.5, and phosphorus concentrations greater than 60 mg/L.



**Fig. 7.** 3D response surfaces indicating the effects of the input parameters (pH, N/P, and  $P_{initial}$ ) on phosphorus recovery (a-b-c) and the enthalpy of the endothermic peak of struvite degradation (d-e-f).

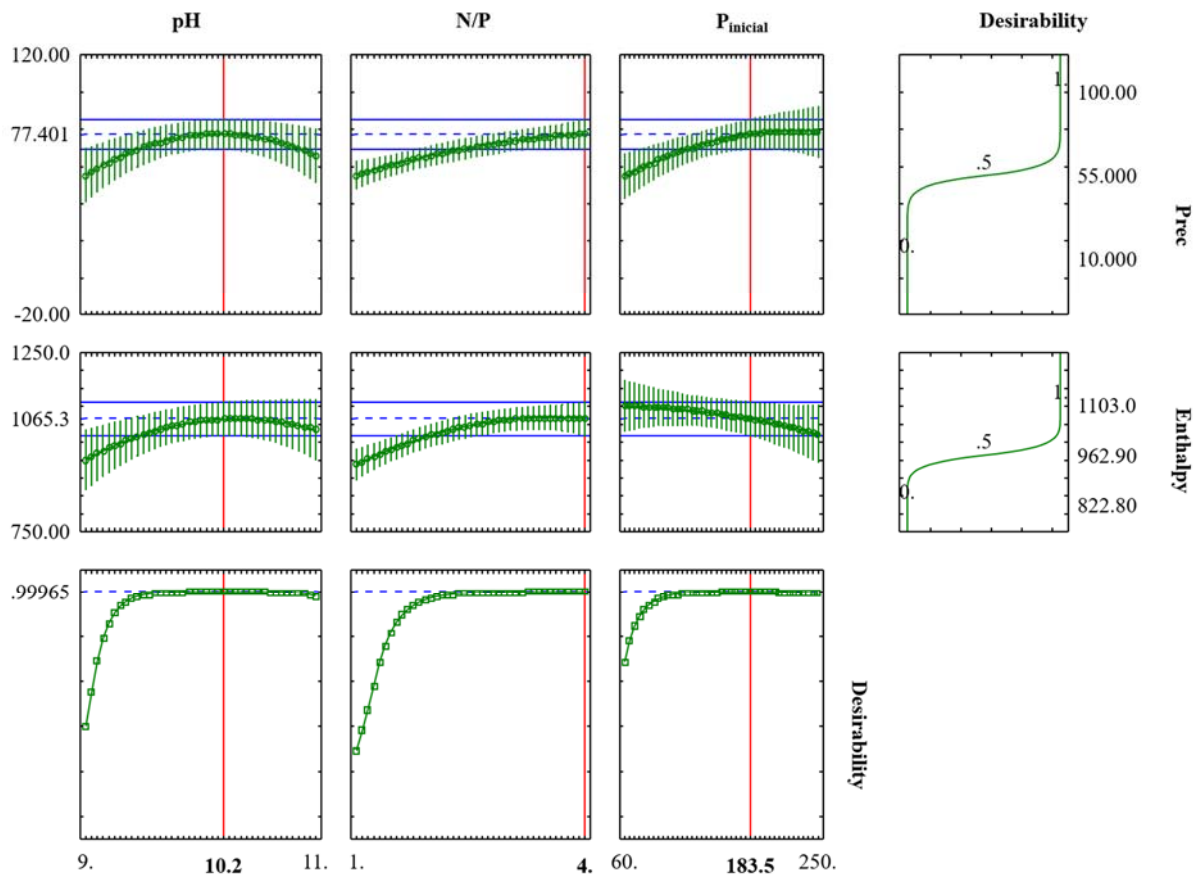
### 3.3.3.1 Simultaneous optimization

Table 9 shows the parameters used in the global desirability function for a better struvite yield, considering phosphorus recovery and the enthalpy variation of the endothermic peak, which represents the decomposition of the formed structure.

**Table 9.** Parameters assumed in the global desirability function.

Response variables	Parameters assumed in optimization				
	Low	Medium	High	s	t
$P_{\text{rec}}$ (%)	10	55	100	2	5
$\Delta H$ (J.g <sup>-1</sup> )	822.8	962.9	1103	2	5

The analysis of the global desirability function in Fig. 8 allowed us to determine the operational conditions to maximize the precipitation of struvite from wastewater. Thus, the pH should be 10.2, the molar ratio N/P should be equal to or greater than 4, and the initial phosphorus concentration should be 183.5 mg/L. The results indicate a global desirability coefficient of 0.99965, which is considered excellent [62].

**Fig. 8.** Profiles of the desirability function for the simultaneous optimization of responses.

## 4 Conclusion

A sequential experimental design methodology was applied to determine the main factors affecting the struvite precipitation process and to determine the optimal points of struvite synthesis for the recovery of nutrients in wastewater, especially phosphorus.

The Plackett-Burman screening plan showed that the most influential factors in the synthesis were the pH, the molar ratio N/P, and the initial phosphorus concentration. In addition, the presence of calcium was shown to be closely related to the formation of the amorphous phase, which makes it detrimental to the expected yield of struvite. The Mg/P and K/P ratios, together with the reaction time and the mixing rate, were not statistically significant; therefore, they did not affect the phosphorus recovery and the associated struvite precipitation.

The second-order design in the Doehlert matrix, in which only the positive significant factors were used, was used to determine an optimized experimental area and to generate regression models with a good fit for the two response variables studied ( $P_{\text{rec}}$  and  $\Delta H$ ). The RSM results show that the optimal points for a good phosphorus recovery yield are pH = 10, N/P ratio  $\geq 4$ , and  $P_{\text{initial}} = 250$  mg/L; for the formation of struvite, as described by the enthalpy variation of the endothermic peak of degradation of its structure, the optimal points of the variables are pH = 9-10, N/P ratio  $> 2.5$ , and  $P_{\text{initial}} > 60$  mg/L. In an optimization involving the two responses simultaneously, the analysis of the desirability function data indicated pH = 10.2, N/P ratio  $\geq 4$ , and  $P_{\text{initial}} = 183.5$  mg/L as optimal points.

The crystallochemical analyses of the synthesis product also demonstrated the efficiency in the formation of struvite within the optimal experimental region. The XRD results show that struvite and its potassium analog were the only phases formed under the synthesis conditions, corroborated by the FTIR and DSC-TG analyses, which showed bands and peaks characteristic of these phases.

The establishment of the main intervening factors and the optimal synthesis values and intervals can be used to determine the best yield ranges for struvite production and phosphorus recovery. Thus, this research has great importance within the global context of the environmental impacts caused by the phosphorus in wastewater and the search for alternative solutions for obtaining fertilizers.

### **Acknowledgments**

The authors thank the Brazilian agency CNPq (Conselho Nacional de Desenvolvimento Científico e Tecnológico) for the following grants: master's scholarship to the first author (131133/2019-5), Research Grand to the second author (RSA, 309176/2019-0) and funding support (MCT/CNPq/Universal No. 28/2018, 429756/2018-6). This study was also financed in part by the Coordenação de Aperfeiçoamento de Pessoal de Nível Superior - Brasil (CAPES) - Finance Code 001. We also thank the Pró-Reitoria de Pesquisa e Pós-Graduação – Universidade

Federal do Pará (PROPESP/UFPA) for funding support (EDITAL PAPQ No. 06/2021). We also thank the Graduate Program in Geology and Geochemistry of UFPA (PPGG/UFPA) for the use of its laboratories and the staff of the Laboratory of Mineral Characterization (LCM/UFPA).

## References

- [1] A. Angert, T. Weiner, S. Mazeh, F. Tamburini, E. Frossard, S.M. Bernasconi, M. Sternberg, Seasonal variability of soil phosphate stable oxygen isotopes in rainfall manipulation experiments, *Geochim. Cosmochim. Acta.* 75 (2011) 4216–4227. <https://doi.org/10.1016/j.gca.2011.05.002>.
- [2] S. Shaddel, S. Ucar, J.P. Andreassen, S.W. Sterhus, Engineering of struvite crystals by regulating supersaturation - Correlation with phosphorus recovery, crystal morphology and process efficiency, *J. Environ. Chem. Eng.* 7 (2019) 102918. <https://doi.org/10.1016/j.jece.2019.102918>.
- [3] R.L. Zimdahl, Phosphorus, in: *Six Chem. That Chang. Agric.*, Elsevier, 2015: pp. 73–88. <https://doi.org/10.1016/B978-0-12-800561-3.00005-5>.
- [4] M.D. Mullen, *Phosphorus in Soils—Biological Interactions*, 2nd ed., Elsevier Inc., 2019. <https://doi.org/10.1016/b978-0-12-409548-9.11992-x>.
- [5] E.K. Bünemann, Assessment of gross and net mineralization rates of soil organic phosphorus - a review, *Soil Biol. Biochem.* 89 (2015) 82–98. <https://doi.org/10.1016/j.soilbio.2015.06.026>.
- [6] D.M. Nash, P.M. Haygarth, B.L. Turner, L.M. Condon, R.W. McDowell, A.E. Richardson, M. Watkins, M.W. Heaven, Using organic phosphorus to sustain pasture productivity: a perspective, *Geoderma.* 221–222 (2014) 11–19. <https://doi.org/10.1016/j.geoderma.2013.12.004>.
- [7] M. Hanhoun, L. Montastruc, C. Azzaro-Pantel, B. Biscans, M. Frèche, L. Pibouleau, Temperature impact assessment on struvite solubility product: A thermodynamic modeling approach, *Chem. Eng. J.* 167 (2011) 50–58. <https://doi.org/10.1016/j.cej.2010.12.001>.
- [8] L. Peng, H. Dai, Y. Wu, Y. Peng, X. Lu, A comprehensive review of phosphorus recovery from wastewater by crystallization processes, *Chemosphere.* 197 (2018) 768–781. <https://doi.org/10.1016/j.chemosphere.2018.01.098>.
- [9] K.C. Ruttenberg, Phosphorus Cycle, *Encycl. Ocean Sci.* (2001) 2149–2162. <https://doi.org/10.1006/rwos.2001.0277>.
- [10] S. Antonini, M.A. Arias, T. Eichert, J. Clemens, Greenhouse evaluation and environmental impact assessment of different urine-derived struvite fertilizers as phosphorus sources for plants, *Chemosphere.* 89 (2012) 1202–1210. <https://doi.org/10.1016/j.chemosphere.2012.07.026>.
- [11] A.G. Capodaglio, A. Muraca, G. Becchi, Accounting for water quality effects of future urbanization: Diffuse pollution loads estimates and control in Mantua’s Lakes (Italy),

- Water Sci. Technol. 47 (2003) 291–298. <https://doi.org/10.2166/wst.2003.0701>.
- [12] M. Lang, P. Li, X. Yan, Runoff concentration and load of nitrogen and phosphorus from a residential area in an intensive agricultural watershed, *Sci. Total Environ.* 458–460 (2013) 238–245. <https://doi.org/10.1016/j.scitotenv.2013.04.044>.
- [13] D. Cordell, J.O. Drangert, S. White, The story of phosphorus: Global food security and food for thought, *Glob. Environ. Chang.* 19 (2009) 292–305. <https://doi.org/10.1016/j.gloenvcha.2008.10.009>.
- [14] V. Smil, *Phosphorus in the Environment: Natural Flows and Human Interferences*, (2000) 53–88.
- [15] C.J. Dawson, J. Hilton, Fertiliser availability in a resource-limited world: Production and recycling of nitrogen and phosphorus, *Food Policy.* 36 (2011) S14–S22. <https://doi.org/10.1016/j.foodpol.2010.11.012>.
- [16] S. van der Kooij, B.J.M. van Vliet, T.J. Stomph, N.B. Sutton, N.P.R. Anten, E. Hoffland, Phosphorus recovered from human excreta: A socio-ecological-technical approach to phosphorus recycling, *Resour. Conserv. Recycl.* 157 (2020). <https://doi.org/10.1016/j.resconrec.2020.104744>.
- [17] D. Cordell, A. Rosemarin, J.J. Schröder, A.L. Smit, Towards global phosphorus security: a systems framework for phosphorus recovery and reuse options, *Chemosphere.* 84 (2011) 747–758. <https://doi.org/10.1016/j.chemosphere.2011.02.032>.
- [18] R.W. Scholz, A.E. Ulrich, M. Eilittä, A. Roy, Sustainable use of phosphorus: A finite resource, *Sci. Total Environ.* 461–462 (2013) 799–803. <https://doi.org/10.1016/j.scitotenv.2013.05.043>.
- [19] E. Desmidt, K. Ghyselbrecht, Y. Zhang, L. Pinoy, B. Van Der Bruggen, W. Verstraete, K. Rabaey, B. Meesschaert, Global phosphorus scarcity and full-scale P-recovery techniques: A review, *Crit. Rev. Environ. Sci. Technol.* 45 (2015) 336–384. <https://doi.org/10.1080/10643389.2013.866531>.
- [20] T.H. Muster, G.B. Douglas, N. Sherman, A. Seeber, N. Wright, Y. Güzükara, Towards effective phosphorus recycling from wastewater: Quantity and quality, *Chemosphere.* 91 (2013) 676–684. <https://doi.org/10.1016/j.chemosphere.2013.01.057>.
- [21] S. Daneshgar, A. Buttafava, A. Callegari, A.G. Capodaglio, Simulations and laboratory tests for assessing phosphorus recovery efficiency from sewage sludge, *Resources.* 7 (2018). <https://doi.org/10.3390/resources7030054>.
- [22] H. Wang, Z. Tian, H. Wang, Q. Yan, Optimization and reaction kinetics analysis for phosphorus removal in struvite precipitation process, *Water Environ. Res.* 92 (2020) 1162–1172. <https://doi.org/10.1002/wer.1311>.
- [23] G. Ferraris, H. Fuess, W. Joswig, Neutron diffraction study of MgNH<sub>4</sub>PO<sub>4</sub>·6H<sub>2</sub>O (struvite) and survey of water molecules donating short hydrogen bonds, *Acta Crystallogr. Sect. B.* 42 (1986) 253–258. <https://doi.org/10.1107/S0108768186098269>.
- [24] K.S. Le Corre, E. Valsami-Jones, P. Hobbs, S.A. Parsons, Phosphorus recovery from wastewater by struvite crystallization: A review, 2009. <https://doi.org/10.1080/10643380701640573>.
- [25] B. Tansel, G. Lunn, O. Monje, Struvite formation and decomposition characteristics for

- ammonia and phosphorus recovery: A review of magnesium-ammonia-phosphate interactions, *Chemosphere*. 194 (2018) 504–514. <https://doi.org/10.1016/j.chemosphere.2017.12.004>.
- [26] P.J. Talboys, J. Heppell, T. Roose, J.R. Healey, D.L. Jones, P.J.A. Withers, Struvite: a slow-release fertiliser for sustainable phosphorus management?, *Plant Soil*. 401 (2016) 109–123. <https://doi.org/10.1007/s11104-015-2747-3>.
- [27] D.M. Morita, R.D.L. Avila, F.N. Aidar, Nucleation in the formation of struvite: State of art, *Eng. Sanit. e Ambient*. 24 (2019) 637–654. <https://doi.org/10.1590/s1413-41522019113711>.
- [28] S. Daneshgar, A. Buttafava, D. Capsoni, A. Callegari, A.G. Capodaglio, Impact of pH and ionic molar ratios on phosphorous forms precipitation and recovery from different wastewater sludges, *Resources*. 7 (2018). <https://doi.org/10.3390/resources7040071>.
- [29] R.V.S.S.N. Ravikumar, A. V. Chandrasekhar, C. Ramakrishna, Y.P. Reddy, X-ray powder diffraction, thermal analysis and IR studies of zinc ammonium phosphate hexahydrate, *Optoelectron. Adv. Mater. Rapid Commun*. 4 (2010) 215–219.
- [30] R. Kumar, P. Pal, Turning hazardous waste into value-added products: Production and characterization of struvite from ammoniacal waste with new approaches, *J. Clean. Prod*. 43 (2013) 59–70. <https://doi.org/10.1016/j.jclepro.2013.01.001>.
- [31] A. Capdevielle, E. Sýkorová, B. Biscans, F. Béline, M.L. Daumer, Optimization of struvite precipitation in synthetic biologically treated swine wastewater-Determination of the optimal process parameters, *J. Hazard. Mater*. 244–245 (2013) 357–369. <https://doi.org/10.1016/j.jhazmat.2012.11.054>.
- [32] S. Daneshgar, P.A. Vanrolleghem, C. Vaneekhaute, A. Buttafava, A.G. Capodaglio, Optimization of P compounds recovery from aerobic sludge by chemical modeling and response surface methodology combination, *Sci. Total Environ*. 668 (2019) 668–677. <https://doi.org/10.1016/j.scitotenv.2019.03.055>.
- [33] M.M. Thant Zin, D.J. Kim, Struvite production from food processing wastewater and incinerated sewage sludge ash as an alternative N and P source: Optimization of multiple resources recovery by response surface methodology, *Process Saf. Environ. Prot*. 126 (2019) 242–249. <https://doi.org/10.1016/j.psep.2019.04.018>.
- [34] W.G. Box, George E. P.; Hunter J. Stuart; Hunter, *Statistics for Experimenters: Design, Innovation, and Discovery* by George E. P. Box; J. Stuart Hunter; William G. Hunter, 2nd ed., New York, 2005.
- [35] B. Li, H.M. Huang, I. Boiarkina, W. Yu, Y.F. Huang, G.Q. Wang, B.R. Young, Phosphorus recovery through struvite crystallisation: Recent developments in the understanding of operational factors, *J. Environ. Manage*. 248 (2019) 109254. <https://doi.org/10.1016/j.jenvman.2019.07.025>.
- [36] S. Polat, P. Sayan, Application of response surface methodology with a Box–Behnken design for struvite precipitation, *Adv. Powder Technol*. 30 (2019) 2396–2407. <https://doi.org/10.1016/j.apt.2019.07.022>.

- [37] H. Ebrahimi-Najafabadi, R. Leardi, M. Jalali-Heravi, Experimental design in analytical chemistry -Part I: Theory, *J. AOAC Int.* 97 (2014) 3–11. <https://doi.org/10.5740/jaoacint.SGEEbrahimi1>.
- [38] S.L.C. Ferreira, W.N.L. Dos Santos, C.M. Quintella, B.B. Neto, J.M. Bosque-Sendra, Doehlert matrix: A chemometric tool for analytical chemistry - Review, *Talanta*. 63 (2004) 1061–1067. <https://doi.org/10.1016/j.talanta.2004.01.015>.
- [39] A. Ouejhani, F. Hellal, M. Dachraoui, G. Lallevé, J.F. Fauvarque, Application of Doehlert matrix to the study of electrochemical oxidation of Cr(III) to Cr(VI) in order to recover chromium from wastewater tanning baths, *J. Hazard. Mater.* 157 (2008) 423–431. <https://doi.org/10.1016/j.jhazmat.2008.01.046>.
- [40] S. Gražulis, D. Chateigner, R.T. Downs, A.F.T. Yokochi, M. Quirós, L. Lutterotti, E. Manakova, J. Butkus, P. Moeck, A. Le Bail, Crystallography Open Database - An open-access collection of crystal structures, *J. Appl. Crystallogr.* 42 (2009) 726–729. <https://doi.org/10.1107/S0021889809016690>.
- [41] M. Mathew, L.W. Schroeder, Crystal structure of a struvite analogue,  $\text{MgKPO}_4 \cdot 6\text{H}_2\text{O}$ , *Acta Crystallogr. Sect. B Struct. Crystallogr. Cryst. Chem.* 35 (1979) 11–13. <https://doi.org/10.1107/s0567740879002429>.
- [42] R.C. de S. Meira, S.P.A. da Paz, J.A.M. Corrêa, XRD-Rietveld analysis as a tool for monitoring struvite analog precipitation from wastewater: P, Mg, N and K recovery for fertilizer production, *J. Mater. Res. Technol.* 9 (2020) 15202–15213. <https://doi.org/10.1016/j.jmrt.2020.10.082>.
- [43] H. Huang, D. Xiao, J. Liu, L. Hou, L. Ding, Recovery and removal of nutrients from swine wastewater by using a novel integrated reactor for struvite decomposition and recycling, *Sci. Rep.* 5 (2015) 1–13. <https://doi.org/10.1038/srep10183>.
- [44] F. Abbona, H.E.L. Madsen, R. Boistelle, The initial phases of calcium and magnesium phosphates precipitated from solutions of high to medium concentrations, *J. Cryst. Growth.* 74 (1986) 581–590. [https://doi.org/10.1016/0022-0248\(86\)90205-8](https://doi.org/10.1016/0022-0248(86)90205-8).
- [45] E. V Musvoto, M.C.M. Wentzel, G.A.M. Ekama, Integrated chemical-physica process modelling-II. Simulating aeration treatment of anaerobic digester supernatants, 34 (2000) 1868–1880.
- [46] D. Crutchik, J.M. Garrido, Struvite crystallization versus amorphous magnesium and calcium phosphate precipitation during the treatment of a saline industrial wastewater, *Water Sci. Technol.* 64 (2011) 2460–2467. <https://doi.org/10.2166/wst.2011.836>.
- [47] L. Hu, J. Yu, H. Luo, H. Wang, P. Xu, Y. Zhang, Simultaneous recovery of ammonium, potassium and magnesium from produced water by struvite precipitation, *Chem. Eng. J.* 382 (2020) 123001. <https://doi.org/10.1016/j.cej.2019.123001>.
- [48] V. Stefov, B. Šoptrajanov, I. Kuzmanovski, H.D. Lutz, B. Engelen, Infrared and Raman spectra of magnesium ammonium phosphate hexahydrate (struvite) and its isomorphous analogues. III. Spectra of protiated and partially deuterated magnesium ammonium phosphate hexahydrate, *J. Mol. Struct.* 752 (2005) 60–67. <https://doi.org/10.1016/j.molstruc.2005.05.040>.



- [49] C.K. Chauhan, M.J. Joshi, In vitro crystallization, characterization and growth-inhibition study of urinary type struvite crystals, *J. Cryst. Growth.* 362 (2013) 330–337. <https://doi.org/10.1016/j.jcrysgro.2011.11.008>.
- [50] V.B. Suryawanshi, R.T. Chaudhari, Synthesis and Characterization of Struvite-k Crystals by Agar Gel, *J. Cryst. Process Technol.* 04 (2014) 212–224. <https://doi.org/10.4236/jcpt.2014.44026>.
- [51] A. Cahil, M. Najdoski, V. Stefov, Infrared and Raman spectra of magnesium ammonium phosphate hexahydrate (struvite) and its isomorphous analogues. IV. FTIR spectra of protiated and partially deuterated nickel ammonium phosphate hexahydrate and nickel potassium phosphate hexahydrate, *J. Mol. Struct.* 834–836 (2007) 408–413. <https://doi.org/10.1016/j.molstruc.2006.11.049>.
- [52] L. Wei, T. Hong, Z. Hu, L. Luo, Q. Zhang, T. Chen, Modeling surface acid-base properties of struvite crystals synthesized in aqueous solution, *Colloids Surfaces A Physicochem. Eng. Asp.* 553 (2018) 237–243. <https://doi.org/10.1016/j.colsurfa.2018.05.035>.
- [53] P. V. Campos, A.R.L. Albuquerque, R.S. Angélica, S.P.A. Paz, FTIR spectral signatures of amazon inorganic phosphates: Igneous, weathering, and biogenetic origin, *Spectrochim. Acta - Part A Mol. Biomol. Spectrosc.* 251 (2021) 119476. <https://doi.org/10.1016/j.saa.2021.119476>.
- [54] S. Zhang, H.S. Shi, S.W. Huang, P. Zhang, Dehydration characteristics of struvite-K pertaining to magnesium potassium phosphate cement system in non-isothermal condition, *J. Therm. Anal. Calorim.* 111 (2013) 35–40. <https://doi.org/10.1007/s10973-011-2170-9>.
- [55] R. Frost, M. Weier, K. Erickson, Thermal decomposition of struvite, *J. Therm. Anal. Calorim.* 76 (2004). <https://doi.org/10.1023/B:JTAN.0000032287.08535.b3>.
- [56] M.I.H. Bhuiyan, D.S. Mavinic, F.A. Koch, Thermal decomposition of struvite and its phase transition, *Chemosphere.* 70 (2008) 1347–1356. <https://doi.org/10.1016/j.chemosphere.2007.09.056>.
- [57] S. Farhana, Thermal decomposition of Struvite : a Novel Approach to Recover Ammonia from Wastewater Using Struvite Decomposition Products, 2015.
- [58] B.E.I. Abdelrazig, J.H. Sharp, Phase changes on heating ammonium magnesium phosphate hydrates, *Thermochim. Acta.* 129 (1988) 197–215. [https://doi.org/10.1016/0040-6031\(88\)87336-2](https://doi.org/10.1016/0040-6031(88)87336-2).
- [59] J. Hövelmann, T.M. Stawski, R. Besselink, H.M. Freeman, K.M. Dietmann, S. Mayanna, B.R. Pauw, L.G. Benning, A template-free and low temperature method for the synthesis of mesoporous magnesium phosphate with uniform pore structure and high surface area, *Nanoscale.* 11 (2019) 6939–6951. <https://doi.org/10.1039/c8nr09205b>.
- [60] A. Kozik, N. Hutnik, K. Piotrowski, A. Mazieniczuk, A. Matynia, Precipitation and Crystallization of Struvite from Synthetic Wastewater under Stoichiometric Conditions, *Adv. Chem. Eng. Sci.* 03 (2013) 20–26. <https://doi.org/10.4236/aces.2013.34b004>.
- [61] A.P. Bayuseno, D.S. Perwitasari, S. Muryanto, M. Tauviqirrahman, J. Jamari, Kinetics and morphological characteristics of struvite ( $\text{MgNH}_4\text{PO}_4 \cdot 6\text{H}_2\text{O}$ ) under the influence of

- maleic acid, *Heliyon*. 6 (2020). <https://doi.org/10.1016/j.heliyon.2020.e03533>.
- [62] Z. Lazić, *Design of Experiments in Chemical Engineering: A Practical Guide*, 2004. <https://doi.org/10.1002/3527604162>.

## 6 CONSIDERAÇÕES FINAIS

Propostas avançadas relacionadas a caracterização química e estrutural, e otimização de processo concernentes a fosfatos foram estabelecidas com base em dois métodos: um analítico (espectroscopia IV) e outro físico-químico (precipitação).

Fosfatos de origem natural, característicos de diferentes localidades da região amazônica, foram qualificados por meio de uma diferenciação genética através do uso da técnica de FTIR. Espectros nas regiões MIR e NIR foram gerados e suas respostas permitiram a determinação das faixas espectrais características das bandas referentes ao grupo fosfato, além de identificar outros grupos funcionais como o  $(\text{CO}_3)^{2-}$  em fosfatos de origem ígnea, o  $\text{Al}_2\text{OH}$  e  $\text{SiO}$  em fosfatos intempéricos e  $\text{NH}_4$  e componentes de Fe nos fosfatos de origem biogenética. Essas informações específicas de cada material permitiram iniciar um banco de dados espectral de FTIR de fosfatos amazônicos, que pode vir a ser de grande utilidade no desenvolvimento de outras pesquisas relacionadas aos fosfatos ou mesmo como uma ferramenta de qualificação de fosfatos dentro do setor industrial.

Uma rota de síntese alternativa e sustentável foi otimizada através de uma metodologia de planejamento experimental sequencial, promovendo assim a recuperação secundária de fosfatos de águas residuais através da precipitação de estruvita. Um planejamento Plackett-Burman definiu estatisticamente a importância do pH, da razão N/P e da concentração inicial de fósforo na obtenção de estruvita, além disso mostrou que a presença de outros íons como o Ca é prejudicial dentro do sistema de síntese. O planejamento de segunda ordem de Doehlert especificou os pontos ótimos de síntese através da aplicação da metodologia de superfície de resposta e da função desejabilidade, gerando assim modelos empíricos baseados por mínimos quadrados.

Tanto o banco de dados de respostas espectrais de FTIR quanto a otimização da síntese de estruvita a partir de águas residuais são tidas como potenciais ferramentas no estudo pertinente aos fosfatos. Essas informações contribuem positivamente no uso sustentável dos recursos fosfáticos e na busca por soluções alternativas para a produção de fertilizantes.

## REFERÊNCIAS

- 4500-P Phosphorus. 2018. In: Rice E. W., Baird R. B., Eaton A. D. *Standard methods for the examination of water and wastewater*. American Public Health Association. <https://doi.org/doi:10.2105/SMWW.2882.093>.
- Aage H. K., Andersen B. L., Blom A., Jensen, I. 1997. The solubility of struvite. *Journal of Radioanalytical and Nuclear Chemistry*, **223**:213–215. <https://doi.org/10.1007/BF02223387>.
- Abbona F. & Boistelle R. 1979. Growth morphology and crystal habit of struvite crystals ( $\text{MgNH}_4\text{PO}_4 \cdot 6\text{H}_2\text{O}$ ). *Journal of Crystal Growth*, **46**:339–354.
- Abbona F., Lundager Madsen H. E., Boistelle R. 1982. Crystallization of two magnesium phosphates, struvite and newberyite: Effect of pH and concentration. *Journal of Crystal Growth*, **57**:6–14. [https://doi.org/10.1016/0022-0248\(82\)90242-1](https://doi.org/10.1016/0022-0248(82)90242-1).
- Abbona, F. Madsen, H. E. L., Boistelle R. 1986. The initial phases of calcium and magnesium phosphates precipitated from solutions of high to medium concentrations. *Journal of Crystal Growth*, **74**:581–590. [https://doi.org/10.1016/0022-0248\(86\)90205-8](https://doi.org/10.1016/0022-0248(86)90205-8).
- Achat D. L., Daumer M. L., Sperandio M., Santellani A. C., Morel C. 2014. Solubility and mobility of phosphorus recycled from dairy effluents and pig manures in incubated soils with different characteristics. *Nutrient Cycling in Agroecosystems*, **99**. <https://doi.org/10.1007/s10705-014-9614-0>.
- Adnan A., Mavinic D. S., Koch F. A. 2003. Pilot-scale study of phosphorus recovery through struvite crystallization examining the process feasibility. *Journal of Environmental Engineering and Science*, **2**:315–324. <https://doi.org/10.1139/s03-040>.
- Aidar F. N. 2012. *Fatores intervenientes na cristalização da estruvita para a recuperação do fósforo de esgoto*. PhD Thesis, Universidade de São Paulo, São Paulo, 137 p. Disponível em: *Teses.Usp.Br*. <http://www.teses.usp.br/teses/disponiveis/3/3147/tde-16072013-164846/en.php>.
- Ali M. I. & Schneider P. A. 2008. An approach of estimating struvite growth kinetic incorporating thermodynamic and solution chemistry, kinetic and process description. *Chemical Engineering Science*, **63**:3514–3525. <https://doi.org/10.1016/j.ces.2008.04.023>.
- Angert A., Weiner T., Mazeh S., Tamburini F., Frossard E., Bernasconi S. M., Sternberg M. 2011. Seasonal variability of soil phosphate stable oxygen isotopes in rainfall manipulation experiments. *Geochimica et Cosmochimica Acta*, **75**:4216–4227. <https://doi.org/10.1016/j.gca.2011.05.002>.
- Antonini S., Arias M. A., Eichert T., Clemens J. 2012. Greenhouse evaluation and environmental impact assessment of different urine-derived struvite fertilizers as phosphorus sources for plants. *Chemosphere*, **89**:1202–1210. <https://doi.org/10.1016/j.chemosphere.2012.07.026>.
- Ariyanto E., Ang H. M., Sem T. K. 2014. Impact of various physico-chemical parameters on spontaneous nucleation of struvite ( $\text{MgNH}_4\text{PO}_4 \cdot 6\text{H}_2\text{O}$ ) formation in a wastewater treatment plant: kinetic and nucleation mechanism. *Desalination and Water Treatment*, **52**:34–36, 6620–6631. <https://doi.org/10.1080/19443994.2013.821042>.

- Attfeld J.P. 2001. Phosphate anions. *In: Mahajan S. Encyclopedia of materials: science and technology*. First Edition, **5**:1–6. Amsterdam; New York, Elsevier.
- Babić-Ivančić V., Kontrec J., Brečević L., Kralj D. 2006. Kinetics of struvite to newberyite transformation in the precipitation system  $\text{MgCl}_2\text{-NH}_4\text{H}_2\text{PO}_4\text{-NaOH-H}_2\text{O}$ . *Water Research*, **40**:3447–3455. <https://doi.org/10.1016/j.watres.2006.07.026>.
- Babić-Ivančić V., Kontrec J., Kralj D., Brečević L. 2002. Precipitation diagrams of struvite and dissolution kinetics of different struvite morphologies. *Croatica Chemica Acta*, **75**:89–106.
- Battistoni P., Pavan P., Prisciandaro M., Cecchi F. 2000. Struvite crystallization: A feasible and reliable way to fix phosphorus in anaerobic supernatants. *Water Research*, **34**:3033–3041. [https://doi.org/10.1016/S0043-1354\(00\)00045-2](https://doi.org/10.1016/S0043-1354(00)00045-2).
- Bendoricchio G., Di Luzio M., Baschieri P., Capodaglio A. G. 1993. Diffuse pollution in the Lagoon of Venice. *Water Science and Technology*, **28**:69–78. <https://doi.org/10.2166/wst.1993.0405>.
- Bhuiyan M. I. H., Mavinic D. S., Koch F. A. 2008. Thermal decomposition of struvite and its phase transition. *Chemosphere*, **70**:1347–1356. <https://doi.org/10.1016/j.chemosphere.2007.09.056>.
- Bitton G. 2010. *Wastewater microbiology*. Fourth Edition p. 119–17). <https://doi.org/10.1002/9780470901243.ch4>.
- Booker N. A., Priestley A. J., Fraser I. H. 1999. Struvite formation in wastewater treatment plants: opportunities for nutrient recovery. *Environmental Technology (United Kingdom)*, **20**:777–782. <https://doi.org/10.1080/09593332008616874>.
- Borgerding J. 1972. Phosphate deposits in digestion systems. *Journal of the Water Pollution Control Federation*, **44**:813–819.
- Bouropoulos N. C. & Koutsoukos P. G. 2000. Spontaneous precipitation of struvite from aqueous solutions. *Journal of Crystal Growth*, **213**:381–388. [https://doi.org/10.1016/S0022-0248\(00\)00351-1](https://doi.org/10.1016/S0022-0248(00)00351-1).
- Bünemann E. K. 2015. Assessment of gross and net mineralization rates of soil organic phosphorus - A review. *Soil Biology and Biochemistry*, **89**:82–98. <https://doi.org/10.1016/j.soilbio.2015.06.026>.
- Cabeza R., Steingrobe B., Römer W., Claassen N. 2011. Effectiveness of recycled P products as P fertilizers, as evaluated in pot experiments. *Nutrient Cycling in Agroecosystems*, **91**:173–184. <https://doi.org/10.1007/s10705-011-9454-0>.
- Capodaglio A. G., Muraca A., Becchi G. 2003. Accounting for water quality effects of future urbanization: Diffuse pollution loads estimates and control in Mantua's Lakes (Italy). *Water Science and Technology*, **47**:291–298. <https://doi.org/10.2166/wst.2003.0701>.
- Carballa M., Moerman W., Windt W., Grootaerd H., Verstraete W. 2009. Strategies to optimize phosphate removal from industrial anaerobic effluents by magnesium ammonium phosphate (MAP) production. *Journal of Chemical Technology and Biotechnology*, **84**:63–68. <https://doi.org/10.1002/jctb.2006>.

- Carey R. O. & Migliaccio K. W. 2009. Contribution of wastewater treatment plant effluents to nutrient dynamics in aquatic systems. *Environmental Management*, **44**:205–217. <https://doi.org/10.1007/s00267-009-9309-5>.
- Castro S. R. 2014. *Precipitação de estruvita: recuperação de nitrogênio e fósforo utilizando fontes alternativas de reagentes*. PhD Thesis, Universidade Federal de Minas Gerais, Belo Horizonte, 157 p.
- Çelen I., Buchanan J. R., Burns R. T., Bruce Robinson R., Raj Raman D. 2007. Using a chemical equilibrium model to predict amendments required to precipitate phosphorus as struvite in liquid swine manure. *Water Research*, **41**:1689–1696. <https://doi.org/10.1016/j.watres.2007.01.018>.
- Chatterjee P., Chakraborty A., Mukherjee A. K. 2018. Phase composition and morphological characterization of human kidney stones using IR spectroscopy, scanning electron microscopy and X-ray Rietveld analysis. *Spectrochimica Acta - Part A: Molecular and Biomolecular Spectroscopy*, **200**:33–42. <https://doi.org/10.1016/j.saa.2018.04.005>.
- Condron L. M., Turner B. L., Cade-Menun B. J. 2015. *Chemistry and Dynamics of Soil Organic Phosphorus*. **46**:87–121. <https://doi.org/10.2134/agronmonogr46.c4>.
- Cordell D., Drangert J. O., White S. 2009. The story of phosphorus: Global food security and food for thought. *Global Environmental Change*, **19**:292–305. <https://doi.org/10.1016/j.gloenvcha.2008.10.009>.
- Daneshgar S., Buttafava A., Callegari A., Capodaglio A. G. 2019. Economic and energetic assessment of different phosphorus recovery options from aerobic sludge. *Journal of Cleaner Production*, **223**:729–738. <https://doi.org/10.1016/j.jclepro.2019.03.195>.
- Daneshgar S., Buttafava A., Capsoni D., Callegari A., Capodaglio A. G. 2018. Impact of pH and ionic molar ratios on phosphorous forms precipitation and recovery from different wastewater sludges. *Resources*, **7**. <https://doi.org/10.3390/resources7040071>.
- Dar S. A. & Khan K. F. 2017. Sedimentary: phosphates. *Earth Systems and Environmental Sciences*, Issue November, 2016. Elsevier Inc. <https://doi.org/10.1016/B978-0-12-409548-9.10509-3>.
- Desmidt E., Ghyselbrecht K., Zhang Y., Pinoy L., Van Der Bruggen B., Verstraete W., Rabaey K., Meesschaert B. 2015. Global phosphorus scarcity and full-scale P-recovery techniques: A review. *Critical Reviews in Environmental Science and Technology*, **45**:336–384. <https://doi.org/10.1080/10643389.2013.866531>.
- Doyle J. D., Oldring K., Churchley J., Price C., Parsons S. A. 2003. Chemical control of struvite precipitation. *Journal of Environmental Engineering*, **129**:419–426. [https://doi.org/10.1061/\(ASCE\)0733-9372\(2003\)129:5\(419\)](https://doi.org/10.1061/(ASCE)0733-9372(2003)129:5(419)).
- Durrant A. E., Scrimshaw M. D., Stratful I., Lester J. N. 1999. Review of the feasibility of recovering phosphate from wastewater for use as a raw material by the phosphate industry. *Environmental Technology (United Kingdom)*, **20**:749–758. <https://doi.org/10.1080/09593332008616870>.
- Elliot J. S., Quaide W. L., Sharp R. F., Lewis L. 1958. Mineralogical studies of urine: the relationship of apatite, brushite and struvite to urinary pH. *The Journal of Urology*,

**80**:269–271. [https://doi.org/10.1016/S0022-5347\(17\)66177-9](https://doi.org/10.1016/S0022-5347(17)66177-9).

Etter B., Tilley E., Khadka R., Udert K. M. 2011. Low-cost struvite production using source-separated urine in Nepal. *Water Research*, **45**:852–862. <https://doi.org/10.1016/j.watres.2010.10.007>.

Farhana S. 2015. *Thermal decomposition of struvite: a novel approach to recover Ammonia from Wastewater Using Struvite Decomposition Products*.

Fattah K. P. 2004. *Pilot scale struvite recovery potential from centrate at Lulu Island Wastewater Treatment Plant* (Issue August).

Fattah K. P., Mavinic D. S., Koch F. A., Jacob C. 2008. Determining the feasibility of phosphorus recovery as struvite from filter press centrate in a secondary wastewater treatment plant. *Journal of Environmental Science and Health - Part A Toxic/Hazardous Substances and Environmental Engineering*, **43**:756–764. <https://doi.org/10.1080/10934520801960052>.

Ferraris G., Fuess H., Joswig W. 1986. Neutron diffraction study of  $\text{MgNH}_4\text{PO}_4 \cdot 6\text{H}_2\text{O}$  (struvite) and survey of water molecules donating short hydrogen bonds. *Acta Crystallographica Section B*, **42**:253–258. <https://doi.org/10.1107/S0108768186098269>.

Forrest A. L., Fattah K. P., Mavinic D. S., Koch F. A. 2008. Optimizing struvite production for phosphate recovery in WWTP. *Journal of Environmental Engineering*, **134**:395–402. [https://doi.org/10.1061/\(ASCE\)0733-9372\(2008\)134:5\(395\)](https://doi.org/10.1061/(ASCE)0733-9372(2008)134:5(395)).

Frost R., Weier M., Erickson K. 2004. Thermal decomposition of struvite. *Journal of Thermal Analysis and Calorimetry*, **76**. <https://doi.org/10.1023/B:JTAN.0000032287.08535.b3>.

Haldar S. K. & Tišljarić J. 2014. Basic mineralogy. In: Haldar S. K. & Tišljarić J. *Introduction to mineralogy and petrology*. <https://doi.org/10.1016/b978-0-12-408133-8.00002-x>.

Hama P. & Zucchini R. 2011. *Certificado de material de referência N° 1908-103* p. 1–3.

He G. X., He L. H., Zhao Z. W., Chen X. Y., Gao L. L., Liu X. H. 2013. Thermodynamic study on phosphorus removal from tungstate solution via magnesium salt precipitation method. *Transactions of Nonferrous Metals Society of China* (English Edition), **23**:3440–3447. [https://doi.org/10.1016/S1003-6326\(13\)62886-1](https://doi.org/10.1016/S1003-6326(13)62886-1).

Huang H., Xiao D., Liu J., Hou L., Ding L. 2015. Recovery and removal of nutrients from swine wastewater by using a novel integrated reactor for struvite decomposition and recycling. *Scientific Reports*, **5**:1–13. <https://doi.org/10.1038/srep10183>.

Huang L. M., Jia X. X., Zhang G. L., Shao M. A. 2017. Soil organic phosphorus transformation during ecosystem development: a review. *Plant and Soil*, **417**:1–2, 17–42. <https://doi.org/10.1007/s11104-017-3240-y>.

Huygens D., Saveyn H. G. M., Tonini D., Eder P., Delgado Sancho L. 2019. Technical proposals for selected new fertilising materials under the Fertilising Products Regulation (Regulation (EU) 2019/1009). *FeHPO CaHPO*. <https://doi.org/10.2760/186684>.

Jones A. G. 2002. *Crystallization process systems*. Oxford, UK, Butterworth-Heinemann, ISBN 9780750655200. <https://doi.org/10.1016/B978-075065520-0/50010-9>.

Kofina A. & Koutsoukos P. 2005. Spontaneous precipitation of struvite from synthetic

- wastewater solutions. *Crystal Growth & Design-Cryst Growth Des*, **5**. <https://doi.org/10.1021/cg049803e>.
- Langergraber G. & Muellegger E. 2005. Ecological sanitation - a way to solve global sanitation problems? *Environment International*, **31**:433–444. <https://doi.org/10.1016/j.envint.2004.08.006>.
- Laridi R., Auclair J. C., Benmoussa H. 2005. Laboratory and pilot-scale phosphate and ammonium removal by controlled struvite precipitation following coagulation and flocculation of swine wastewater. *Environmental Technology*, **26**:525–536. <https://doi.org/10.1080/09593332608618533>.
- Le Corre K. S. 2006. *Understanding struvite crystallisation and recovery* (Issue October). PhD Thesis, Cranfield University, United Kingdom, 211 p.
- Le Corre K. S., Valsami-Jones E., Hobbs P., Parsons S. A. 2007. Kinetics of struvite precipitation: effect of the magnesium dose on induction times and precipitation rates. *Environmental Technology*, **28**:1317–1324. <https://doi.org/10.1080/09593332808618891>.
- Le Corre K. S., Valsami-Jones E., Hobbs P., Parsons S. A. 2009. Phosphorus recovery from wastewater by struvite crystallization: a review. *Critical Reviews in Environmental Science and Technology*. **39**. <https://doi.org/10.1080/10643380701640573>.
- Li B., Boiarkina I., Yu W., Huang H. M., Munir T., Wang G. Q., Young B. R. 2019. Phosphorous recovery through struvite crystallization: challenges for future design. *Science of the Total Environment*, **648**:1244–1256. <https://doi.org/10.1016/j.scitotenv.2018.07.166>.
- Loewenthal R. E., Kornmüller U. R. C., van Heerden E. P. 1994. Modelling struvite precipitation in anaerobic treatment systems. *Water Science and Technology*, **30**:107–116. <https://doi.org/10.2166/wst.1994.0592>
- Mayer B. K., Baker L. A., Boyer T. H., Drechsel P., Gifford M., Hanjra M. A., Parameswaran P., Stoltzfus J., Westerhoff P., Rittmann B. E. 2016. Total value of phosphorus recovery. *Environmental Science and Technology*, **50**:6606–6620. <https://doi.org/10.1021/acs.est.6b01239>.
- Mehta C. M. & Batstone D. J. 2013. Nucleation and growth kinetics of struvite crystallization. *Water Research*, **47**:2890–2900. <https://doi.org/10.1016/j.watres.2013.03.007>.
- Meira R. C. S. 2020. *Otimização da síntese de estruvita e seus análogos visando a recuperação de fósforo, magnésio, nitrogênio e potássio de águas residuais*. PhD Thesis, Universidade Federal do Pará, Belém, 129 p.
- Morita D. M., Avila R. D. L., Aida F. N. 2019. Nucleation in the formation of struvite: State of art. *Engenharia Sanitaria e Ambiental*, **24**:637–654. <https://doi.org/10.1590/s1413-41522019113711>.
- Mullen M. D. 2019. Phosphorus in soils-biological interactions. In: Elias S. A. *Reference module in earth systems and environmental sciences*. 2nd ed. Issue November. Elsevier Inc. <https://doi.org/10.1016/b978-0-12-409548-9.11992-x>.
- Münch E. V. & Barr K. 2001. Controlled struvite crystallisation for removing phosphorus from anaerobic digester sidestreams. *Water Research*, **35**:151–159.



[https://doi.org/10.1016/S0043-1354\(00\)00236-0](https://doi.org/10.1016/S0043-1354(00)00236-0).

Muster T. H., Douglas G. B., Sherman N., Seeber A., Wright N., Güzükara Y. 2013. Towards effective phosphorus recycling from wastewater: quantity and quality. *Chemosphere*, **91**:676–684. <https://doi.org/10.1016/j.chemosphere.2013.01.057>.

Negrea A., Lupa L., Negrea P., Ciopec M., Muntean C. 2010. Simultaneous removal of ammonium and phosphate ions from wastewaters and characterization of the resulting Product. *Chemical Bulletin of "Politehnica" Univ.*, **55**:136–142.

Novotny C. 2011. *Ammonia removal and recovery using heated struvite as an adsorbent* (Issue February). <https://circle.ubc.ca/handle/2429/31595>.

Ohlinger K. N., Young T. M., Schroeder E. D. 1998. Predicting struvite formation in digestion. *Water Research*, **32**:3607–3614. [https://doi.org/10.1016/S0043-1354\(98\)00123-7](https://doi.org/10.1016/S0043-1354(98)00123-7).

Parsons S. A. & Doyle J. D. 2002. Struvite formation, control and recovery. *Water Research*, **36**:3925–3940.

Paz S.P.A., Torres P.W.T.S., Angélica R.S., Kahn, H. 2017. Synthesis, rietveld refinement and DSC analysis of Al-goethites to support mineralogical quantification of gibbsitic bauxites. *J Therm Anal Calorim* **128**, 841–854. <https://doi.org/10.1007/s10973-016-5987-4>

Ptáček P. 2016. Phosphate rocks. In: Ptáček P. *Apatites and their synthetic analogues - synthesis, structure, properties and applications*. (BoD–Books on Demand). **1**:13. InTech. <https://doi.org/10.5772/62214>.

Rahaman M. S., Ellis N., Mavinic D. S. 2008. Effects of various process parameters on struvite precipitation kinetics and subsequent determination of rate constants. *Water Science and Technology*, **57**:647–654. <https://doi.org/10.2166/wst.2008.022>.

Rahman M. M., Salleh M. A. M., Rashid U., Ahsan A., Hossain M. M., Ra C. S. 2014. Production of slow release crystal fertilizer from wastewaters through struvite crystallization - a review. *Arabian Journal of Chemistry*, **7**:139–155. <https://doi.org/10.1016/j.arabjc.2013.10.007>.

Ravikumar R. V. S. S. N., Chandrasekhar A. V., Ramakrishna C., Reddy Y. P. 2010. X-ray powder diffraction, thermal analysis and IR studies of zinc ammonium phosphate hexahydrate. *Optoelectronics and Advanced Materials, Rapid Communications*, **4**:215–219.

Regy S. 2001. Phosphate recovery by struvite precipitation in a stirred reactor. *Ceep*, **2**:1–66.

Rittmann B. E., Mayer B., Westerhoff P., Edwards M. 2011. Capturing the lost phosphorus. *Chemosphere*, **84**:846–853. <https://doi.org/10.1016/j.chemosphere.2011.02.001>.

Römer W. & Steingrobe B. 2018. Fertilizer effect of phosphorus recycling products. *Sustainability (Switzerland)*, **10**. <https://doi.org/10.3390/su10041166>.

Ronteltap M., Maurer M., Hausherr R., Gujer W. 2010. Struvite precipitation from urine - Influencing factors on particle size. *Water Research*, **44**:2038–2046. <https://doi.org/10.1016/j.watres.2009.12.015>.

- Ruttenberg K. C. 2001. Phosphorus cycle. *Encyclopedia of Ocean Sciences*, 2149–2162. <https://doi.org/10.1006/rwos.2001.0277>.
- Saerens B. 2020. Thermal decomposition of struvite. *Journal of Thermal Analysis and Calorimetry*. <https://doi.org/10.13140>.
- Schuiling R. D. & Andrade A. 1999. Recovery of struvite from calf manure. *Environmental Technology United Kingdom*, **20**:765–768. <https://doi.org/10.1080/09593332008616872>.
- Shih Y. J., Abarca R. R. M., de Luna M. D. G., Huang Y. H., Lu M. C. 2017. Recovery of phosphorus from synthetic wastewaters by struvite crystallization in a fluidized-bed reactor: effects of pH, phosphate concentration and coexisting ions. *Chemosphere*, **173**:466–473. <https://doi.org/10.1016/j.chemosphere.2017.01.088>.
- Siciliano A., Limonti C., Curcio G. M., Molinari R. 2020. Advances in struvite precipitation technologies for nutrients removal and recovery from aqueous waste and wastewater. *Sustainability (Switzerland)*, **12**. <https://doi.org/10.3390/su12187538>.
- Smil V. 2000. Phosphorus in the environment : natural flows and human interferences. *Annual Review of Energy and the Environment*, **25** (1): 53–88.
- Stefov V., Šoptrajanov B., Kuzmanovski I., Lutz H. D., Engelen B. 2005. Infrared and Raman spectra of magnesium ammonium phosphate hexahydrate (struvite) and its isomorphous analogues. III. Spectra of protiated and partially deuterated magnesium ammonium phosphate hexahydrate. *Journal of Molecular Structure*, **752**:60–67. <https://doi.org/10.1016/j.molstruc.2005.05.040>.
- Suzuki K., Tanaka Y., Kuroda K., Hanajima D., Fukumoto Y., Yasuda T., Waki M. 2007. Removal and recovery of phosphorous from swine wastewater by demonstration crystallization reactor and struvite accumulation device. *Bioresource Technology*, **98**:1573–1578. <https://doi.org/10.1016/j.biortech.2006.06.008>.
- Talboys P. J., Heppell J., Roose T., Healey J. R., Jones D. L., Withers P. J. A. 2016. Struvite: a slow-release fertiliser for sustainable phosphorus management? *Plant and Soil*, **401**:109–123. <https://doi.org/10.1007/s11104-015-2747-3>.
- Tansel B., Lunn G., Monje O. 2018. Struvite formation and decomposition characteristics for ammonia and phosphorus recovery: a review of magnesium-ammonia-phosphate interactions. *Chemosphere*, **194**:504–514. <https://doi.org/10.1016/j.chemosphere.2017.12.004>.
- Taylor A. W., Frazier A. W., Gurney E. L. 1963. Solubility products of magnesium ammonium and magnesium potassium phosphates. *Transactions of the Faraday Society*, **59**:1580–1584. <https://doi.org/10.1039/tf9635901580>.
- Uysal A., Yilmazel Y. D., Demirer G. N. 2010. The determination of fertilizer quality of the formed struvite from effluent of a sewage sludge anaerobic digester. *Journal of Hazardous Materials*, **181**:248–254. <https://doi.org/10.1016/j.jhazmat.2010.05.004>.
- Van Straaten P. 2002. *Rocks for crops: agrominerals of sub-Saharan Africa*. Toronto, ICRAF International Centre for Research in Agroforestry.
- Van Straaten P. 2007. *Agrogeology : the use of rocks for crops*. [S.l, s.n].

- Veneklaas E. J., Lambers H., Bragg J., Finnegan P. M., Lovelock C. E., Plaxton W. C., Price C. A., Scheible W. R., Shane M. W., White P. J., Raven J. A. 2012. Opportunities for improving phosphorus-use efficiency in crop plants. *New Phytologist*, **195**:306–320. <https://doi.org/10.1111/j.1469-8137.2012.04190.x>.
- Verstraete W., Van de Caveye P., Diamantis V. 2009. Maximum use of resources present in domestic “used water.” *Bioresource Technology*, **100**:5537–5545. <https://doi.org/10.1016/j.biortech.2009.05.047>.
- Vollmar R. C. 1967. Physical properties. *Analytical Chemistry*, **39**:177–178. <https://doi.org/10.1021/ac60249a025>.
- Whitaker A. & Jeffery J. W. 1970. The crystal structure of struvite,  $MgNH_4PO_4 \cdot 6H_2O$ . *Acta Crystallographica Section B Structural Crystallography and Crystal Chemistry*, **26**:1429–1440. <https://doi.org/10.1107/s0567740870004284>.
- Withers P. J. A., Sylvester-Bradley R., Jones D. L., Healey J. R., Talboys P. J. 2014. Feed the crop not the soil: Rethinking phosphorus management in the food chain. *Environmental Science and Technology*, **48**:6523–6530. <https://doi.org/10.1021/es501670j>.
- Zhang T., He X., Deng Y., Tsang D. C. W., Jiang R., Becker G. C., Kruse A. 2020. Phosphorus recovered from digestate by hydrothermal processes with struvite crystallization and its potential as a fertilizer. *Science of the Total Environment*, **698**. 134240. <https://doi.org/10.1016/j.scitotenv.2019.134240>.
- Zimdahl R. L. 2015. Phosphorus. In: Zimdahl R. L. *Six chemicals that changed agriculture*. Colorado USA, Academic Press. p. 73–88. Elsevier. <https://doi.org/10.1016/B978-0-12-800561-3.00005-5>.

## APÊNDICE A – COMPROVANTE DE SUBMISSÃO DO ARTIGO 02

03/05/2021

Gmail - Submission Confirmation



Paulo Victor Campos &lt;pvcamps97@gmail.com&gt;

---

### Submission Confirmation

1 mensagem

---

**Chemical Engineering Journal** <em@editorialmanager.com>  
Responder a: Chemical Engineering Journal <cej@elsevier.com>  
Para: Paulo Victor Campos <pvcamps97@gmail.com>

3 de maio de 2021 22:05

Dear Dr. Campos,

Your submission entitled "A SEQUENTIAL PLACKETT-BURMAN AND DOEHLERT DESIGN TO OPTIMIZE STRUVITE PRECIPITATION FOR PHOSPHORUS RECOVERY FROM WASTEWATER AIMING FERTILIZER PRODUCTION", article type "Research Paper" has been received by Chemical Engineering Journal

You may check on the progress of your paper by logging on to the Editorial Manager as an author. The URL is <https://www.editorialmanager.com/cej/>.

Your username is: [pvcamps97@gmail.com](mailto:pvcamps97@gmail.com)

If you do not know your confidential password, you may reset it by clicking this link: <https://www.editorialmanager.com/cej/login.asp?i=1818030&l=KPXXBEO8>

Your manuscript will be given a reference number once an Editor has been assigned.

Thank you for submitting your work to this journal.

For further assistance, please visit our customer support site at <http://help.elsevier.com/app/answers/list/p/7923>. Here you can search for solutions on a range of topics, find answers to frequently asked questions and learn more about EM via interactive tutorials. You will also find our 24/7 support contact details should you need any further assistance from one of our customer support representatives.

Kind regards,

Editorial Manager  
Chemical Engineering Journal

---

In compliance with data protection regulations, you may request that we remove your personal registration details at any time. (Use the following URL: <https://www.editorialmanager.com/cej/login.asp?a=r>). Please contact the publication office if you have any questions.